

# INAUGURAL-DISSERTATION

Zur Erlangung der Doktorwürde

der

Gesamtfakultät für Mathematik, Ingenieur- und Naturwissenschaften

Ruprecht-Karls-Universität Heidelberg

Vorgelegt von

Philipp Baur M. Sc. M. Sc.

Aus Hildesheim

Tag der mündlichen Prüfung: 05.05.2023



THE BIOLOGICAL FUNCTION OF  
PATELLAMIDES AND THEIR COPPER COMPLEXES

Gutachter:

Prof. Dr. Peter Comba

Zweitgutachter:

Prof. Dr. Franziska Thomas

This thesis has been accomplished at the Institute of Inorganic Chemistry of the Ruperto Carola University Heidelberg from May 2019 until April 2023 and was supervised by Prof. Dr. Peter Comba and the thesis advisory committee members: Prof. Dr. Franziska Thomas, Prof. Dr. Annika Guse, Prof. Dr. Kai Johnsson. Synchrotron experiments were performed at the DESY in Hamburg and the PSI in Switzerland. Field studies were performed in collaboration with Prof. Bernhard Degnan from the University of Queensland, Brisbane, and were done on Heron Island, Queensland, Australia. Experimental work in Australia was performed in the group of Prof. Dr. David Fairlie, in direct collaboration with Dr. Tim Hill, Dr. James Lim and Dr. Kathy Wu, and Prof. Dr. Jeff Harmer at the University of Queensland, Brisbane. Solid phase peptide synthesis was done in collaboration with the group of Prof. Dr. Franziska Thomas at Heidelberg University, mainly together with Truc Lam Pham. ICP-OES experiments were performed at the Department of Geology by Dr. Christian Scholz. Computational research was performed in collaboration with Dr. Velmurugan Gunasekaran of the Comba group using the bwForCluster as well as the compute servers at the IWR.

The thesis was done in the graduate program of the Max Planck School *Matter to Life*

**Parts of this thesis have been published in scientific Journals:**

**P. Baur**, M. Kühl, P. Comba, L. Behrendt, *Marine Drugs*, **2022**, *20*, 119

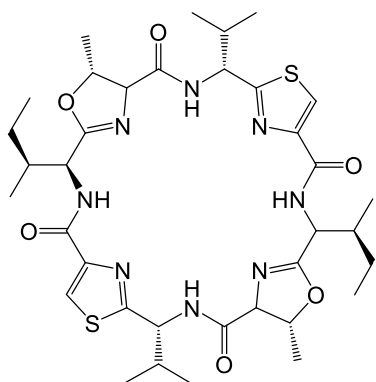
**P. Baur**, P. Comba, V. Gunasekaran, *Chem. Eur. J.*, **2022**, *28*, e202200249

**P. Baur**, L. R. Gahan, P. Comba, C. Scholz, *Aust. J. Chem*, **2022**, *76(1)*, 44-48

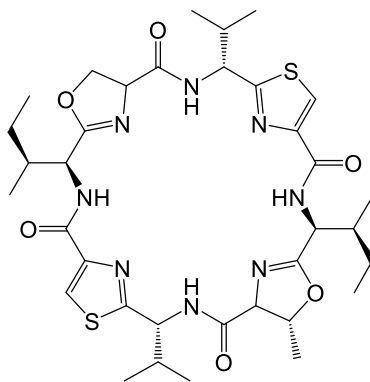


FOR  
MY  
FAMILY

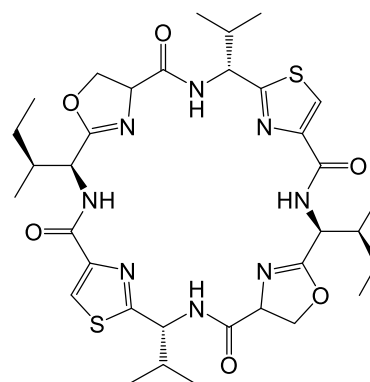
## Table of Molecules



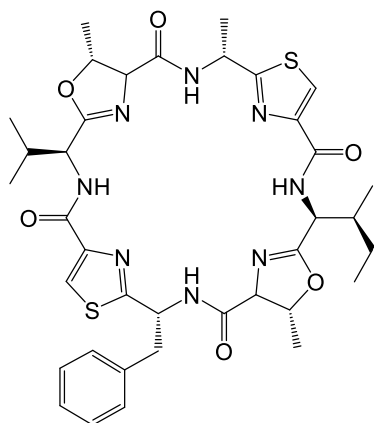
**Ascidiacyclamide (Asc)**



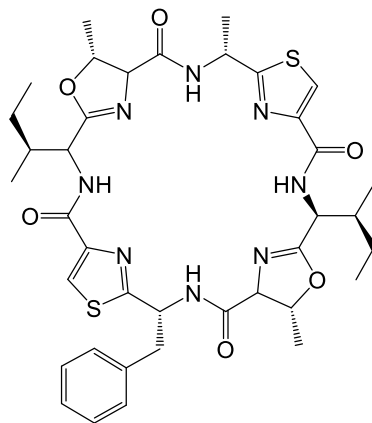
**Patellamide A (PatA)**



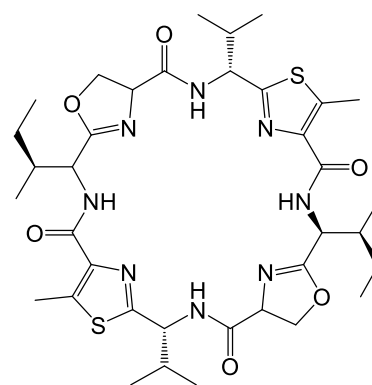
**Patellamide Analogue PB  
(Asc-0M)**



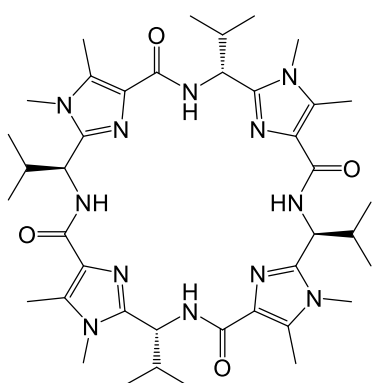
**Patellamide C (PatC)**



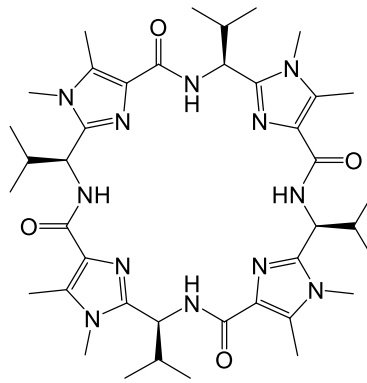
**Patellamide D (PatD)**



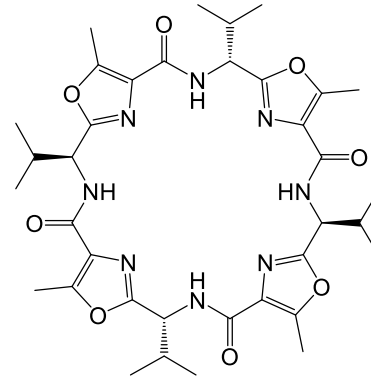
**Patellamide Analogue SO<sub>RS</sub>  
(PASO<sub>RS</sub>)**



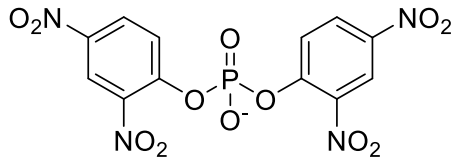
**Patellamide Analogue NN<sub>RS</sub>  
(PANN<sub>RS</sub>)**



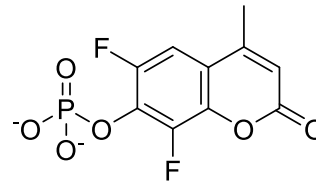
**Patellamide Analogue NN<sub>SS</sub>  
(PANN<sub>SS</sub>)**



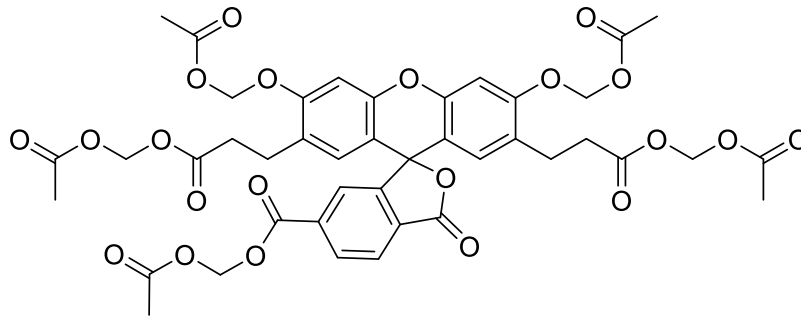
**Patellamide Analogue OO<sub>RS</sub>  
(PAOO<sub>RS</sub>)**



**bis(2,4-Dinitrophenyl) phosphate**  
**BDNPP**



**6,8-Difluoro-4-methylumbelliferyl phosphate**  
**DiFMUP**



**2',7'-bis-(2-Carboxyethyl)-5-(and-6)-carboxyfluorescein, acetoxymethyl ester**  
**BCECF/AM**



## List of abbreviations

A	<i>α</i> -Thr	<i>allo</i> -Threonine
	atm	physical atmosphere
	Ala	Alanine
	APCI	atmospheric pressure chemical ionisation
	aq	aqueous solution
	ATP	Adenosine triphosphate
B	BDNPP	Bis(2,4-dinitrophenyl)phosphate
	Bn	Benzyl
	Boc	<i>tert</i> -Butylcarboxycarbonyl
	Bu	Butyl
C	c	concentration
	CAPS	N-Cyclohexyl-3-aminopropanesulfonic acid
	calcd.	calculated
	Cbz	Carboxybenzyl
	CHES	2-( <i>N</i> -Cyclohexylamino)ethanesulfonic acid
	Chl	Chlorophyll
	COMU®	(1-Cyano-2-ethoxy-2-oxoethylideneaminoxy)dimethyl-aminomorpholino-carbenium hexafluorophosphate
	COSY	correlated spectroscopy
	CW	continuous wave
	Cys	Cysteine
D	DCM	Dichloromethane
	DEPT	distortionless enhancement by polarization transfer
	DIEA	<i>N,N</i> -Diisopropylethylamine
	DFT	density functional theory
	DNA	Desoxyribonucleic acid
	DMF	Dimethylformamide
	DMSO	Dimethylsulfoxide
	DWF	Debye-Waller factors

E	<i>E. coli</i>	<i>Escherichia coli</i>
	EPR	electron paramagnetic resonance
	eq.	equivalents
	Eq.	equation
	ESI	electrospray ionisation
	Et	Ethyl
	Et <sub>2</sub> O	Diethylether
	EtOAc	Ethyl acetate
	EtOH	Ethanol
	ε	extinction coefficient
	EXAFS	extended X-Ray absorption fine structure
F	FDPP	Pentafluorophenyl diphenylphosphinate
	FCM	flow cytometry
	Fmoc	Fluorenylmethoxycarbonyl
G	G	Gauss
	GH	Glycoside hydrolase
	GTP	Guanosine-5'-triphosphate
H	H	Hydrogen
	HEPES	4-(2-Hydroxyethyl)-1-piperazineethanesulfonic acid
	HF	HARTREE FOCK
	His	Histidine
	HMBC	heteronuclear multiple bond correlation
	HPLC	high performance liquid chromatography
	HR	high resolution
	HSQC	heteronuclear single quantum coherence
I	IC	inhibitory concentration
	<i>i.e.</i>	<i>id est</i> (that is)
	Ind	indicator
	Int.	intensity
	IR	infrared (spectroscopy)
	ISC	intersystem crossing
	IUGS	International Union of Geological Sciences

J	$J$	coupling constant
K	$k_{\text{cat}}$	first order rate constant
	$K_{\text{M}}$	MICHAELIS constant
L	$\lambda$	wavelength
	LDA	local density approximation
	LMCT	ligand metal charge transfer
	<i>L.p.</i>	<i>Lissoclinum patella</i>
M	m	multiplet
	M	molar [mol/L]
	MD	molecular dynamics
	Me	Methyl
	MeCN	Acetonitrile
	MeOH	Methanol
	MES	2-( <i>N</i> -Morpholino)ethanesulfonic acid
	Met	Methionine
	MM	molecular mechanics
	mol	number of moles of compound
	MS	mass spectrometry
N	neg.	negative
	NMM	<i>N</i> -Methylmorpholine
	NMR	nuclear magnetic resonance (spectroscopy)
	NRP	non-ribosomal pathway
O	OTf <sup>-</sup>	Trifluoromethane sulfonate

P	<i>p.a.</i>	<i>pro analysis</i>	
	<i>P.d.</i>	<i>Prochloron didemni</i>	
	PA	patellamide analogue	
	PAM	pulse amplitude modulation	
	PAP	Purple acid phosphatase	
	PEEK	Polyether ether ketone	
	Ph	Phenyl	
	Phe	Phenylalanine	
	PKS	Polyketide synthase	
	PMT	photomultiplier tubes	
	POM	Polyoxymethylene	
	pos.	positive	
	PS	polymer-supported	
	R	RMS	root mean square
		rt	room temperature
ROS		reactive oxygen species	
S	s	second(s)	
	SEM	scanning electron microscopy	
	Ser	Serine	
	SD	standard deviation	
	SPPS	solid phase peptide synthesis	
T	t	time	
	Thr	Threonine	
	TFA	Trifluoroacetic acid	
	TFMSAA	Trifluoromethane sulfonic acid anhydride	
	TON	turnover number	
	TRIS	(Tris-hydroxymethyl)-aminomethane	
U	UV	ultraviolet light	
	UPLC	ultra-performance liquid chromatography	
V	vis	visible light	
	Val	Valine	
	<i>vs.</i>	<i>versus</i>	

X	XAS	X-ray absorption spectroscopy
	XANES	X-ray absorption near edge spectroscopy
Z	Z	Carboxybenzylate

## Abstract

Patellamides are a group of cyclic peptides, found in the sea squirt (ascidian) *Lissoclinum patella*. These macrocycles are produced by the obligate symbiotic cyanobacterium *Prochloron didemni* in large quantities but their biological function remains unclear. Due to the rigid backbone of patellamides and various possible coordination sites, the complexation behavior with different metal ions has been studied in the past. The highest affinity and a wide range of catalytic properties were found with copper(II) ions. The resulting complexes show an extremely efficient carbonic anhydrase activity as well as phosphoesterase, glucosidase, and  $\beta$ -lactamase activity. However, the existence and structure of copper(II)-patellamide complexes in the organism have not directly been confirmed experimentally so far.

This work explores possible biological functions of patellamides, focusing on the detection of copper(II)-patellamide complexes in biological samples and testing hypotheses concerning their bioactivity. To obtain synthetically produced patellamides in appropriate quality and quantity, a new method for the synthesis of natural patellamides has been developed. For biological investigations, a field excursion to Heron Island, Queensland, Australia was undertaken, to collect colonies of *Lissoclinum patella*. A key observation is that injecting copper(II) into the living organism leads to a significant increase in the concentration of different patellamides. Furthermore, copper K-edge XAS measurements of the biological samples suggest that most of the copper within the organism is indeed bound as copper(II). Interestingly, with algae of the genus *Nannochloropsis spp.* it was observed that, while metal-free patellamides appear to have little effect on the algae, together with copper(II) they can have strong effects: while a rapid death of the algae at high copper(II) concentrations (0.5 mM copper, 0.05 mM patellamide) was observed, no adverse effects and a higher photosynthesis rate were observed at the physiological, low copper(II) concentrations (0.015 mM copper, 0.05 mM patellamides).

Based on these and previously published results, it is hypothesized that a main biological function is as a carbonate transporter from the cloacal cavity into the *Prochloron* cells.

## Zusammenfassung

Patellamide sind eine Gruppe zyklischer Peptide, die in der Seescheide (Aszidie) *Lissoclinum patella* vorkommen. Sie werden von ihrem obligat symbiotischen Cyanobakterium *Prochloron didemni*, in großen Mengen produziert, jedoch zu unbekanntem Zweck. Aufgrund des starren Rückgrats mit verschiedenen potenziellen Koordinationsstellen, wurde bereits früh ihr Komplexierungsverhalten mit verschiedenen Metallionen untersucht. Die höchste Metallaffinität und vielfältige katalytische Aktivitäten wurden mit Kupfer(II) festgestellt, darunter die als eine der schnellsten bekannten Carboanhydrasen, sowie als Phosphoesterase, Glucosidase und  $\beta$ -Lactamase. Bisher wurden Kupferkomplexe der natürlichen Patellamide und deren Struktur jedoch nicht experimentell in den Seescheiden nachgewiesen.

In dieser Arbeit wird die biologische Funktion der Patellamide untersucht, mit Schwerpunkten auf den Nachweis von Kupfer(II)-Komplexen in biologischen Proben und der Prüfung verschiedener Hypothesen zu möglichen Bioaktivitäten. Um reine Patellamide in ausreichender Menge als Referenzsubstanz zu erhalten, wurde eine neue Methode zur Synthese natürlicher Patellamide entwickelt. Für biologische Versuche wurde eine Exkursion nach Heron Island, Queensland, Australien unternommen, um Kolonien von *Lissoclinum patella* zu sammeln. Es wurde beobachtet, dass die Injektion von Kupfer(II) in den lebenden Organismus zu einem signifikanten Anstieg der Konzentration verschiedener Patellamide führt. Zudem legen Kupfer K-Kanten Röntgenabsorptionsmessungen nahe, dass der Großteil des Kupfer(II) im Organismus an Patellamide gebunden ist. Bei Experimenten mit Algen des Genus *Nannochloropsis spp.* wurde beobachtet, dass Patellamide selbst keinen Effekt auf die Algen haben, jedoch zusammen mit Kupfer(II) starke Effekte haben: hohe Konzentrationen (0.5 mM Kupfer, 0.05 mM Patellamid) führen zu einem schnellen Tod der Algen während bei niedrigen Konzentrationen (0.015 mM Kupfer, 0.05 mM Patellamid) kein Absterben sondern eine Zunahme der Photosynthese-Rate beobachtet wurde.

Basierend auf diesen und literaturbeschriebenen Resultaten wird die Hypothese aufgestellt, dass eine Hauptfunktion der Patellamide die eines Transporters für Carbonat aus der Kloake der Seescheide in die *Prochloron*-Zellen ist.

## Contents

	<b>Table of Molecules</b> .....	1-7
	<b>Abstract</b> .....	1-14
	<b>Zusammenfassung</b> .....	1-15
	<b>Contents</b> .....	1-16
<b>1.</b>	<b>Introduction</b> .....	<b>1</b>
<b>2.</b>	<b>State of the Art</b> .....	<b>3</b>
<b>2.1</b>	<b>Biological background</b> .....	<b>3</b>
2.1.1	<i>Lissoclinum patella</i> .....	3
2.1.2	<i>Prochloron didemni</i> .....	8
<b>2.2</b>	<b>Chemical background</b> .....	<b>11</b>
2.2.1	Structural elements of patellamides and other cyanobactins .....	11
2.2.2	Metal complexation .....	14
2.2.3	Synthesis and biosynthesis of patellamides .....	16
<b>2.3</b>	<b>Properties of patellamides</b> .....	<b>18</b>
2.3.1	Medical properties .....	18
<b>3.</b>	<b>Patellamide synthesis</b> .....	<b>21</b>
3.1	Introduction .....	21
3.2	Synthesis in the liquid phase using heterocyclic building blocks .....	22
3.3	Solid phase synthesis .....	26
<b>4.</b>	<b>Characterization of copper(II)-patellamide complexes <i>in vivo</i></b> .....	<b>28</b>
4.1	<i>In vivo</i> detection of copper(II)-patellamide complexes using X-ray absorption spectroscopy .....	28
4.1.1	Method .....	28
4.1.2	Introduction .....	30
4.1.3	Measurements .....	31
4.1.4	Results .....	33
4.2	Determination of the copper concentration in <i>Lissoclinum patella</i> .....	38
4.3	Interrelation of the concentration of patellamides and the concentration of copper(II) .....	41
<b>5.</b>	<b>Biological studies on patellamides and their producers</b> .....	<b>45</b>



5.1	Determination of the intracellular pH value within <i>Prochloron didemni</i> ....	45
5.2	Bioactivity of patellamides and their copper complexes on algae .....	49
5.3	Catalytic activity of dicopper(II)-patellamide complexes.....	52
	5.3.1 Phosphoesterase activity with small molecules .....	52
	5.3.2 Phosphodiesterase activity with DNA .....	56
5.4	Discovery of a new species of parasite within <i>Lissoclinum patella</i> .....	60
<b>6.</b>	<b>Conclusions and outlook.....</b>	<b>62</b>
<b>7.</b>	<b>Experimental Section .....</b>	<b>65</b>
	7.1 Materials and methods .....	65
	7.2 Field Experiments and Sample Collection .....	70
	7.3 X-ray Absorption Spectroscopy .....	72
	7.4 Synthesis.....	74
<b>8.</b>	<b>References .....</b>	<b>95</b>
	<b>Appendices .....</b>	<b>102</b>
	Synthesis – Maldi-MS spectra of linear peptides made by SPPS.....	102
	XAS Data.....	103
	Copper Concentration Measurements.....	107
	Patellamide concentration dynamics dependent on copper .....	114
	Determination of the intracellular pH value in <i>Prochloron didemni</i> .....	120
	Patellamide bioactivity towards <i>Nannochloropsis spp.</i> .....	123
	Phosphodiesterase activity.....	125
	<b>Danksagung .....</b>	<b>129</b>



# 1. Introduction

In the pursuit of steadily expanding the array of available medication, especially against cancer and infectious diseases, researchers look for new molecules with pharmaceutical properties wherever is deemed promising. Apart from exploiting new computational and synthetic techniques, the search is increasingly expanded to natural substances found between the highest mountains<sup>[8]</sup> and the deepest seas<sup>[9]</sup>. Some of the most successful drugs such as Aspirin<sup>[10]</sup>, Digoxin<sup>[11]</sup>, and morphines<sup>[12]</sup> are derived from terrestrial natural products. While the sea covers over 70% of our planet only little is known about many of the organisms that inhabit it – and about potentially useful substances they might contain.

One of these studies, aiming at identifying new medically interesting substances<sup>[13]</sup> discovered a group of cyclic peptides found in large amounts within the ascidian *Lissoclinum patella*. Unlike many marine cyclic peptides, they did not show significant cytotoxicity or palatability changes towards any of the tested marine organisms<sup>[14]</sup>. They showed cytotoxicity towards different human cell lines<sup>[15]</sup> and Patellamide D has been shown to act as a selective antagonist in multidrug-resistant leukemia cell lines<sup>[16]</sup>. However, none of these properties seemed likely to be correlated to their natural function, as the effects were related to competitive binding to overexpressed transport proteins. All molecules from the patellamide family show a similar structure, being cyclized pseudo-octapeptides with two oxazoline and two thiazole heterocycles as well as hydrophobic side chains with two amino acids next to the thiazole showing inverted stereochemistry (the structure and biosynthesis are introduced in detail in **2.2**).

Notably, the evaluation of the genome of the ascidian as well as its obligate symbiont, the cyanobacterium *Prochloron didemni*, revealed that only the cyanobacterium has the genes required for the synthesis of the patellamides<sup>[17]</sup>. Thus, the question arose for which purpose the molecule is made, especially on its role in the symbiosis and why it is exported to the host in such large amounts<sup>[18-19]</sup>. While *Prochloron didemni* has proven to be an obligate symbiont for the ascidian host (the biological background will be introduced in detail in **2.1**), no studies are addressing the question of whether the patellamides have a function for the host or whether they are produced by the cyanobacterium for its benefit.

Already few years after the discovery of the patellamides, their metal-binding properties were studied, as one would expect the molecule to form stable metal complexes due to the rigid cyclic backbone with eight nitrogen donors. Metal binding studies<sup>[20-22]</sup> have shown that patellamides have the highest affinity towards copper(II) and that copper(I) does not only bind stronger than other metals but that it can bind two Cu<sup>2+</sup>-ions cooperatively (this is discussed in detail in **2.2.2**) The resulting dinuclear copper(II) complexes of the patellamides have shown to be highly catalytically active towards different substrates <sup>[23-24]</sup>. While the copper(II)-patellamide complexes have so far not been found *in natura*, a recent study used a fluorescence-tagged patellamide analogue showing the ability to bind copper(II) *in vivo*<sup>[25]</sup>.

Despite the numerous patellamide studies *in vitro* in the last years, the biological function of the molecules remained unclear. This thesis aims to apply new synthetic and experimental approaches to clarify whether dicopper(II)-patellamide complexes do exist *in vivo* and what their biological function might be.

## 2. State of the Art

### 2.1 Biological background

The patellamides are found in the organism *Lissoclinum patella*, produced by their most important symbiont, *Prochloron didemni*. Both species have some interesting properties that set them apart from other members of their respective families. Their most important properties are discussed in the following sections.

#### 2.1.1 *Lissoclinum patella*

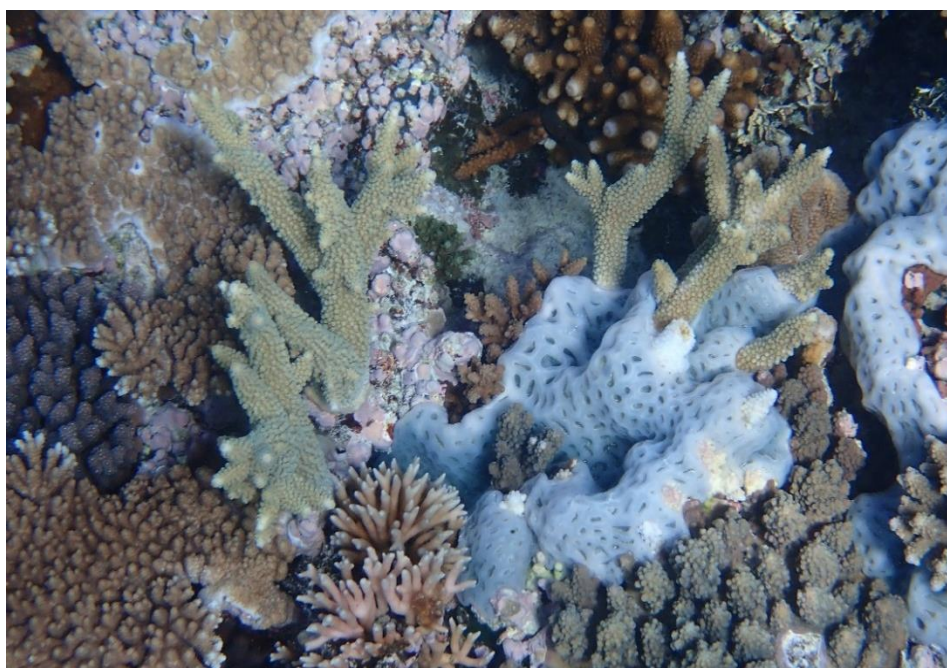


Figure 1: One colony of *Lissoclinum patella* growing on a coral (photo taken in 2022 at a depth of 1.2m at the Blue Pools Dive Site, Heron Island).

The didemnid ascidian *Lissoclinum patella* (*L.p.*) is a colonial tunicate organism (Figure 1), found near different reefs in the Western Pacific<sup>[26]</sup>. While most ascidians are sea squirts that sustain themselves by filtering nutrients out of the surrounding water, most didemnids such as *L.p.* contain a photosynthetic symbiont, in this case the cyanobacterium *Prochloron didemni* (*P.d.*). The cyanobacterium is an obligate symbiont for *L.p.*, and there have been no confirmed cases of the two organisms found without the other. *L.p.* usually reproduces sexually by cross- and self- fertilization, where different behavioral and structural mechanisms<sup>[27-28]</sup> ensure transmission of the symbiont.

Inside and on the outside of the ascidian a complex microbiome of resident microflora is found. The symbionts assume important functions such as nitrogen fixation<sup>[29-30]</sup> or photosymbiosis (*Prochloron didemni*) or produce cytotoxic substances (e.g. *Candidatus Endolissoclinum faulkneri* <sup>[31]</sup> produces the highly cytotoxic patellazoles for the ascidian). Especially the presence of these photosynthetic symbionts seems to be essential for the organism, as shading of the colony and the resulting drop in photosynthesis rates leads to slower growth of the ascidian<sup>[32]</sup>.

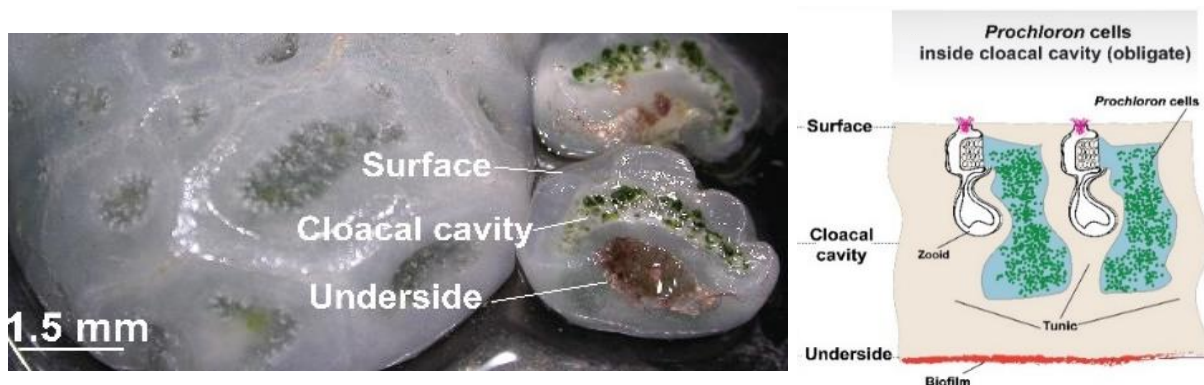


Figure 2: Left: Cross-section through a colony of *Lissoclinum patella*, Right: Schematic representation of the ascidian anatomy. <sup>[1]</sup>

Each ascidian colony consists of multiple individual animals (“zooids”), embedded in a common tunic, which is immobilized on the coral or rock the organism is growing on <sup>[26, 33]</sup>. Several individual ascidians share one common colonial cloaca, which is inhabited by *P.d.*<sup>[34]</sup>. The individual colonies can grow quite large to sizes of up to one square meter\*, but more commonly are significantly smaller, in the range of 10-50 cm<sup>2</sup>, and are up to 1 cm thick<sup>[26]</sup>. They have a firm gelatinous, smooth, white surface with multiple opaque rounded ridges and transparent concave indentations in between, which contain the cloacal and zooid openings of one sub-colony of ascidian zooids (Figure 2). For one subcolony, the number of openings to the common cloaca is small compared to ascidians who rely on filter-feeding<sup>[35]</sup>. The individual zooids are vertical and parallel to each other and have an ingestion opening with 16 oral tentacles (this opening is visible as the bright spots in the transparent area of the surface, seen in Figure 2). The thorax is between 4 rows of 14 elongated stigmata, the stomach and the intestine form a simple loop, which is flexed ventrally at an angle to the thorax. The reproductive organs are located beneath the loop of the gut.<sup>[26, 36]</sup> At the bottom of the

\* Based on personal correspondence with Prof. Bernard Degnan

colony, an additional red-colored biofilm is found, inhabited mostly by cyanobacteria and proteobacteria as well as Bacteroidetes. As most of the visible light is absorbed in the surface and the cloacal cavity of the ascidian, the remaining light on the bottom is mostly in the near infrared-region<sup>[37]</sup>.

Behrendt et al. (2012) found that unlike in other parts of the organism, the colonial cloacal cavity shows strongly varying parameters such as pH and oxygen saturation<sup>[29]</sup>, depending on the photon irradiance. The pH can vary between 6-7 in darkness and 8.5-10.5 in light, while the oxygen saturation (relative to the saturation in equilibrium with the atmosphere) can vary between around 60% under irradiation and nearly 0% in darkness<sup>[29]</sup>. However, it is unclear what mechanism causes these fluctuations and whether they are caused by *L.p.* or are imposed onto it by the photosymbiont *P.d.*.

Ascidians in general are known to accumulate different metals and particularly vanadium is found in unusually high amounts<sup>[38]</sup>. In some organisms and for some elements these accumulations correspond to the metal ion concentrations in the surrounding water<sup>[39]</sup> which might indicate that the accumulation is a non-selective, passive side effect of the filter feeding. Most species of ascidians rely on filter-feeding and resultingly have a quite different anatomy to species such as *L.p.*, which rely on a symbiotic cyanobacterium in the cloacal cavity. Filter-feeding ascidians often are vase-shaped and have a large cloaca and large cloacal openings and exits, as they pump up to several hundred milliliters of sea water per minute per gram of animal through the cloaca<sup>[40]</sup>. In the case of *L.p.*, the exact water transport rate has not been measured but can be assumed to be much lower. Free flow of water is limited as the common cloaca is surrounded on all sides by ascidian mantle tunic to immobilize the cyanobacteria. On the outer surface of *L.p.*, the cloacal openings with the feeding apparatus of the individual zooids can easily be seen as pale spots on the surface, while an exit hole usually is not visible (but has been reported in some cases<sup>[4]</sup>).



Figure 3: Larvae of the ascidian *Lissoclinum patella*. Both have a green color due to the presence of *Prochloron*. The larvae on the right shows the tadpole tail used for movement, the one at the left starts its transition to the immobile, adult phase<sup>[41]</sup>. (Photo credit: Oxford Scientific Films).

While a subcolony split from its original colony can survive and grow on its own, colonial didemnid ascidians such as *L.p.* usually reproduce sexually. Each individual zooid has reproductive organs, usually a testis and an egg or early embryo, which in the course of its development is moved into the basal tunic for brooding<sup>[41]</sup>. In the later stages of embryonic development, a tail is developed, which allows the larvae (Figure 3) or “tadpole” to swim for up to a few minutes, usually not dispersing further than 2m from the parent colony. As the colonies rely on the photosynthetic cyanobacterial symbionts<sup>[42]</sup>, the larvae have a photoreceptor and show a preference to settle in a location with a certain irradiation level, usually preferring a depth between 15m and 20m where possible<sup>[42]</sup>. If the larvae are forced to settle in shallow waters with high photon fluxes, the cyanobacterial symbionts usually die, leading to the death of the new colony. The ascidians’ adaptation to the light demands of the photosynthetic symbionts becomes evident from the time of the larval release at midday, unlike that of most nonsymbiotic ascidians, which spawn at dawn or dusk<sup>[43]</sup>. Additionally, adult colonies were found to produce dark bladder cells to protect the symbionts from high irradiation levels (Figure 4). Also, the swimming behavior of the larvae is different, as they start by swimming upwards for ~1m, followed by a descend to a preferred depth<sup>[42]</sup>. In shallow waters with many potential predators, typical for the habitats of the ascidians, a vast majority of about 95% of the larvae are eaten by other organisms such as fish, or get entangled within



the tentacles of corals (zoanthids)<sup>[42]</sup>. In deeper waters, this number can decrease to 70%, leading to an overall success rate of 5%-25% for the reproduction, depending on the depth. This ratio might seem low, but is high compared to many marine species e.g. turtles, where only 1 in 1000 turtle hatchlings reaches adulthood and maturity<sup>[44-45]</sup>.

During the development of the larvae, several adaptations ensure that all larvae leaving the colony have some of the symbiotic cyanobacteria *P.d.* in them. During the development of the ascidian embryo, the outer membrane of the developing egg initially is adhesive, trapping cyanobacteria onto it<sup>[4, 27-28]</sup>.

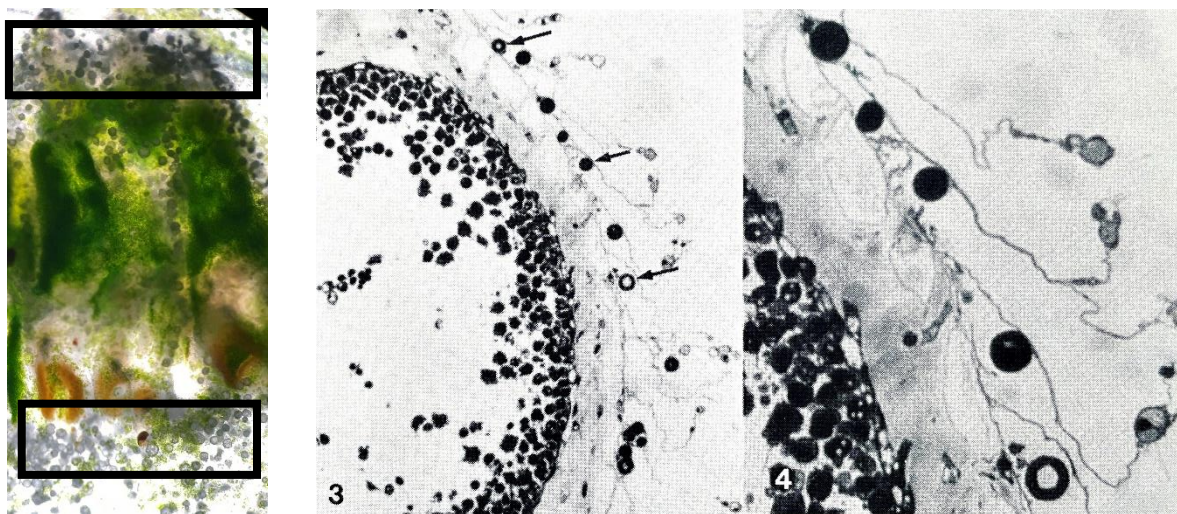


Figure 4: Left: Cut through a colony of *Lissoclinum patella*. The dark spheres inside the rectangles are bladder cells produced by the ascidian to protect from UV radiation. Center and Right: The trapping of *Prochloron didemni* cyanobacteria within the outer surface of the ascidian larvae. This anatomic preorganization, ensuring the transmission of the symbiont, indicative of the obligate nature of the symbiosis (Photo used with permission of L. Cheng<sup>[4]</sup>).

### 2.1.2 *Prochloron didemni*

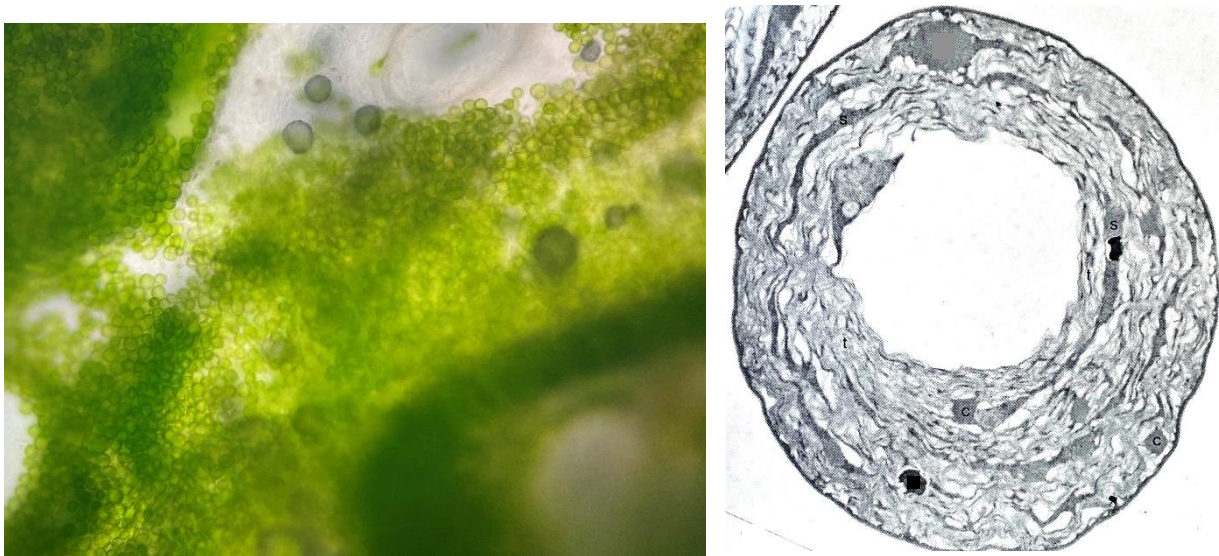


Figure 5: Left: *Prochloron didemni* inside the colonial cloacal cavity of L.p., a didemnid ascidian (2022, Heron Island). Right: Microscopy of an individual cyanobacterium. (Photo with permission of L. Cheng<sup>[4]</sup>)

Having evolved over 3 billion years<sup>[46]</sup>, cyanobacteria are one of the oldest species on earth and key contributors to the great oxygenation event 2.4-2 billion years ago that initiated the subsequent evolution of higher species. In general, cyanobacteria only possess chlorophyll A and use phycobilisomes<sup>†</sup> as antennae to increase the light-harvesting efficiency<sup>[47]</sup>, which gives them a red-brown color. However, Lewin et al. have discovered *Prochloron didemni* as a species in a new family of green-colored cyanobacteria having both chlorophyll a and b but no phycobilisomes<sup>[48]</sup>. Initially, it was suggested that the *prochloron* family might be an important missing link in the endosymbiotic evolutionary path from unicellular organisms to plants<sup>[49-50]</sup>. Given the presence of both types of chlorophyll together with other aspects such as appressed thylakoids it was assumed that *Prochloron* might be an oxygenic phototrophic bacterium, from which green plastids had evolved. This inspired the name *Prochloron* and led to its classification as a prochlorophyte<sup>[51]</sup>. To this bacterial group other cyanobacteria, i.e., *Prochlorococcus* and *Prochlorothrix*, with similar, unusual photo pigmentation were later added. However, more current studies based on molecular ecology, have shown that prochlorophytes most likely represent a different line among cyanobacteria, and no evidence was found that green plastids are evolutionarily linked to *Prochloron*<sup>[52-53]</sup>. *P. didemni* was initially discovered as symbiotic cyanobacterium associated with the surface of *Didemnum*

<sup>†</sup> Phycobilisomes: the light harvesting antennae of photosystem II in cyanobacteria.

colonies in the Pacific and with *Diplosoma virens* near Hawaii<sup>[48]</sup>, but it was soon discovered in other species, including *Lissoclinum patella*<sup>[54-55]</sup>.

Generally, *Prochloron* are single-celled, spherical cyanobacteria (~10–25 µm) that engage in symbiosis with different didemnid ascidians (tunicates) and in some cases with marine invertebrates such as Porifera and holothurians (sponges and sea cucumbers)<sup>[4]</sup>. The obligate symbiotic relationship between the ascidians and *Prochloron* is the only known example of obligate photo-symbiosis in chordates<sup>‡</sup>. There are some examples of *Prochloron* found in coral reef water, able to persist in a free-living state<sup>[56]</sup>, it is usually found on the interior or exterior surface of didemnid ascidians<sup>[54-55, 57]</sup> and needs a host organism to survive. There are different variants of the symbiotic relationship between the two organisms<sup>[51-52]</sup>, where the cyanobacterium can either be *i*) an obligate symbiont hosted intracellularly in tunic cells (e.g. in *Lissoclinum punctatum*) or, more commonly, in shared inner colonial cloacal cavities (see Figure 5 e.g. in *Lissoclinum patella*, *Diplosoma spp.*) and tunic (e.g. some *Didemnum* and *Trididemnum* species) of the ascidian, or *ii*) facultatively associated, where *Prochloron* is found in a biofilm on the external tunic surface like on *Didemnum candidum* and some non-didemnid ascidians.

As *Prochloron* inhabits the cloacal cavity of *L.p.* with its widely varying pH and oxygen saturation levels and high metal concentrations, it must be well adapted to these conditions<sup>[29]</sup> or might even influence them. Given that the cultivation of the cyanobacterium under standard conditions has been mostly unsuccessful with only one report describing a successful cultivation in a low salinity medium and with slightly increased concentrations of different metal salts such as Cu<sup>II</sup>, Fe<sup>II</sup>, Mn<sup>II</sup><sup>[58]</sup>, *P.d.* might even depend on the availability of these metals. While *P.d.* lives within the cloacal cavity of *L.p.*, there are other types of phycobilisome-containing cyanobacteria inhabiting the biofilm at the bottom side of the ascidian. In direct comparison to *P.d.*, they show much lower PSII quantum yield and relative photosynthesis rates, which is an indication, that the prevailing conditions are ideal for *P.d.*<sup>[29]</sup>. For the fixation and utilization of carbon, *P.d.* like most similar organisms uses carboxysomes<sup>[59]</sup>, small microcompartments containing carbonic anhydrase and RuBisCO that have formed to prevent a substrate competition of O<sub>2</sub> with CO<sub>2</sub> for RuBisCO<sup>[60]</sup>.

---

<sup>‡</sup> chordates: members of the animal phylum of chordates, to which most animals belong.

While both, the ascidian host and *Prochloron* have been shown to be in an obligate symbiotic relationship, both are unable to thrive without each other. The benefit of the symbiosis for *L.p.* is more obvious as *P.d.* provides the host with photosynthesis products and intermediates<sup>[61]</sup> to an extent, that up to 60% of the host's demand for carbon is met<sup>[30]</sup>. This agrees with the observation that limiting the photosynthetic activity by shading the ascidian slows the growth<sup>[32]</sup>. However, the reliance of the host on the photosynthesis products is likely to vary with different biological and environmental factors<sup>[30, 62]</sup> to a hitherto unknown degree. *Prochloron* was found to participate in the recycling of nitrogen<sup>[30, 63-64]</sup> and possibly even in nitrogen fixation<sup>[65]</sup>. Besides getting a habitat in a controlled environment, a possible export of nitrogen-based waste from the host to the symbiont could be one of the benefits *Prochloron* obtains from the symbiosis.

Besides assisting the host in the carbon- and nitrogen metabolism, *Prochloron didemni* produces large amounts of cyclic peptides, the patellamides, and exports them to the host<sup>[66]</sup>. The cyclic peptides have been reported to be present in amounts of up to several percent of the animal's dry mass<sup>[17]</sup>. Since *P.d.* itself only accounts for a small percentage of the animals' dry mass, the production of patellamides must be quite resource intense for the cyanobacteria. Due to the large amounts of patellamides found in all parts of the animal<sup>[18]</sup> they obtained their initial name after the putative producer *Lissoclinum patella*<sup>[13]</sup>. Only later studies proposed *P.d.* as the likely producer<sup>[18]</sup>. The analysis of the full genome of both organisms revealed that only *P.d.* has the genes required for the patellamide biosynthesis<sup>[17]</sup>. The characteristic properties of the patG gene, it is coding for multiple enzymes required for the synthesis of the patellamides that are not substrate specific and disassembled afterward, the patellamides were classified as secondary metabolites. Generally, secondary metabolites are not involved in the growth, development, or reproduction of the organisms, and are relevant for long-term strategies such as control of the local environment or defense<sup>[67]</sup>. This makes some initially proposed functions such as an enzymatic role in the primary metabolism of carbon or nitrogen unlikely.

## 2.2 Chemical background

### 2.2.1 Structural elements of patellamides and other cyanobactins

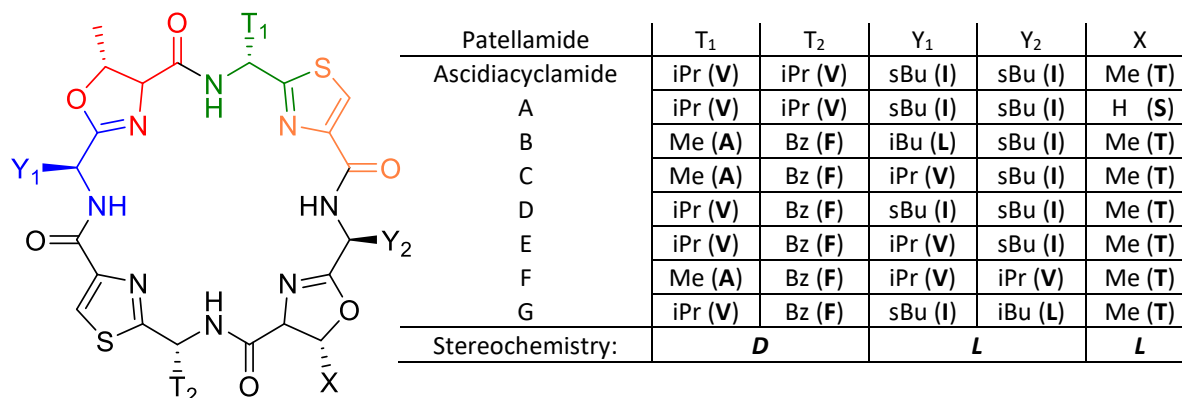


Figure 6: Fundamental Structure of all patellamides. All patellamides contain **cysteine** (yellow) heterocyclized with a **hydrophobic amino acid with D-stereochemistry** (green) and **threonine** (red serin in case of Patellamide A) heterocyclized **with a hydrophobic amino acid with L-stereochemistry** (blue). The table shows all known patellamides with the nature of their respective hydrophobic side chains and the amino acid encoded in the sequence<sup>[7]</sup>.

All molecules from the patellamide family share common structural characteristics (Figure 6). They are quasi-octapeptidic macrocycles consisting of four heterocycles with side chains, alternating between two thiazoles and two oxazolines with a methyl group in  $\alpha$ -position of the oxygen and *trans* relative to the amide. They are made from eight amino acids, alternating between a hydrophilic amino acid (cysteine, serine, threonine) and a hydrophobic amino acid (alanine, isoleucine, leucine, phenylalanine, valine). Each of the hydrophilic amino acid side chain heteroatoms forms a heterocycle with the carbonyl group of the peptide bond of the neighboring (N-sided) neighboring amino acid to form thiazole or methyl-oxazoline (oxazoline in the case of patellamide A). The hydrophobic side chains next to the oxazolines have an *S*-stereocenter while the hydrophobic side chains next to the thiazole always have an *R*-stereocenter, despite the respective free *D*-amino acid not being present in the organism i.e., only the corresponding *L*-amino acid is encoded in the gene.

The structure of the patellamides has been extensively studied, both in solution and in the solid state<sup>[68-73]</sup>. The resulting systems form a 24-membered ring which in its metal-free state commonly assumes a figure-of-eight configuration, in which the two thiazoles are parallel and close to each other while the amide hydrogens are forming hydrogen bonds to proximate oxygen atoms from the peptide carbonyl groups and the heterocycles (Figure 7)<sup>[69]</sup>. In addition

to the figure-of-eight conformer, a saddle/square-shaped conformer with hydrogen bonds between the amide hydrogen and the neighboring nitrogen from the heterocycles was identified<sup>[2, 69]</sup>. Due to the structural restrictions from the macrocyclic shape as well as the rigidity of the heterocycles, the nitrogen atoms of the heterocycles and the peptide bonds point to the inside of the macrocycle, and the peptide side chains to the outside, making the molecule well suited for metal-binding. This structural preorganization as well as the accumulation of different metal ions within ascidians enticed researchers for many years to extensively study the metal ion chemistry of the patellamides and their analogues as well as the resulting coordination properties of the metal complexes both experimentally and theoretically<sup>[2, 5, 20, 23, 74-83]</sup>.

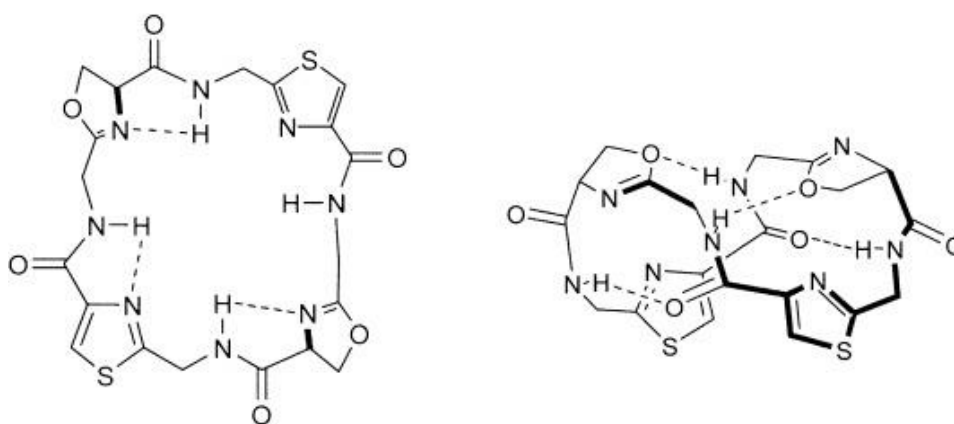


Figure 7: Comparison of the saddle-shaped and the figure-of eight configurations of the fully protonated patellamides<sup>[1-2]</sup>.

In addition to the patellamides produced by *Prochloron didemni*, there are several other cyclic molecules, found within *L.p.* that share some structural features with the patellamides (Figure 8). Amongst these are the lissoclinamides and ulicyclamide, which consist of seven amino acids instead of the eight found in the patellamides, with similar hydrophobic amino acids such as phenylalanine and valine, but with three instead of four azol(in)es, two thiazoles, one oxazoline (instead of a second oxazoline, there is a proline pyrrolidine ring built into the backbone)<sup>[84]</sup>. The different lissoclinamides and ulicyclamide only differ in the hydrophobic side chains and the oxidation state of the thiazole rings, of which none, one, or both can be thiazolines instead. Another example is ulithiacyclamide, which shares many of the structural characteristics with the patellamides like the number and nature of heterocycles and macrocyclic ring size. However, the side chains next to the oxazoline are cysteines, which have been found to form a disulfide bridge through the middle of the macrocycle, which would

make metal binding unlikely<sup>[85]</sup> but increases the rigidity and stability of the macrocycle. Lissoclinamides, ulicyclamides, and ulithiacyclamides are also produced by *Prochloron didemni* and the genes for their biosynthesis are in the same cluster as for the patellamides<sup>[86]</sup>.

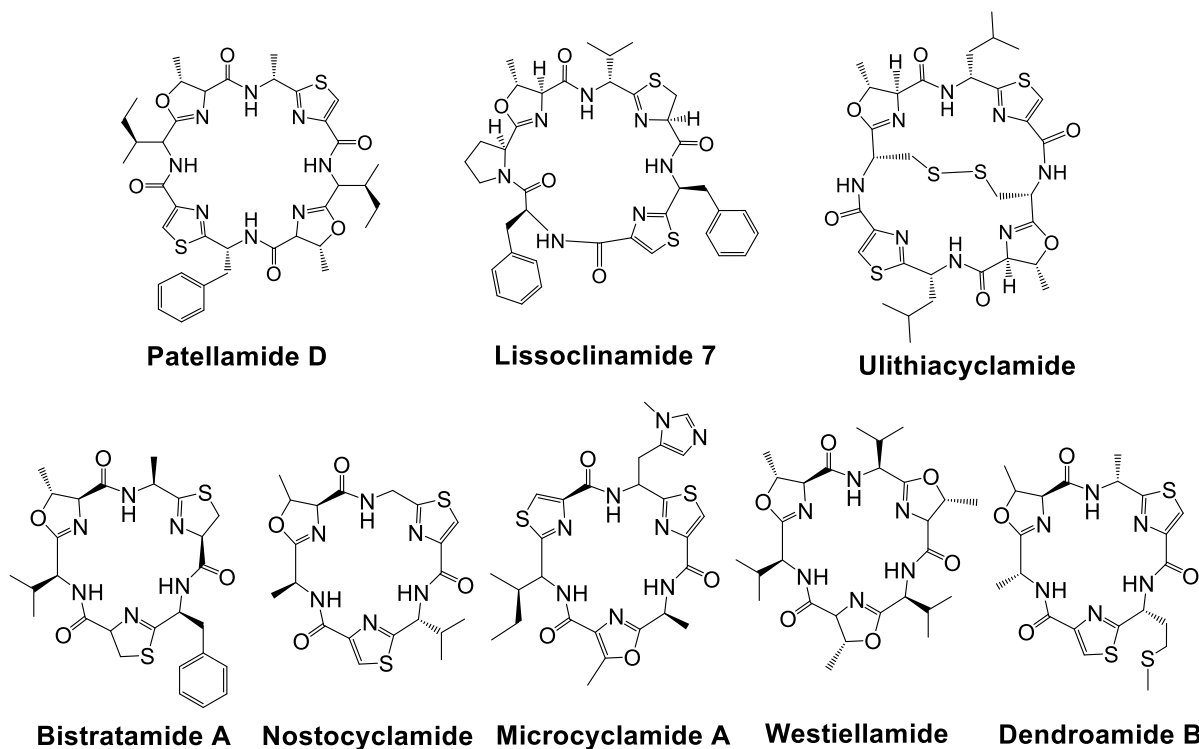


Figure 8: Selected examples of heterocycle-containing cyclic peptides from marine sources.

While all these molecules have four heterocycles, the patellamides and ulithiacyclamide are octapeptides but the lissoclinamides and ulicyclamides are heptapeptides. There is another class of similar hexapeptide compounds, found in other species that often share the same habitat. Within *Lissoclinum bistratum*, one can find the bistratamides, produced also by *Prochloron didemni*, which are smaller macrocycles with three heterocycles (thiazole, methyl-oxazoline or oxazole) and the same side chains but in all cases with the naturally occurring *L*-stereoisomers of the hydrophobic amino acids. In the ascidian *Didemnum mole*, the similar didmolamides are found, one of which supposedly features a non-heterocyclized threonine side chain and can be found with the *D*-stereoisomers of the amino acids as well. In the cyanobacterium *Westiellopsis prolifica* the westiellamide is found, which unlike the others has three identical methyloxazoline heterocycles<sup>[87]</sup>. The nostocyclamides found in the nitrogen-fixating cyanobacterium *Nostoc 31* and the tenuencyclamides<sup>[88]</sup> from *Nostoc spongiaeforme* unlike all others feature a side chain-less glycine<sup>[89]</sup>. In *Oscillatoria raoi* the raocyclamides were isolated, which contain oxazoline without methyl groups<sup>[90]</sup>. One of the

microcyclamides isolated from *Microcystis aeruginosa* possesses N-methylated histidine as a side chain. Some further members of the family of heterocycle-containing cyclic hexapeptides are the venturamides from the cyanobacterium *Oscillatoria s.p.*, the aerucyclamides from *Microcystis aeruginosa*<sup>[91]</sup> and the dendroamides from the cyanobacterium *Stigonema dendroideum*<sup>[92]</sup>. While these azol(in)e containing macrocycles are produced by many different cyanobacteria, in most cases the possible function attributed to them in literature is molecular defense.

### 2.2.2 Metal complexation

The described structural aspects, specifically the rigid heterocycle-containing macrocyclic backbone with several potential nitrogen donors remind of an expanded version of the commonly found porphyrin rings, however, they are less rigid and do not have an aromatic backbone. As a result, many researchers started to study the metal-binding properties of these molecules shortly after their discovery<sup>[21-22, 74]</sup>. Metal binding studies have shown, that while many metal ions can weakly bind to the patellamides<sup>[93]</sup>, zinc(II) and especially copper(II) bind more strongly, and in the case of copper(II), not only one, but two copper(II) ions can bind. Furthermore, copper(II) was assumed to be present at concentrations increased by a factor of  $10^4$  in the animals with respect to the surrounding sea water<sup>[20, 74]</sup> (during experiments in this work, this value was found to be incorrect as described in **4.2**). Notably, the binding of the first copper(II) to the patellamide results in a structural change into a saddle-shape which facilitates the binding of a second copper(II)<sup>[83, 94]</sup>. This cooperative binding in addition to the higher affinity indicated that this might be an essential feature. As the most common oxidation state of copper in an aqueous environment is two, the research on the complex chemistry of patellamides focused on copper(II). The resulting complexes have been studied extensively by crystallography, EPR- UV/Vis and CD- spectroscopy as well as computationally in order to understand the structural characteristics and the resulting properties of different dicopper(II)-patellamide complexes in solution and as solids.



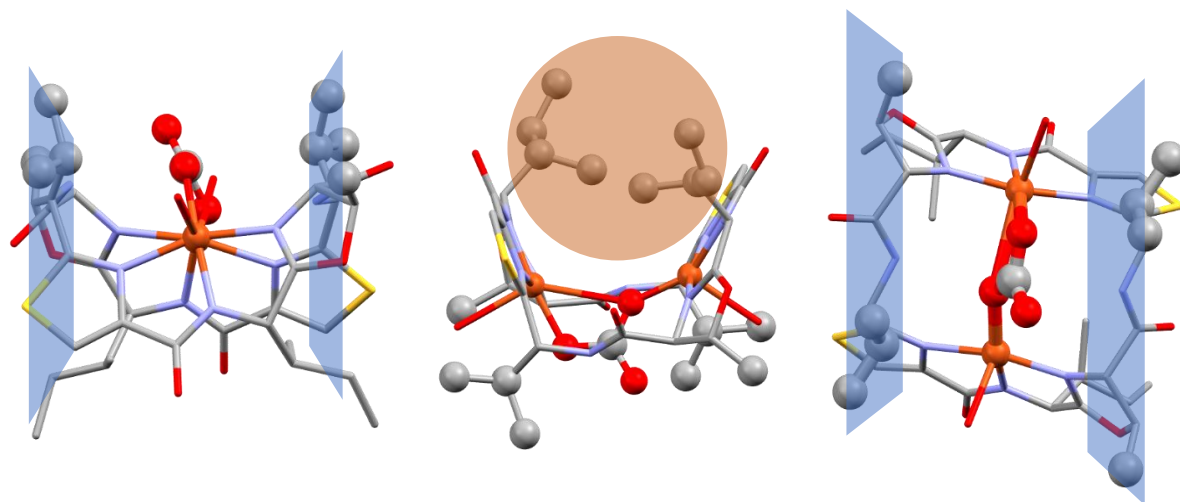


Figure 9: Crystal structure of the dinuclear copper(II) complex of ascidiacyclamide, bridged by carbonate. The isobutyl side chains from the *D*-valines lie in one plane with the methyl group from the oxazolines (colored blue), parallel to the plane containing the  $\text{Cu}^{\text{II}}\text{-CO}_3^{2-}\text{-Cu}^{\text{II}}$  site<sup>[5]</sup>.

Both copper(II) ions bind to three nitrogen atoms from the patellamide backbone, two from the azol(in)e heterocycles, and one from a deprotonated peptide bond, and the patellamide, therefore, is in a dianionic state. In an aqueous solution, the remaining binding sites of the copper(II) ions are usually coordinated to a bridging carbonate and/or  $\text{OH}_2$  or  $\text{OH}^-$ . The structural rearrangement following the binding of the first copper(II) ion, causes the final complex to assume a saddle-shaped structure<sup>[2]</sup>. In the resulting structure, the hydrophobic side chains next to the thiazoles, due to the non-natural *D*-configuration point outwards of the coordination plane, parallel to the plane containing the  $\text{Cu}^{\text{II}}\text{-CO}_3^{2-}\text{-Cu}^{\text{II}}$  site<sup>[1]</sup> (Figure 9, blue planes), while the hydrophobic side chains with *L*-configuration next to the oxazolines are oriented towards the inside of the saddle, posing a certain steric obstacle in that area (Figure 9, orange circle). The valine-containing planes might therefore act as a pocket for the catalytically active site, helping to stabilize the intermediate.

As many of the patellamides differ only in the size of the hydrophobic side chains, the differences in metal binding affinities that have been observed for very similar molecules, can therefore only be influenced by differences in the hydrophobic side chains. In the case of patellamides C and A, the stability constants for copper(II) are  $2.0 \times 10^4$  for patellamide A and  $6.8 \times 10^4$  for patellamide C, respectively<sup>[20]</sup>. Furthermore, major side chain differences cannot only lead to a different steric arrangement around the binding site but are expected to affect the bending angle and rigidity of the entire saddle-shaped structure. The azol(in)e-type heterocycles are important for the binding properties, and this was demonstrated in a

recently published study<sup>[95]</sup> showing that for a similar cyclic cyanobactin, the lissoclinamide, the ability to bind copper(II) is significantly decreased by interchanging the heteroatoms in the thiazole ring: when binding copper(II), the backbone strongly deformed to allow coordination to the nitrogen donors. Apart from structural differences between flat, aromatic azoles and the bent, non-aromatic azolines, the difference in  $pK_a$  between the different heterocycles ( $pK_a$  of  $pK_a$ , imidazole: 7.0, thiazole: 2.5, oxazoline: 4.75, oxazole: 0.8)<sup>[6, 96]</sup> leads to different binding behavior.

### 2.2.3 Synthesis and biosynthesis of patellamides

When the patellamides originally were discovered in 1981 by Ireland et al.<sup>[13]</sup>, they published a first initial guess of their structure, which involved directly fused thiazole and oxazoline heterocycles. When Hamada et al. in 1985 developed the first synthesis for different patellamides, they noticed that the resulting compounds analytically differed from the natural patellamides and proposed a corrected version of the patellamide structure<sup>[97-98]</sup>. This was later confirmed by crystallography and EPR-spectroscopy<sup>[70]</sup>. In the following years, different synthetic approaches, mostly combining peptide coupling approaches with heterocyclizations have been developed, shifting away from tedious or dangerous heterocyclization reactions such as the Hantzsch synthesis<sup>[97-98]</sup> or even heterocyclization using an overpressure of H<sub>2</sub>S-gas. Haberhauer et al. developed a building block-based approach in 2003 enabling a straightforward and cheap synthetic route to different analogues of the patellamides<sup>[99]</sup>. This resulted in good availability of the produced analogues for functional studies, especially of analogues containing 1,5-dimethylimidazole heterocycles instead of the natural ones. The proposed method for the synthesis of thiazole heterocycles however, using Lawesson's reagent can only lead to 5-methylthiazole, as the starting material needs to have two secondary carbonyls. A few years later in 2008 García-Reynaga et al. developed a new total synthetic approach using the more modern Fmoc-based peptide synthesis<sup>[100]</sup>.

Based on the building block-approach and the Fmoc-based peptide chemistry, a new synthetic approach was developed in course of this work: it is versatile and allows to prepare any desired natural or non-natural patellamide while moving the potentially yield-determining oxazoline heterocyclization step to the third step of the respective building block synthesis<sup>[6]</sup>.

As an alternative to the chemical approaches for the synthesis of patellamides, the biosynthetic route undertaken by the cyanobacteria was studied to understand and reproduce the synthesis. Firstly, the gene cluster “*pat*” responsible for the synthesis of patellamides was identified, isolated, amplified, and subsequently introduced into *E. coli* to successfully produce the patellamides in other organisms<sup>[17]</sup>. It was discovered that, apart from the eight amino acids used as precursor peptide for the biosynthesis, the majority of the gene encodes different enzymes required for many of the modifications needed to obtain the final patellamide, such as a protease, a heterocyclase/cyclodehydratase, an oxidase, a macrocyclase and possibly more enzymes in parts of the gene that are yet to be understood<sup>[101]</sup>. The macrocyclase and the heterocyclase have been found to be quite flexible and powerful enzymatic tools for macrocyclizations<sup>[3, 102]</sup> or heterocyclizations<sup>[103-104]</sup> of different substrates, making them interesting for different biosynthetic applications.

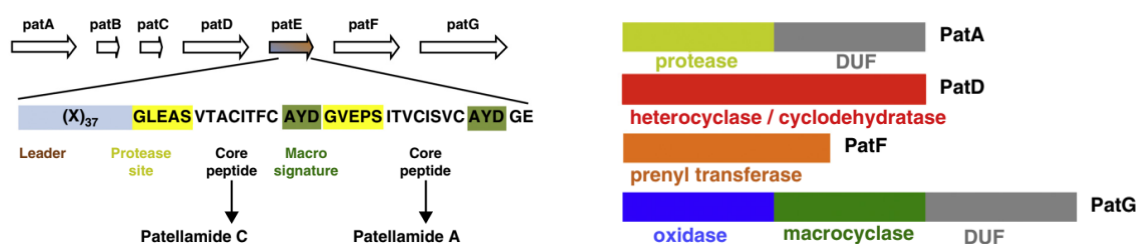


Figure 10: Contents of the *pat* gene, containing all the enzymes and the precursor peptides required for the biosynthesis of the patellamides (adapted from Koehnke, Naismith et al.)<sup>[3]</sup>.

Generally, the biosynthesis involves the synthesis of the enzymes encoded in the subgenes *patA*, *patB*, *patC*, *patD*, *patF* and *patG* and of large amounts of the precursor peptide contained in subgene *patE*. This precursor peptide contains the eight amino acids forming the final patellamides, which is cut from the precursor peptide with three additional amino acids (AYD), that are removed in the macrocyclization step. After being cut out by the protease, the precursor peptide needs to undergo a heterocyclization step of the cysteines to the thiazolines and an oxidation of the thiazolines to the thiazoles<sup>[101]</sup>, a heterocyclization of the threonines/serines to the oxazolines as well as the macrocyclization. The function of the different domains of unknown function within *patA* and *patG* is not fully understood, as is the exact order in which these enzymatic reactions occur. However, it is assumed that the heterocyclization steps occur first<sup>[105]</sup>.

## 2.3 Properties of patellamides

### 2.3.1 Medical properties

Many marine cyclic peptides were discovered by medical researchers, looking for potentially interesting new drugs – and generally the tests done with the molecules were toxicity assays<sup>[106]</sup>. Resultingly, in most cases the possible function discussed in literature is molecular defense. In case of the patellamides, these cyclic peptides do not have noteworthy toxicity against any microbial enemy or competitor of *P.d.*<sup>[107]</sup> and do not seem to affect the feeding behavior of larger predators<sup>[14]</sup>, which raises the interesting and so far unanswered question for what purpose the molecules are made. The period of the ascidian life cycle, in which they are most at risk, is the embryotic stage, during which a majority of the larvae are eaten by predators at similar rates as larvae of other ascidian species not containing patellamides<sup>[42]</sup>.

The patellamides were discovered by collecting several kilograms of ascidians and homogenizing them, extracting, and separating the natural products. They were noticed due to their cytotoxicity against L1210 murine leukemia cells at 2-4 µg/mL and of patellamide A against the acute lymphoblastic leukemia cell line CeM with an IC<sub>50</sub> of 0.028 µg/mL<sup>[13]</sup>. A more striking activity was discovered by Williams et al., who have shown that patellamide D at 3.3 µM concentrations acts as a selective antagonist in multidrug-resistant CEM/VLB<sub>100</sub> cell lines<sup>[16]</sup>. They observed that the IC<sub>50</sub> value of different chemotherapeutics in some cases could be reduced from 1000 ng/mL to 110 ng/mL, the effectiveness generally was comparable to verapamil, a previously used drug resistance modifier. The authors hypothesize that the anti-MDR activity works via competitive binding to p-glycoprotein, preventing the efflux of the drug. A key issue with pharmaceutically interesting compounds from biological sources is that, while extraction can be done on a drug-discovery scale, for medical use a stable supply of a large amount in consistent quality is needed. Therefore, typically an efficient synthesis is required. To date, there are various examples where, after a synthesis for the natural product was developed, the compound found use in clinical routine<sup>[108]</sup>, while others are still being tested<sup>[109-112]</sup>. In addition to the patellamides, several structurally similar cyclic peptides mentioned previously show pharmaceutical potential, such as the dendroamides<sup>[92]</sup> and the lissoclinamides<sup>[84]</sup>.

### 2.3.2 Reactivity and possible biological functions

As the patellamides, like many cyanobactins, have been discovered by medical researchers evaluating the antibacterial and antineoplastic properties of compounds in marine organisms. These properties were the only ones explored initially, and for the ascidian they were proposed to assume a defensive function<sup>[13]</sup>. However, in the case of the patellamides, no toxic properties or even palatability changes could be identified for the metal-free peptides<sup>[14, 42]</sup>. After the discovery of their interesting metal binding properties<sup>[5, 74]</sup>, researchers started to consider the possibility that the function of the patellamides might be related to their copper(II) binding properties. It was noticed that, whenever the copper(II) complexes of the patellamides are measured in presence of air, carbonato-bridged complexes were commonly found<sup>[2, 5]</sup>, which led researchers to evaluate the carbonic anhydrase reactivity of the complexes<sup>[79-80, 113]</sup>. It was concluded, that the patellamides indeed have a quite high carbonic anhydrase activity, showing activities only two orders of magnitude slower than the highly efficient zinc-based carbonic anhydrases<sup>[79, 113]</sup>, despite being solely copper-based and dinuclear. The reaction mechanism has been extensively studied using stopped-flow kinetic measurements, isotope labeling as well as quantum-chemical calculations. In these measurements, only a range of analogues, such as PANN<sub>RS</sub>, PANN<sub>SS</sub>, and PASO<sub>RS</sub> have been studied and it could not be evaluated whether this activity of the patellamides is of biological relevance for the cyanobacterium or its host.

Apart from carbonic anhydrase activity, the copper(II)-patellamide complexes show several other catalytic activities, including phosphoesterase<sup>[23, 81, 114]</sup> as well as glucosidase and  $\beta$ -lactamase<sup>[24]</sup>. While the phosphodiesterase reaction like the carbonic anhydrase reaction occurs at physiologically relevant pH ranges of 6-7<sup>[23, 81]</sup>, the other activities have only been observed at high pH values (over 10), and are thus unlikely to be of relevance<sup>[24]</sup>. For any relevance *in vivo* of these reactions, the copper(II) patellamide complexes would need to exist within the animal. While they have not directly been measured yet, a recent study has shown that the binding of copper(II) to fluorescence-tagged patellamide analogues occurs *in vivo*, which suggests a possible existence of the copper(II) complexes of patellamides *in situ*<sup>[25]</sup>. All the catalytic properties studied so far have been studied *in vitro* under controlled conditions and often in solvents or buffer conditions that differ from the natural conditions. To study these reactions *in vivo* other, more biocompatible methods are needed. Furthermore, while

for all reactions different patellamide analogue derivatives have shown differing reactivities, in agreement with the respective calculations, little is known about the influence of differences in heterocycles or side chains. A further indication of a possible enzyme-like function is the close proximity of the two copper(II)-ions within the macrocycle, which can be between 3.5 Å and 4.5 Å, similar to most dicopper-based enzymes<sup>[115]</sup>.

Apart from assumptions of an enzyme-like catalytic function, there have been other hypotheses concerning possible biological functions of the patellamides and their complexation behavior<sup>[21]</sup>. An interesting hypothesis is the activation and mobilization of CO<sub>2</sub><sup>[74]</sup>. A possible purpose of this transport function is the formation of CaCO<sub>3</sub> for the internal skeleton, but so far no indication of this has been found. However, the purpose of activation and transport of CO<sub>2</sub>/CO<sub>3</sub> between the cloacal cavity and the cyanobacterial cytoplasm to maximize the amount of available carbonate for photosynthesis would explain both the large amounts of patellamides produced as well as the CO<sub>2</sub> binding and carbonic anhydrase activity.

Another hypothesized function is to render the free copper(II) within the cloaca harmless<sup>[21]</sup>, as would be necessary for survival within the cloaca, given the reported high copper concentrations within the ascidians and the fact that copper is toxic to many (marine) microorganisms<sup>[116]</sup>.

A further, possible function could be the transport of copper(II) within the ascidian or in the colonial cloaca. While the stability constants of the patellamides for copper(II) are generally moderate compared to other copper(II)-binding molecules, Cu<sup>II</sup> is the metal ion for which they show the highest affinity, 1-2 orders of magnitude higher than for zinc(II) and several orders of magnitude higher than for calcium(II)<sup>[1, 113, 117]</sup>. However, new data on the actual copper concentrations in the animal makes this hypothesis less likely, also since the ascidians might have other, easier mechanisms to selectively translocate or accumulate copper(II).

## 3. Patellamide synthesis

### 3.1 Introduction

Investigating versatile and interesting copper(II) binding chemistry of the patellamides requires synthetic access to the molecules. Various synthetic approaches have been developed for the synthesis of these patellamide analogues<sup>[82, 94, 99, 118]</sup>. The few approaches for the synthesis of the natural patellamides reported in literature<sup>[97-98, 100, 119]</sup> often use long, outdated, or not easily adaptable synthetic methods. Thus, as part of this work, a new synthetic approach for the synthesis of natural patellamides was developed, combining the adaptability and efficiency of convergent building block approaches as described by Haberhauer et al.<sup>[99]</sup> with the more commonly used Fmoc-based chemistry described by VanNieuwenhze et al.<sup>[100]</sup>.

Concerning the general classification and nomenclature of patellamides and their analogues, based on the distinct structural properties shared by the natural patellamides and setting them apart from similar peptides from other organisms, we define the term patellamide as “macrocyclic octapeptide with a backbone alternating between azol(in)e heterocycles and hydrophobic side chains, with twice inverted *D*-amino acids next to thiazoles and twice *L*-amino acids next to oxazolines” (herein abbreviated Pat). In contrast, all similar derivatives violating at least parts of the definition are referred to as patellamide analogues (abbreviated PA), as long they consist of a 24-membered ring with four azol(in)e heterocycles bridged by four peptide bonds. To quickly and easily describe the nature of the azol(in)e heterocycles, the abbreviation PA is followed by two letters, describing the second heteroatom (other than the former amide nitrogen) in the two pairs of heterocycles (e.g., PANN: four imidazoles, PAOO: four oxazoles, PASO: two thiazoles, two oxazoles). This abbreviation is followed by two letters in subscript (e.g. PANN<sub>RS</sub> or PANN<sub>SS</sub>), describing the stereochemistry of the two pairs of side chains. This nomenclature allows to quickly and efficiently include the most important properties of the respective analogue and avoids the ambiguous numbering system used in previous works.

### 3.2 Synthesis in the liquid phase using heterocyclic building blocks<sup>†</sup>

The heterocyclization is a crucial step in the synthesis route and has been performed by a wide range of reactions in the past, such as a Hantzsch synthesis<sup>[119]</sup>, the application of Burgess or Lawesson's reagent<sup>[99, 120]</sup>, using thionyl chloride to create an acid chloride *in situ*<sup>[97]</sup>, by a modified Appel reaction or using the Hendrickson's reagent<sup>[121-122]</sup>. All these approaches have been considered as possible strategies for the synthesis of heterocyclic peptides. However, the Hantzsch synthesis requires several steps, hazardous chemicals such as H<sub>2</sub>S-gas<sup>[123]</sup> and a long temperature-controlled reaction, Lawesson's reagent requires two (secondary) carbonyls as starting material and thus could not be used with the natural amino acids and can only lead to methylated thiazoles, which are not found in nature, Burgess reagent has proven to not reliably afford high yields and often requires long reaction times at reflux temperatures, making the desired transition to the solid phase difficult.

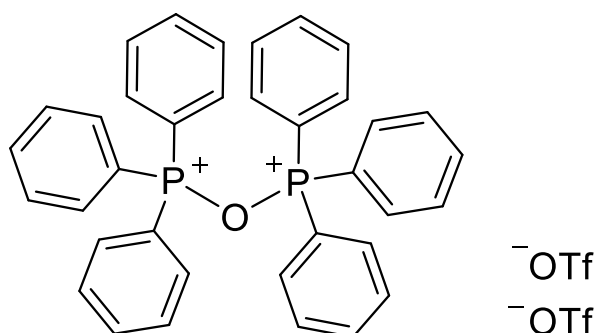


Figure 11: Active Form of the Hendrickson's "POP" reagent. It is produced *in situ* by adding Trifluoromethanesulfonic acid anhydride to a solution of triphenylphosphine oxide.

The synthetic methods described by You et al. in 2003, based on the Hendrickson "POP" reagent<sup>[121-122, 124-125]</sup> (Figure 11) have been used first for the thiazole, and have then successfully been used for the direct synthesis of oxazolines and methyl-oxazolines from the amino acids serine and threonine, respectively. The direct synthesis of oxazoline heterocycles from natural amino acids appears to be the first one reported using Hendrickson's reagent, as for oxygen-containing azoles, usually oxazoles were synthesized after first oxidizing the alcohol to a carbonyl<sup>[121]</sup>, and oxazolines were synthesized using a different, heterocyclic POP

<sup>†</sup> The contents of this chapter have in parts been published in [6] P. Baur, P. Comba, G. Velmurugan, Chem. Eur. J. 2022, 28, e202200249.



analogue<sup>[125]</sup>. An overview comparing the different heterocyclization approaches attempted in this work is given in Table 1.

Table 1: Attempted approaches for the heterocyclization step

Target Heterocycle	Approach	Result
Oxazoline	Burgess-Reagent linear octapeptide	Incomplete heterocyclization, only 15% desired product
Oxazoline	Burgess-Reagent building block	~50% yield after 8h reflux, harsh conditions (>80°C)
Oxazoline	Hendrickson's Reagent Linear octapeptide (SPPS)	Incomplete heterocyclization after 5h, but ~50% desired product
Oxazoline	Hendrickson's Reagent Building block	Up to 85% yield (PG: OtBu) with PG, lower yields without PG (50%)
Thiazole	Lawesson's-Reagent Building block	Good yields (80%), but can't produce the natural non-methylated thiazoles
Thiazole	Hantzsch Reaction Building block	Very long reaction times, dangerous substances, mediocre yields (40%)
Thiazoline	Hendrickson's reagent Linear octapeptide (SPPS)	Incomplete heterocyclization after 5h, but ~50% desired product
Thiazole	Hendrickson's reagent, oxidation with MnO <sub>2</sub> Building block	Good yields (75% over 2 steps), compatible with natural amino acids

The Hendrickson's reagent has proven to be the best choice for the synthesis of both azol(in)e building blocks. Therefore, it was decided to attempt a convergent synthetic strategy, which involves the parallel synthesis of the different building blocks for patellamides with one side chain and one heterocycle each, allowing to perform the possible yield-decreasing and challenging heterocyclization earlier in the synthesis. Additionally, the building block approach can very easily be extended, using the same synthetic approach with different

amino acids to allow an adaptable synthesis, which should allow the synthesis of any desired patellamide derivative.

After identifying the most suitable heterocyclization strategy, for the synthesis of the patellamides a contemporary peptide synthesis strategy involving Fmoc-protecting groups was employed, as it is widely used and can easily be adapted to allow synthesis in the solid phase. For the acid protecting group different possibilities (methyl, allyl, benzyl) were considered, and it was decided to use the allyl group, as it is easy to selectively protect and deprotect the molecules under mild conditions. For the hydrophilic side chains, different protecting groups (*tert*-butyl, trityl, benzyl), as well as approaches with no protecting groups, were attempted, showing that depending on the amino acid, either trityl (for cysteine and serine) or *tert*-butyl (for *allo*-threonine) are best suited. For the peptide synthesis steps, HBTU/HOBt/DIEA was used as coupling reagent, as the mixture of HBTU and HOBt is known to minimize the racemization that tends to occur when carbodiimides are used in peptide coupling reactions<sup>[126]</sup>. The heterocyclic building blocks then are subsequently deprotected, coupled, and cyclodimerized using FDPP (scheme in Figure 12).

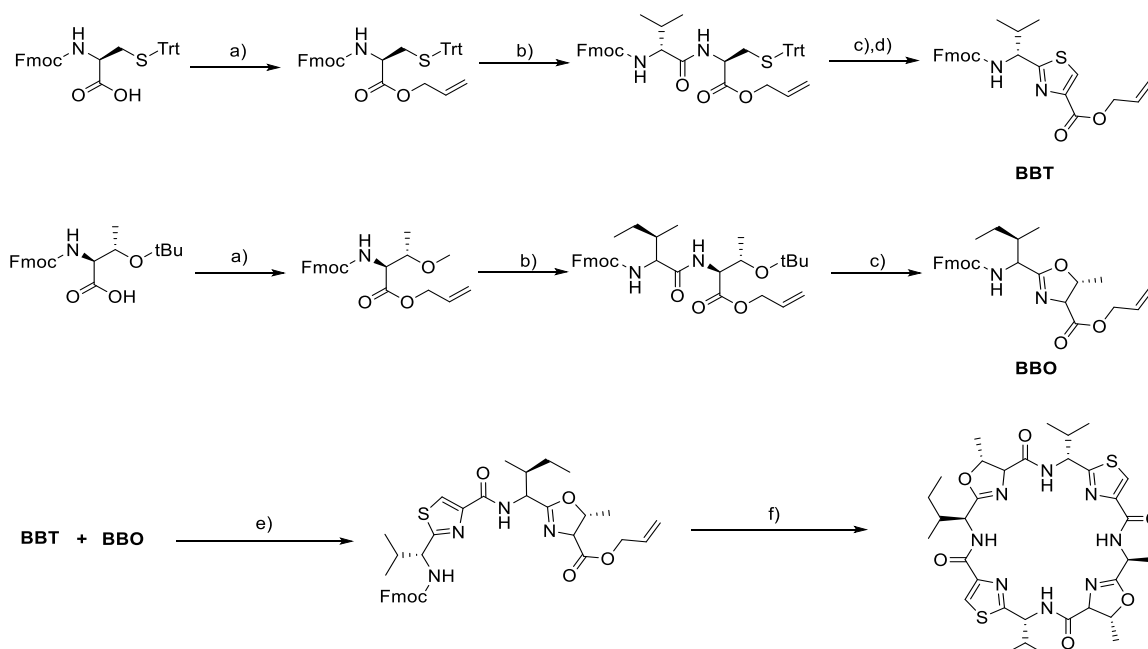
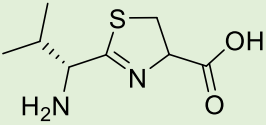
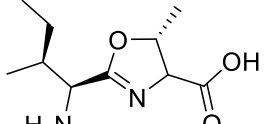
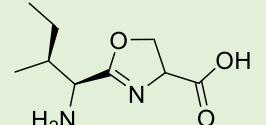
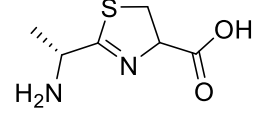
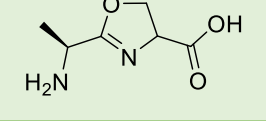
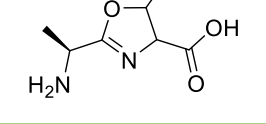
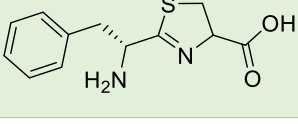
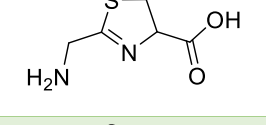
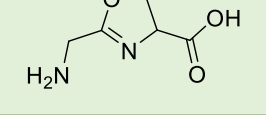


Figure 12: Reaction Scheme of the patellamide synthesis, using ascidiacyclamide as example. The general steps for the building block synthesis are a) allyl protection (12h, rt, DMF) using allyl alcohol and HBTU/HOBt/DIEA, b) Fmoc-deprotection using piperidine 20% in DMF, followed by peptide coupling with Fmoc-*D*-valine/*L*-Isoleucine using HBTU/HOBt/DIEA, c) heterocyclization using Ph<sub>3</sub>PO and Tf<sub>2</sub>O (4h, <-20 °C, DCM), d) in case of thiazoles followed by oxidation with activated MnO<sub>2</sub>-nanoparticles (48h, rt, DCM). Successively the building blocks are coupled e) by deprotecting and coupling the building blocks using HBTU/HOBt/DIEA (24h, rt, DMF), followed by f) macrocyclization using FDPP (48h, rt, MeCN)<sup>[6]</sup>.

The Hendrickson's reagent POP has been used to heterocyclize the cysteine-containing dipeptides to thiazolines followed by an oxidation step using activated MnO<sub>2</sub> nanoparticles, as described by Young and Kelly<sup>[121]</sup>. An overview of different building blocks produced using this method is given in Table 2.

Table 2: Synthesized heterocyclic building blocks. If the stereochemistry is not specified, the naturally available *L*-amino acid was used. All thiazolines shown were subsequently oxidized to the respective thiazoles. For each reaction, the highest yield obtained is given.

Peptide	Desired Product	Yield	Notes
<b>D-Val-Cys</b>		80%	Confirmed by NMR, ESI-MS
<b>Ile-<i>allo</i>-L-Thr</b>		88%	Confirmed by NMR, ESI-MS
<b>Ile-Ser</b>		77%	Confirmed by NMR, ESI-MS
<b>Ala-Cys</b>		91%	Confirmed by NMR, ESI-MS
<b>Ala-Ser</b>		85%	Confirmed by NMR, ESI-MS
<b>Ala-Thr</b>		89%	Confirmed by NMR, ESI-MS
<b>Phe-Cys</b>		75%	Confirmed by NMR, ESI-MS
<b>Gly-Cys</b>		-	Unsuccessful
<b>Gly-Ser</b>		-	Unsuccessful

Generally, the method was used successfully to heterocyclize various amino acids, one exception was glycine (Gly), as with both cysteine (Gly-Cys) or serine (Gly-Ser) the heterocyclization of the dipeptides has not led to the desired products. It is noteworthy that for some heterocyclizations the choice of protecting group can impact the yield significantly.

### 3.3 Solid phase synthesis

In the last decades, solid state peptide synthesis (SPPS) has become the predominant technique in the synthesis of peptides. Apart from allowing a much faster synthesis, especially of longer peptides in hours rather than days or weeks, the yield of the desired peptide is also significantly higher than possible in the liquid phase. The Hendrickson's reagent has proven versatile and efficient in the liquid phase. However, in liquid phase, the synthesis requires multiple long reaction steps and multiple time-consuming and yield-decreasing purification steps. As the reaction conditions for the Hendrickson's reagent are in general compatible with solid-phase strategies, therefore we attempted to transfer the heterocyclization approach to the solid phase. Generally, it would be preferred to have as many steps as possible being transferred to the solid phase. Thus, different general strategies have been devised and tested:

1. Synthesis of the linear octapeptide on an acid-labile resin (chlorotriyl **ClTrt**), followed by a one-step heterocyclization of all heterocycles, cleavage off the resin, and subsequent oxidation and macrocyclization in solution.
2. Synthesis of the linear octapeptide on acid-stabile resin (Wang), followed by a heterocyclization of all heterocycles and thiazoline oxidation on resin with subsequent cleavage and macrocyclization in solution.
3. Synthesis of the linear octapeptide on an acid-stabile resin (Wang) using the pre-synthesized thiazole building block, followed by the heterocyclization of oxazolines on resin with subsequent cleavage and macrocyclization in solution.
4. Synthesis of the linear octapeptide on an acid-labile resin (**ClTrt**) using the premade thiazole building block, followed by a one-step heterocyclization of oxazolines and cleavage off the resin with subsequent macrocyclization in solution.

The first strategy (1) did not show any success, and this was expected, as with the many reactive sites, the occurrence of many unintended side-reactions and racemization is quite likely. However, it was still attempted as it would be by far the most time-efficient approach. For strategies 2. and 3. the success of the steps on-resin could be confirmed by Maldi-MS (Appendix A-S1), although the heterocyclization has led to a mixture of only partly and fully heterocyclized peptides. In the case of strategy 4, the heterocyclization on-resin occurs, but only one of the four heterocycles was formed, possibly because the cleavage step affected the reaction.

Another possible approach that will be attempted in the future is the synthesis of the linear octapeptide on an acid stable resin (Wang), linked to the resin perpendicular by replacing one of the hydrophobic side chains such as Val/Ile with lysine, followed by on-resin heterocyclization, oxidation, and macrocyclization, followed by cleavage of the final Lys-containing patellamide analogue<sup>[127]</sup>.

## 4. Characterization of copper(II)-patellamide complexes *in vivo*

### 4.1 *In vivo* detection of copper(II)-patellamide complexes using X-ray absorption spectroscopy

#### 4.1.1 Method

XAS (X-ray Absorption Spectroscopy) is a well-established and increasingly important technique offered at most synchrotron sources in the world. In an XAS measurement, the sample is subjected to an intense X-ray beam, the energy of which is varied while the absorption by the sample is determined, considering the ratio of the intensity of the X-ray beam transmitting the sample and the intensity of the incoming beam. Once the energy of the incoming X-rays exceeds the binding energy of a core electron of the metal of interest, the radiation is absorbed, forming a photoelectron core-hole pair. This newly available absorption channel significantly increases the absorption of the X-ray beam by the sample at this energy value, causing a jump in the absorption in the spectrum which is referred to as absorption edge. The energy range of the incoming beam is therefore chosen close to the specific absorption edge of an element of interest present in the sample. As the energy required to promote an electron from a core level to a higher energy level or into the continuum is different for every element, the measurements are element specific. Dependent on the energy of the incoming photons, the electron promoted can originate from different energy levels with varying quantum numbers. The edges are named according to the principal quantum number of the excited electron: K-edge for  $n=1$ , L-edge for  $n=2$ , and M-edge for  $n=3$ . As samples with a low concentration of the metal of interest, such as many biological samples would only cause a small change in absorption, the emission of by the sample is measured instead. This fluorescence is caused by one of the electrons in higher energy levels filling the hole left behind by the excited electron.

The X-ray absorption spectrum can be divided into three regions of interest, the pre-edge, the edge, and the continuum. In a XANES (X-ray Absorption Near Edge Spectroscopy) analysis, the pre-edge and edge are the main regions of interest, while the continuum is interpreted for an EXAFS (Extended X-ray Absorption Fine Structure) analysis. The applicability of XAS techniques on metal complex samples and specifically copper active sites have been discussed and proven in many studies and papers<sup>[128-129]</sup>.

Close to the energy of the absorption edge as well as on the edge several features can be found that correspond to transitions of the excited core electron to higher levels. Thoroughly analyzing the edge features allows to obtain information such as the oxidation state and the local coordination sphere of the absorbing atom. The pre-edge generally allows the estimation of the ligand-field, the spin-state, and the site symmetry of the sample, while the edge (also: rising-edge) can allow the determination of the geometric structure, the metal-ligand overlap, the ligand arrangement, and the charge on the metal center. The identification and assignment of certain pre-edge and edge features of copper K-edge spectra have proven to be a reliable way to identify the oxidation state of copper<sup>[130]</sup>.

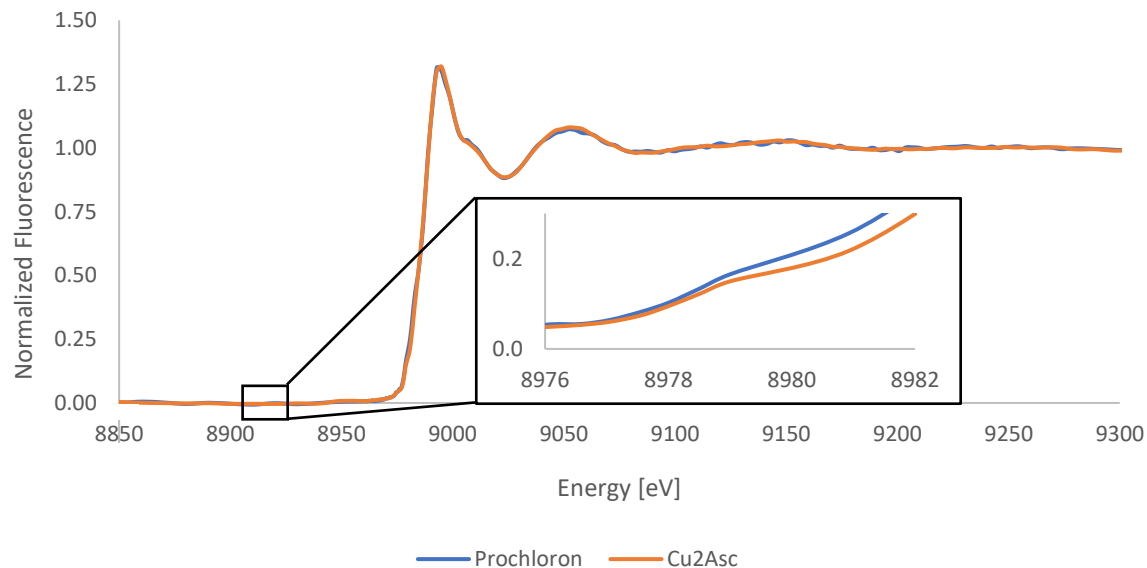


Figure 13: Copper K-Edge X-ray absorption spectrum of the biological sample of *Prochloron didemni* and a synthetically produced Cu<sup>II</sup>-ascidiacyclamide-complex. In the magnification, the pre-edge 1s→3d transition, characteristic for Cu<sup>II</sup> is visible. A characteristic and intense 1s→4p transition in the rising-edge region, which would indicate the presence of Cu<sup>I</sup> is not visible. The XAS was measured during the beamtime in August 2022 at the SuperXAS beamline of the PSI in Switzerland using a 5-channel silicon drift detector (SDD).

At energies higher than the edge energy, in the XAS region, corresponding to a photoelectron being emitted from the absorbing atom, the periodic oscillations can be interpreted in course

of an EXAFS analysis. The EXAFS can be calculated as shown in Equation 1.1 and is usually shown as a graph of the dimensionless positive or negative value of  $\chi$  as a function of the wavenumber  $k$ , which due to its relationship with the absorption energy Equation 1.2 increases with the distance to the absorber atom. When evaluating the EXAFS of a sample, the starting point for a fit generally is a known structure or initial guess, containing information about surrounding atoms and their distances – for which the EXAFS is calculated. The parameters of this assumed structure are then altered until the simulated EXAFS agrees well with the measured EXAFS. In many cases, this requires knowledge about the atom arrangement in the structure of interest and ideally reference samples to compare the measurements to.

$$\chi(k) = \sum_j \frac{N_j S_0^2}{k R_j^2} F_j(k) e^{-\frac{2R_j}{\lambda_j(k)}} e^{-2k^2 \sigma_j^2} \sin[2kR_j + \Phi_j(k)] \quad (1.1)$$

$$k = \frac{2\pi}{\lambda} = \sqrt{\frac{2m_e(E-E_0)}{\hbar^2}} \quad (1.2)$$

Equation 1: Mathematical function used to model EXAFS data with  $k$  being the photoelectron wavenumber  $E$  the X-ray energy,  $E_0$  the absorption edge energy,  $m_e$  the mass of the electron,  $F_j$  the photoelectron backscattering amplitude,  $N_j$  the coordination number,  $R_j$  the interatomic distance,  $\sigma_j^2$  the Debye-Waller factors (DWF), the mean-square disorder in shell  $j$ ,  $\Phi_j^2$  the corresponding back-scattering phase,  $\lambda_j(k)$  the photoelectron inelastic mean free path, and  $S_0^2$  the amplitude reduction factor\*.

#### 4.1.2 Introduction

So far, the most interesting properties of the patellamides, such as bioactivities and catalytical efficiency, have only been observed for copper(II) complexes. To understand, whether these observed properties are of biological relevance, it is important to know whether the patellamide copper(II) complexes can be found *in vivo*. Recent studies have shown that when attaching a fluorescent copper(II)-probe to a patellamide analogue, copper(II) binds to them *in vivo* – suggesting that the *in vivo* conditions allow for the formation of these complexes<sup>[25]</sup>. Furthermore, it was reported that the concentration of patellamides makes up to a few percent of the organism's dry mass<sup>[17]</sup>. Considering the recently updated concentrations of less than 1 ppm copper in the organism<sup>[131]</sup>, it appears that the concentration of patellamides

---

\* Equation and definition taken from the Online Dictionary of Crystallography (20.3.2022).



is not on a similar level to the copper concentration but at least 100 times higher. Given the concentration of the patellamides and their affinity for copper(ii)<sup>[21, 83, 132]</sup> it is therefore expected, that the majority of excess copper not bound to enzymes is complexed by patellamides. Most common laboratory techniques do not allow to unequivocally test this in the very heterogenous biological samples, as these methods are impaired by other metal ions, or it would otherwise require very extensive sample preparation with uncertainty that the measurement might not be representative for the biological conditions. Optical and vibrational spectroscopies (UV-VIS, CD, IR) cannot selectively detect copper(II)-patellamide compounds due to the weak and not well-enough resolved spectra. On the other hand, EPR spectroscopy is a technique that can be used to selectively investigate copper complexes. However, this technique presents a challenge when applied to photosynthetic organisms like *P.d.* due to the naturally abundant manganese in these organisms, which creates a strong and well-resolved signal of Mn<sup>II</sup> that overlaps with the signal from copper.

X-ray absorption spectroscopy has been established as an important technique in bioinorganic chemistry, allowing specific measurement of single elements – and obtaining a wide range of information from both the XANES region and the EXAFS region<sup>[133-136]</sup>. Recently, the method has been used successfully to detect specific metal complexes in the biological sample *in vivo*<sup>[137]</sup>. Resultingly, it was attempted to detect the copper complex of patellamides *in vivo/ex vivo* by collecting fresh biological samples, measuring an XAS, and comparing it with the spectra of synthetically produced patellamides and fitting them using the literature-reported crystal structure<sup>[5]</sup>.

A short description of the performed measurements is given here, see experimental section 7.3 for a more detailed description of the sample collection, preparation, measurement parameters, and data treatment.

#### 4.1.3 Measurements

Due to the travel restrictions in 2020-2021, a field collection of fresh samples for the XAS studies was not possible, such that frozen samples of *Prochloron didemni*, collected in 2016 by our collaborator Lars Behrendt from the University of Uppsala, have been used for preliminary measurements. These samples were used for initial synchrotron measurements for which a trial beamtime was allocated to us at beamline P65 of the Petra III synchrotron at

the DESY in Hamburg. In this beamtime, the frozen centrifugates of *P.d.* were diluted with glycerol to prevent the formation of ice crystals measured in a self-designed holder for liquid samples which is fixed to a sample rod within a helium-cooled sample chamber cooled to 4 °K. Additionally, synthetically produced ascidiacyclamide and patellamide analogues were complexed at the beamline and measured as well. While the measurements of the synthetically produced patellamides gave a good signal, the signals from the biological samples were too weak for a thorough analysis, as the germanium multichannel fluorescence detector that would have allowed more meaningful measurements of low concentration, was not available during the beamtime, and a much less sensitive PIPS diode detector had to be used. This was not sensitive enough to obtain interpretable spectra of the copper K-edge in concentrations as low as in these biological samples.

Once a field trip for sample collections was planned for 2022, a new series of test beamtimes was performed at the SuperXAS beamline at the SLS synchrotron of the PSI in Villigen, Switzerland. For this series of measurements, a 5-channel silicon drift fluorescence detector (SDD) was used, and the samples were filled in quartz glass capillaries or Kapton tubes and into different sample-holders for liquid samples cooled by a liquid-nitrogen cryojet, cooling the sample down to 100° K. The modified experimental setup significantly increased the signal-to-noise ratio. However, the signal was still significantly weaker than expected from literature-reported copper(II) concentrations in the ppm-range<sup>[20, 74]</sup>.

After the field sample collection, a third series of measurements was performed at the PSI with the same setup, using freshly collected samples of *L.p.* and *P.d.* from Heron Island in Australia. For this series of measurements, four days of beamtime were received. While the optimum setup found during the test measurements was used, but as the new measurements of the copper(II) concentration in the biological samples have shown<sup>[131]</sup> that the total copper content is approximately 100-1000 times lower than initially expected, the biological samples were freeze-dried in a lyophilizer for the measurement them to optimize the copper concentration.

#### 4.1.4 Results

In all synchrotron experiments, the copper(II) complexes of patellamides could be measured successfully. While in the biological samples initially the signal-to-noise ratio was too low for a thorough analysis of the data, in the third series of measurements the combination of a large number of measurements (20x20 minutes), a more sensitive detector, the increase in copper(II) concentration by freeze-drying and the measurement within Kapton tubes instead of quartz capillaries has allowed to obtain datasets with a sufficiently clean signal-to-noise ratio.

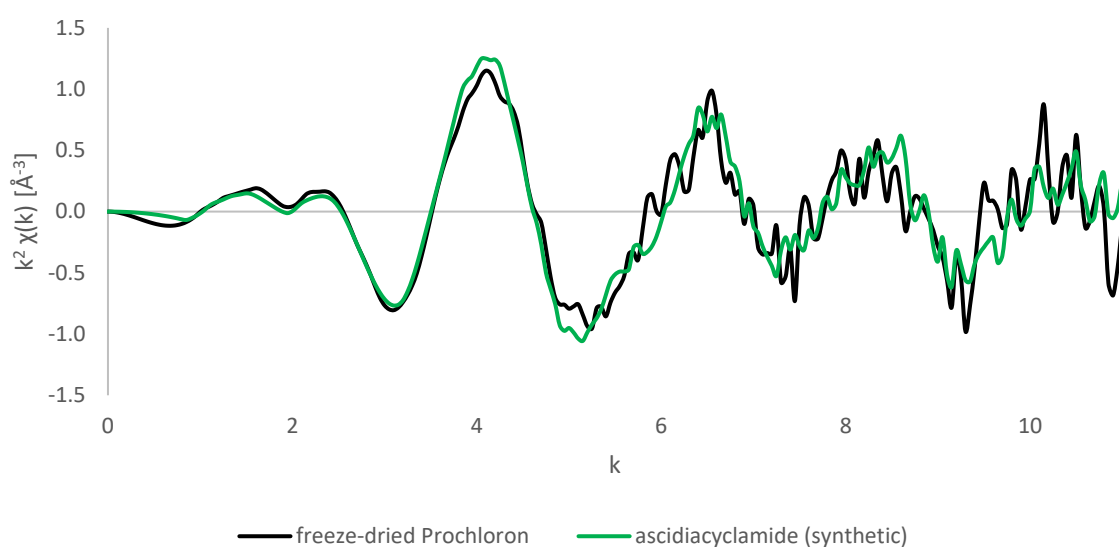


Figure 14: Overlay of the EXAFS-Signal from freeze-dried Prochloron didemni (collected during the field experiments in 2022), with the EXAFS of synthetically produced  $\text{Cu}^{\text{II}}$ -ascidiacyclamide (in DMSO:H<sub>2</sub>O, 4 mM/L, with  $\text{Bu}_4\text{N}^+\text{MeOH}^-$  with a ratio Asc/Cu/base of 1/2/5) complexes. Measured at the SuperXAS beamline of the PSI in Switzerland using an SDD. The biological sample data was merged over 20 scans of 20 minutes at different spots, the synthetic sample data was merged over 6 scans of 20 minutes at different spots.

In this series of measurements like in the previous ones, the copper complexes of synthetically produced patellamides were measured as reference material to the biological samples and give rise to a very similar EXAFS (Figure 14). While especially the distinctive features in the low wavenumber region appear similar, the differences in the higher wavenumber region can be explained by the fact, that in the biological samples a mixture of different patellamides (at least patellamides A, B, C, D, ascidiacyclamide). While these patellamides share very similar first-shell paths (the first coordination sphere around the ion) they differ significantly at longer distances. In the first shell, the copper(II) ions are coordinated to two azol(in)e nitrogens as well as a deprotonated amide in all patellamides and are coordinated to water and in most cases carbonate, resulting in a nearly identical environment until about 2.5 Å. At

larger distances from the copper(II) center, the differences between the patellamides resulting from the different side chains impact the spectrum more strongly, by a different number of atoms or by changes in distances and angles in the backbone.

The synthetic efforts were primarily focused on ascidiacyclamide due to the crystal structure of its dicopper(II) complex being the only one measured among the patellamide derivatives, to match the biological samples (see Experimental Section for a detailed description). By using the feff10 software package<sup>[138]</sup> on the crystal structure (Figure 15) to obtain the expected scattering and interference paths around the absorbing copper with the most important parameters such as the distance, the atomic scattering amplitudes, and the phase shifts, the most important paths (estimated based on their feff-ranking) of the crystal structure can be fitted to the measured spectrum as shown in Table 3.

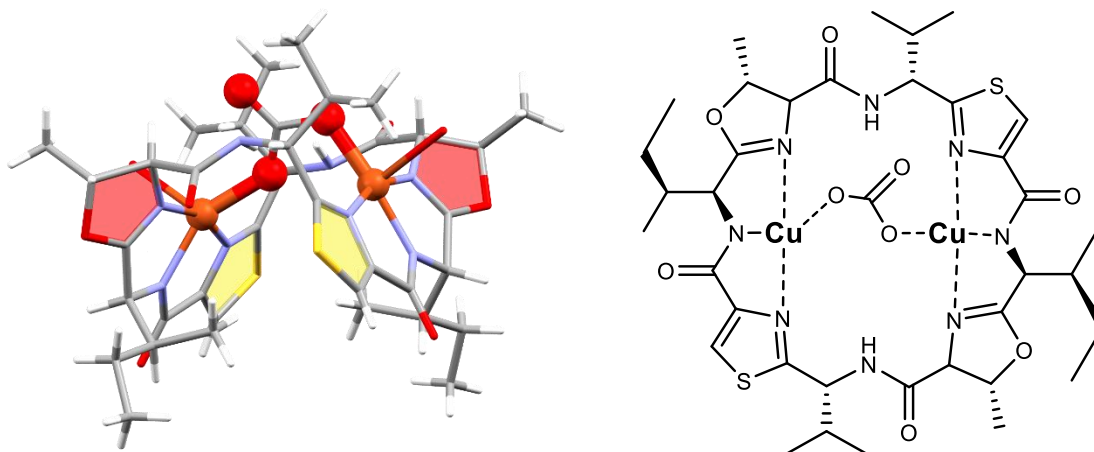


Figure 15: : Structure of the carbonato-bridged dinuclear copper(II) complex of ascidiacyclamide. The crystal structure of the complex was published by van den Brenk et al. in 1994<sup>[5]</sup>.

In all possible fits, the most significant single-scattering paths expected based on the crystal structure showed very similar values of distance and Debye-Waller factors (DWF,  $\sigma^2$ ). In the patellamide structure<sup>[5]</sup>, the first shell contains at a distance of 1.94 Å the three coordinated nitrogen atoms from the patellamide and the 1-2 oxygen atoms from the bridging carbonate as well as the oxygen atoms of the one or two coordinated water molecules (as copper(II) usually is found 6-coordinate). While these parameters fit the crystal structure of the carbonato-bridged patellamide very well, it remains uncertain, whether the remaining atom paths correspond to carbonate or are just three coordinated water molecules.

Table 3: EXAFS fitting parameters of the fit of the freeze-dried biological sample. All shown paths correspond to single scattering paths in the crystal structure of the carbonato-bridged dinuclear copper(II) complex of ascidiacyclamide<sup>[5]</sup>. As elements with similar atomic number cannot be distinguished on these short distances, the respective paths were united. For the first path, coordination numbers of 5 or 5.5 lead to similar fitting parameters. However, since in the crystal structure one copper is expected to be 6- coordinate, while the other is 5-coordinate, 5.5 was used for the fit.

	Path(s)	Number of paths	Distance [Å]	Debye-Waller factors ( $\sigma^2$ )	$E_0$	F-Factor
Without Cu-Cu path	Cu-N/O	5.5	1.94	824	<b>-8.34</b>	<b>0.49</b>
	Cu-C	4	2.87	686		
	Cu-C/O	5	3.18	357		
	Cu-C/N	6	4.23	916		
With Cu-Cu path	Cu-N/O	5.5	1.94	828	<b>-8.38</b>	<b>0.49</b>
	Cu-C	4	2.87	588		
	Cu-C/O	5	3.17	315		
	Cu-C/N	6	4.17	111		
	Cu-Cu	1	4.34	72		

In the next shell, the 4 closest carbon atoms from the backbone can be fitted at a distance of about 2.9 Å. This path can be fit with a fifth carbon atom, corresponding to the carbonate C atom. However, this leads to DWF of over 1000, which can either mean that too many atoms are fitted into the path or that at least one of them has a higher thermal position uncertainty. This would apply to the carbon in a bridging carbonate being significantly less fixed than the atoms in the rigid patellamide backbone. In the next two paths, the remaining backbone, heterocyclic and side chain carbon atoms, and oxygens from the peptide carbonyl groups and the oxazoline ring can be fitted in average distances of 3.18 Å and 4.20 Å. Comparing the fitted EXAFS with the experimental result (Figure 16) shows that the fit quite fully and accurately represents the measured spectrum and the Fourier-Transform (Appendix Figure A-XA4) shows that, while most of the main features are well represented, there is missing intensity in the fit at distances around 4.4 Å. At this distance, the Cu-Cu path would be expected and

including this in the fit fills the gap, but the calculated path shows very low DWF and has a higher intensity than the experimental data in this range.

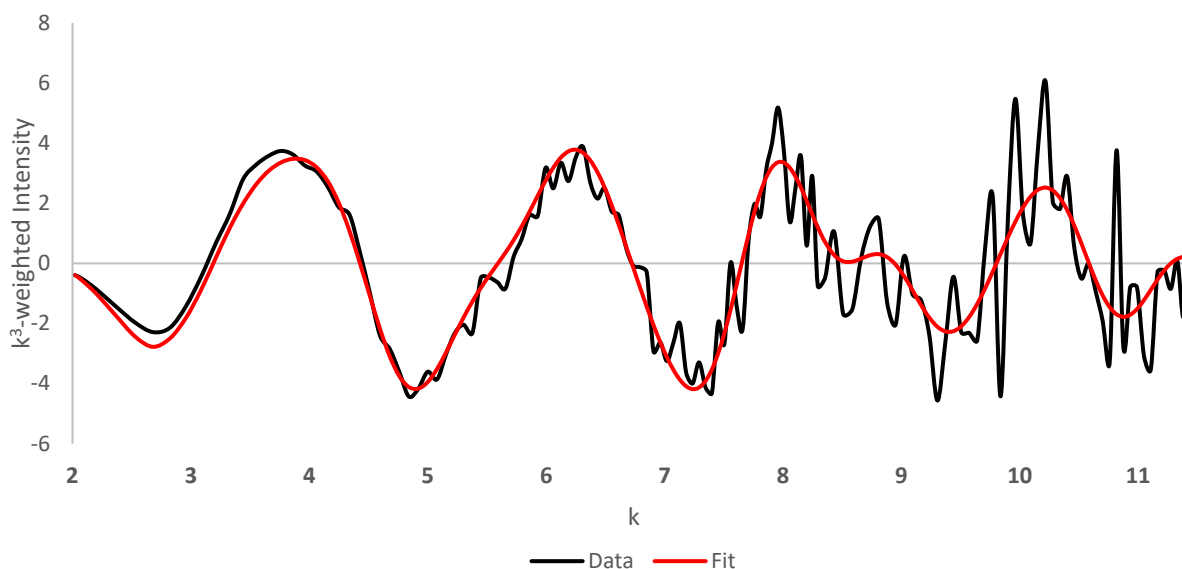


Figure 16: Overlay of the  $k$ -weighted EXAFS of the measured biological sample (black) and the fitted EXAFS (red) in the ( $k$  range of  $k = 2-11.5$ ). Measured at the SuperXAS beamline of the PSI in Switzerland using an SDD. The biological sample data was merged over 20 scans of 20 minutes at different spots.

Generally, while especially the closer paths (up to  $4.2 \text{ \AA}$ ) could be fitted very well, the longer distances impact the high- $k$  region of the EXAFS. As in an EXAFS the X-ray absorption data after the edge is multiplied by  $k^3$ , the signal-to-noise ratio becomes significantly worse at high values of  $k$ , making it difficult to reliably fit these longer paths. One factor additionally impacting the noise intensity, was the lack of a helium-cryostat, allowing to measure at minimum measurement temperatures of  $100^\circ \text{ K}$  at the SuperXAS beamline. While this temperature is sufficient to minimize the photodamaging of the samples, lower temperatures would be required to obtain a less noisy spectrum in the high- $k$  region. Additionally, it must be considered that the sample for the crystal structure used for the simulation and the synthetic XAS sample only contained the single patellamide derivative ascidiacyclamide, while the biological sample used for the XAS experiments (see Figure 14 and Figure 16) contains a mixture of several different patellamides (at least A, C/F, B/D and ascidiacyclamide). While in the first shells, their EXAFS should be identical as the copper(II) ion is at the same position in the backbone with the same surrounding atoms in the first  $3.5 \text{ \AA}$ , the different side chains of the derivatives lead to different paths at  $3.8 \text{ \AA}$  and above (as at this distance the side chain carbon atoms impact the spectrum).

Since copper(II) is present in concentrations in the nanomolar region in the cloaca<sup>[131]</sup> but patellamides supposedly strongly exceed that concentration<sup>[17]</sup> and show relatively large complex stabilities ( $\log K \sim 6-8$ )<sup>[21]</sup>, the majority of copper(II) in the cloaca is coordinated to patellamides. The copper K-edge X-ray absorption data based on measurements of synthetic and biological samples at the PSI SLS synchrotron strongly suggest that this is indeed the case (Figure 14), as the XAS data from the freeze-dried biological samples shares great similarity with synthetically produced patellamides and can be fitted using the crystal structure of a dicopper(II)-ascidiacyclamide complex. A comparison of the Fourier-transform of spectra from samples collected during the day and at night, when the pH inside the cloacal cavity varies between 9-10 (day) and 6-7 (night) respectively, shows that at night the spectra have a feature predominantly in the low-k region (Appendix Figure A-XA3). This is expected, as at the less basic pH values at night the protonation equilibrium of the patellamides is shifted to the protonated form not available for complexation.

While one of the reasons to use XAS rather than the more easily available EPR spectroscopy to characterize the dicopper(II) complexes *in vivo* is that the copper(II) concentration is not only too low to give a well-resolved EPR signal, it also is overlaid by the significantly more intense Mn<sup>II</sup> signal. However, extracting the homogenate of prochloron from the cloaca with DCM may extract both the patellamides and their copper(II) complexes<sup>[20]</sup>. After concentrating this extract, a copper(II) signal could be observed in the EPR spectrum, possessing a half-field signal as well (Appendix Figure A-XA5), and this indicates the presence of the dinuclear copper(II) complexes. While this signal is not disturbed by a Mn<sup>II</sup> signal, it is not well enough resolved for further discussion. In future, a larger amount of the organic phase needs to be concentrated, to allow the measurement of a sufficiently resolved copper(II) EPR spectrum.

Additional confirmation of the presence of the dicopper(II) patellamide complexes *in vivo* was attempted by mass spectrometry. However, the low concentration of the complexes, the harshness of most commonly available ionization techniques, and the acidity of the commonly used columns made this method unsuitable for a direct and straightforward detection. In addition to the analytical techniques performed here, the experiments by Eisenschmidt et al.<sup>[25]</sup> further confirm the ability of patellamide analogues to bind copper(II) *in vivo*.

#### 4.2 Determination of the copper concentration in *Lissoclinum patella*<sup>†</sup>

One reason for the focus of researchers on the chemistry of the copper(II)-patellamide complexes rather than metal-free cyclic peptides were the suggestions in previous literature, that copper is strongly concentrated by *L.p./P.d.* to about  $10^4$  times higher concentrations compared to the surrounding seawater<sup>[21, 74, 80]</sup>. This would result in concentrations of copper on a level similar to the concentration of patellamides<sup>[17]</sup>. The main reference in support of this number is an *Inorg. Chem.* paper published by van den Brenk et al. in 1994, which has since been cited multiple times<sup>[21, 74, 80, 139-140]</sup>. In this paper, the copper concentration in *L.p.* is given as 1.56 ppm (dry weight), compared with surrounding seawater concentrations at high and low tide of 0.08 ppb and 0.027 ppm, respectively. However, these numbers are reported as ‘unpublished results’ without any specification on the experimental procedure and have never been published since<sup>[74]</sup>. With this reported accumulation of copper, the resulting concentration in the organism would be expected to be in a micromolar/ppm range, which would give rise to well-measurable and well-resolved copper(II) EPR spectra. When attempting to measure the EPR spectra of biological samples collected on Heron Island, Australia, at the Center of Advanced Imaging of the University of Queensland, Brisbane, it was observed that the EPR signal was barely detectable. Comparing the intensity of the signal to pure copper(II) salts suggested, that the actual concentration of copper(II) is much lower than previously assumed.

Therefore, for different biological samples collected during the Heron Island field trip in 2022 (and an old reference sample collected by colleagues on Heron Island in 2011) the concentration of copper and other metal ions (Ca, Mn, Fe, Cu, Zn) more accurately by ICP-OES (and for Cu by ICP-MS). Samples from three different *L.p.* colonies of the 2022 specimens (1–3) were used, as well as samples of two colonies from the 2011 samples (4, 5). There are five types of samples from colonies 1 and 2, i.e. finely minced and rough cut whole colony (a, b), prochloron homogenate (c), and the aqueous contents of the entire colony (filtered d, or unfiltered e). The third specimen of the 2022 field trip was divided into two parts, in one part additional copper was added by syringe ( $3 \times 2$  mL 14.2 mM  $\text{Cu}(\text{SO}_4) \cdot 6\text{H}_2\text{O}$  into the cloacal cavities) of the living colony (see Experimental Section 7.1; the second part was only injected

---

<sup>†</sup> Main parts of this chapter have been published in [131] P. Baur, P. Comba, L. R. Gahan, C. Scholz, *Aust. J. Chem.* **2022**. The data and figures presented, and parts of the text were used as published.



with water, Experimental Section 7.1). From each of these sub-colonies, two types of samples were used, i.e. prochloron homogenate (3.1b, 3.2b), and aqueous phase (3.1c, 3.2c). From specimens 4 and 5, the prochloron homogenate was measured (4b, 5b). Each of the samples was freeze-dried and further prepared as described in the Experimental Section 7.1. The results of the ICP-OES measurements, corrected for the loss of water, are shown in Table 4.4.1 (the raw data, reference values, water-loss corrections, and results of the ICP-MS measurements can be found in the Appendix, tables A-Cu1 – A-Cu5).

Table 4: Copper concentrations in mg/kg (ppm); concentration determined in the dry sample, values in this table are corrected for the loss of water upon drying and thus correspond to the actual “wet” concentration, see Appendix Tables A-Cu1 – A-Cu5).

Sample Type	Colony 1	Colony 2	Colony 3		Colony 4
			no copper added	copper added <sup>a</sup>	
<b>Piece of Colony</b>	0.27	0.89			0.31
<b>cyanobacteria (homogenized)</b>	0.12	0.49	0.52	3.64	0.79
<b>water inside cloaca</b>	0.05	0.06 <sup>b</sup>	0.13	0.52	

<sup>a</sup> injection of copper(II) into the colony and preparation of the sample for the measurement 24h after injection (for details see Experimental Section)

<sup>b</sup> after filtration through a syringe filter (Cellulose Acetate, 0.45µm), all other cloaca samples were centrifuged instead

As the copper concentration in different colonies of *L.p.* collected from different locations around Heron Island and at different times shows consistently to be significantly higher within the colony or the cyanobacteria than within the water within the cloacal cavity, which suggests, that most of the copper is found in ascidian cells or cyanobacteria, rather than within the cloacal cavity. This makes some hypotheses concerning possible biological functions of patellamides such as catalytic activities of the dicopper(II) complexes in the cloacal cavity unlikely. The absolute values of the copper concentrations of 0.05-1 ppm within the ascidian remain consistent with previously reported values [21, 74]. It is noteworthy, that the observation that 24 hours after the injection of copper(II), the measure concentration in the colony remains significantly increased, both in the cyanobacteria and in the cloacal liquid.

For the concentration of copper within sea water, several values can be found in the literature (Table 4.3.2). While some of the more recent values are of a more general nature or focused

on different waters that might not be representative of the Great Barrier Reef, especially the copper concentrations reported by Denton et al.<sup>[141]</sup> are of interest, as they have been determined at a similar time as the first reports of the 10<sup>4</sup>-fold copper accumulation<sup>[74]</sup>.

Table 5: Literature data for the concentration of copper in seawater at various locations, reported over the last two decades and determined by a range of different methods. Measurements marked with <sup>a</sup> or <sup>b</sup> were excluded from the calculation of the average, as the values reported are unlikely to be representative of the ocean in general.

Year	Place	range [ppb]	average [ppb]	ref
1979	Global	0.15	0.15	[142]
1983	Northwest Atlantic	0.13-0.19	0.16	[143]
1985	North-East Atlantic, deep open water <sup>a</sup>	0.073-0.094	0.09	[144]
1986	Great Barrier Reef (Heron Island)	0.12-0.24	0.14	[141]
1988	Northeast Pacific, deep open water <sup>a</sup>	0.038	0.038	[145]
1994	Heron Island <sup>b</sup>	0.08-27	13.5	[146]
1998	Global	0.04-10	not rep.	[147]
2001	Global	0.25	0.25	[148]
2011	Red Sea <sup>a</sup>	2.08-5.23	3.244	[149]
2014	Northern Pacific Ocean, (in the Indian Ocean)	0.0378-0.29	0.07	[150]
2018	Global Values	0.5-3.18	0.5	[151]
<b>Average</b>			0.21	

Most of the reported copper concentrations are within a similar range of 0.15-0.4 ppb with an average of ~0.2 ppb. There are no other reports other than the generally cited data from van den Brenk et al.<sup>[74]</sup>, mentioning large tidal variations in the metal concentrations of 1000-fold differences between high and low tide. This, therefore, is difficult to understand and justify – especially since no experimental data is provided for the concentration values. Thus, it is assumed that the reported value is in error. Based on the newly determined values of the copper concentration within parts of the whole colony (~0.3 ppm), the cyanobacteria (0.5 ppm) and the water in the cloaca (0.05 ppm), as well as the average of the literature, reported values of 0.2 ppb (Table 4), the concentration of copper in the water within the cloacal cavity of *L.p.*, in general, is less than 500 times as high as in the surrounding sea water, and in the tissue and cells about 2000-3000 times as high. While these accumulation factors are lower than the previously reported ones, they remain significant and are higher by a factor of ~10 than in fish found around Heron Island<sup>[152]</sup>. However, it appears that compared to other ascidian species, *L.p.* might not accumulate copper particularly strongly<sup>[93]</sup>.

#### 4.3 Interrelation of the concentration of patellamides and the concentration of copper(II)

The detection of copper(II) complexes of patellamides *in vivo/ex vivo* is of importance for the evaluation of possible bioactivities of the patellamides but the presence of dicopper(II)-patellamide complexes alone is not necessarily proof that the function of the macrocycles is correlated to copper-binding. If the patellamides are indeed produced to complex copper, changes in the copper(II) concentration within the ascidian cloaca, should change the concentration of patellamides accordingly. As this has not been evaluated previously, it was decided to test this hypothesis with one of the colonies collected during the 2022 field trip to Heron Island. Copper(II) was injected into several sub-colonies (darker/transparent areas, shown exemplarily in Figure 17) on one half of the animal, and the other half of the animal was injected with sea water only.



Figure 17: One colony of *Lissoclinum patella*. Some of the sub colonies, identifiable by the darker transparent openings in the ascidian mantle are marked by red circles.

24 hours after injection of copper(II), the ascidian was removed from the aquarium, divided into the copper-treated and water-treated halves, and the cloaca water as well as the cyanobacteria were carefully extracted from the cloacal cavities. The water from the cloaca was subsequently filtered and the cyanobacteria were homogenized and centrifuged (details on the sample collection and preparation are given in the Experimental Section). The collected and filtered samples were measured using Sciex TripleTOF 5600 and 6600 mass spectrometers (see Experimental Section).

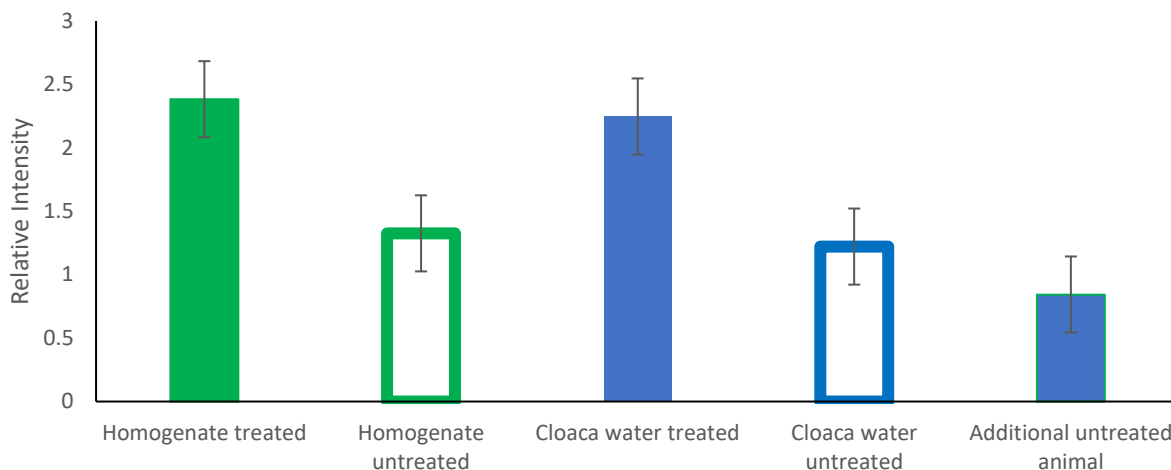


Figure 18: Comparison of the intensity of the peak corresponding to patellamide D/B in the MS chromatogram, measured at the Sciex TripleTOF 5600.

For the measurements, the extracts were first separated by HPLC, with continuous measurement at different retention times, which resulted in a chromatogram consisting of several mass spectra, each with respective fragmentation triple-TOF data. The analysis of all samples showed that, for both the filtered water extracted from the cloaca and the homogenized cyanobacteria, the concentration of patellamides was significantly increased in the sub-colonies that have been injected with copper(II). As the chromatography data is not quantitatively interpretable, the intensity of the peaks of different patellamides was compared to the average intensity of the large signal of the non-separated remains rinsed off the column at the end of the chromatogram, which had a comparable intensity for all samples. For the determination of the relative intensity, patellamide D or B (masses identical) was used, since the signal of this derivative was distinctly interpretable, not overlapping with other derivatives (one exemplary chromatogram is shown in Figure 19, the remaining ones are shown in the supporting information).

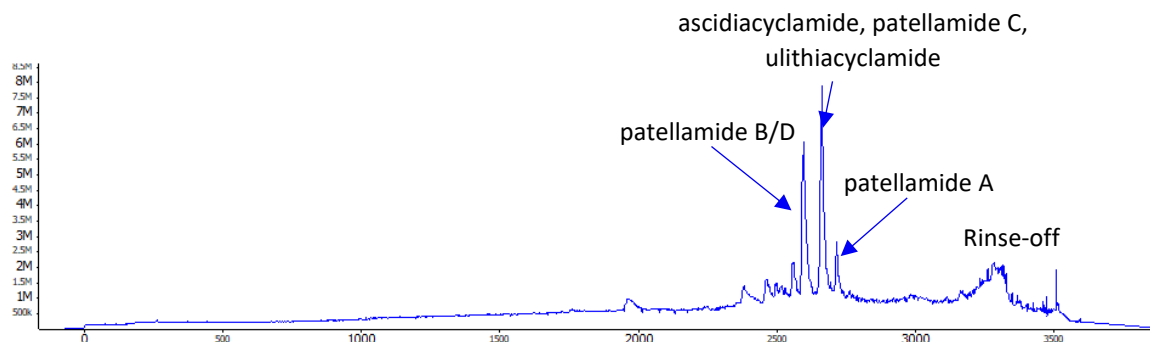


Figure 19: Chromatogram of one sample of homogenized cyanobacteria. The three distinct peaks correspond to 1. patellamide B/D, 2. Ascidiacyclamide, patellamide C and ulithiacyclamide, 3. patellamide A. Measured with a Sciex TripleTOF 6600.

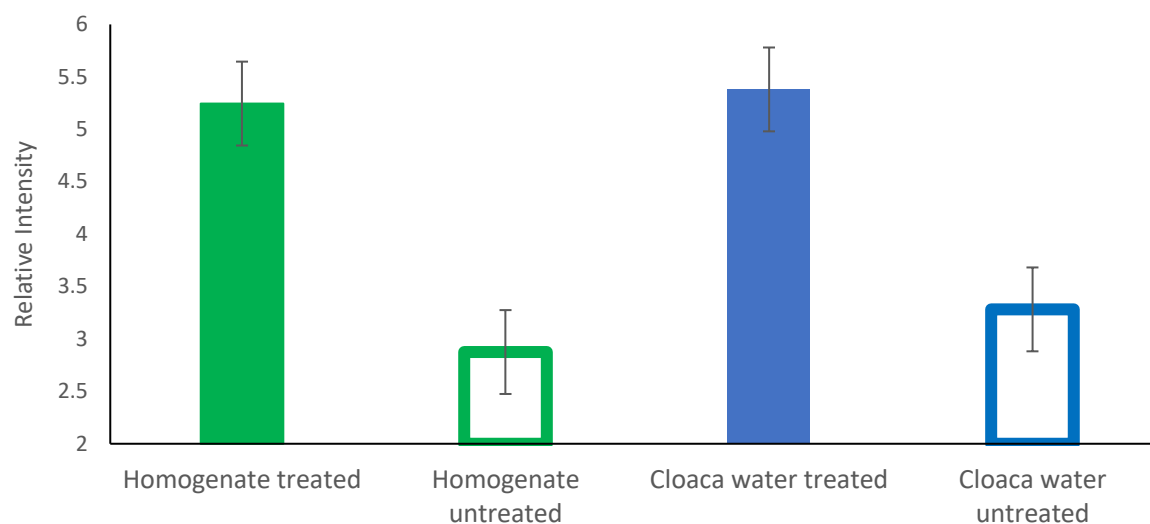


Figure 20: Comparison of the intensity of the peak corresponding to patellamide D/B in the MS chromatogram, for the samples of the homogenate of *P.d.* and the cloaca water with and without addition of copper(II), measured at the Sciex TripleTOF 6600.

As evident (Figure 18, Figure 20), the relative intensity of the signal of patellamide D is significantly more intense in the samples from the sub-colonies that have been injected with additional copper, leading to in some cases a twice as high peak in the chromatogram (the two-dimensional raw data can be found in the Appendix). While the data obtained from the newer Sciex TripleTOF 6600 (Figure 20) generally have better quality and higher intensity, the results of the TripleTOF 5600 (Figure 18) allow to draw the same conclusions, and these are therefore shown as well. As mass spectrometry does not allow quantifying the patellamide content and the different mass spectrometric data can only be compared in a normalized way. Therefore, the total concentration of protein in the water extracted from the cloaca was additionally analyzed by the Bradford assay (Figure 21). The Bradford protein assay is a colorimetric assay and one of the most used methods to measure the concentration of proteins in a solution quickly and accurately<sup>[153-154]</sup>. The assay is based on the absorption shift of the used dye Coomassie brilliant blue as it binds noncovalently to the proteins<sup>†</sup>. Using this method was possible to determine the total protein concentration to verify the increase of the protein concentration following the injection of copper(II) that was seen in the MS-data. While the Bradford-assay only allows drawing conclusions about the total protein content and not about specific ones (i.e., the patellamides), the HPLC-MS (Figure 18, Figure 20) chromatograms only allow to estimate qualitative changes of concentrations for specific

<sup>†</sup>Coomassie brilliant blue (G250) is a triphenylmethane-based dye, widely used in qualitative and quantitative protein detection methods due to its ability to non-covalently bind to protein end groups and side chains.

proteins. The water extracted from the cloacal cavity of the ascidians is mostly fresh sea water that has been passed through the digestive system of the ascidian zooids with some nutrient removal by filtration. Thus, it is not expected that significant amounts of proteins can be found in this solution. However, surprisingly the HPLC-MS data suggests that other than minor amounts of various debris, the cloacal water contained significant amounts of patellamides but hardly any other proteins in noteworthy concentrations.

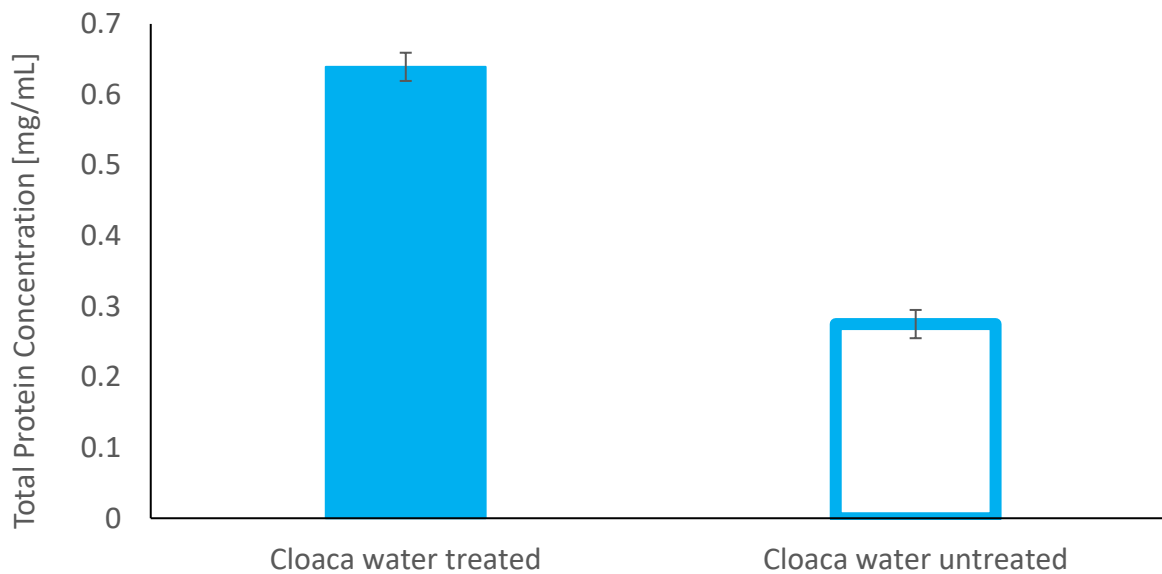


Figure 21: Protein Concentration in the water extracted from the cloacal cavity, compared between the sub colonies with and without injection of additional copper, determined by a Bradford assay. The data given each, the error bar is based on the maximum deviation between the samples.

The fact that patellamides are that abundant in the entire cloaca agrees with the suggestions in the literature, that patellamides are found in all parts of the ascidian, and that they can have concentrations of a few percent of the ascidian dry mass<sup>[17-18]</sup>. The new results presented here suggest for the first time, that an increase in the copper concentration in the animal causes the cyanobacteria to produce more patellamides, acting as additional important evidence for possible copper(II)-based bioactivity. However, further experiments are needed, to reproducibly show that this effect occurs and whether the increase in patellamide concentration is only caused by copper(II) or also by other metal ions. In addition, changes in the expression rate of the patG gene, responsible for the biosynthesis of patellamides, should be measured after the injection of copper(II).

## 5. Biological studies on patellamides and their producers

Many of the experiments reported in chapter 4 focus on the molecular properties of the patellamides and their copper(II) complexes. Since the objective of this work is to explore the biological role of the patellamides, whilst the results in this chapter are not directly related to the patellamides and their copper complexes, they are required to better understand their local chemical and biological environment.

### 5.1 Determination of the intracellular pH value within *Prochloron didemni*

As the patellamides can only bind copper(II) after the deprotonation of two amides from peptide bonds in the macrocycle, the solution pH is an important factor for the ability of patellamides to form copper(II) complexes. Moreover, the different catalytic reactions of the patellamides (phosphatase, carbonic anhydrase, etc.) only occur in specific pH/pK<sub>A</sub>-ranges. While the pH values within different parts of the ascidian, including their cloacal cavities, have been thoroughly studied along with their dynamics within the circadian rhythm<sup>[29, 155]</sup>, the pH value in the producer of the patellamides, *Prochloron didemni*, has not been studied yet. Most cyanobacteria and algae have intracellular pH values in the range of 7.0-7.5<sup>[156-158]</sup>, in cyanobacteria, the intracellular pH values are suggested to be even higher, to reduce the leakage of carbonate<sup>[159]</sup>. As carbon fixation is a key function of *P.d.* for the symbiosis with the ascidians, this probably applies also to this cyanobacterium.

For the measurement of the intracellular pH value in *P.d.*, the ratiometric fluorescent dye BCECF/AM (2',7'-bis-(Carboxyethyl)-5(6')-carboxyfluorescein-acetoxymethylester), was used. While the BCECF acid is the luminous signaling form of the dye, the acetoxymethyl ester is membrane permeable and hydrolyzed by esterases inside the cells, allowing easy loading of the dye into the cells as well as a selective luminosity inside the cell. Two living specimens of *L.p.* were transported from Heron Island to the laboratory in Brisbane, to allow for the collection of fresh and intact specimens of *P.d.*, since the cyanobacteria often die within 1-3 days when separated from their host. This could be confirmed experimentally by following

their photosynthetic efficiency, using a PAM (Pulse Amplitude Modulation) chlorophyll fluorometer. The cyanobacteria were freshly collected from the animal and incubated with BCECF/AM as described by the producer<sup>[160]</sup>, once at room temperature for 30 minutes, or after subjecting the cyanobacteria to an acid shock (50mM HCl for 5 minutes). While the acid shock led to the death of the cyanobacteria, making these measurements unusable, the incubation at room temperature with BCECF/AM gave a sufficient load of the dye into the cells and left the organisms alive. As reference for the measurements, BCECF/AM was dissolved in a lysate of *E. coli*, which was set to different pH values, to create a set of reference spectra and the respective regression curve for the dataset (see Appendix Figures A-pH1 – A-pH2). The experimental procedure is described in more detail in the Experimental Section.

To verify the success of the loading procedure and to confirm, that the signal measured originates from within the cyanobacteria and not from the surrounding aqueous solvent, the incubated cells were measured with a confocal fluorescence microscope (Figure 22). As evident from the figure, using the same excitation and emission settings, the negative control only shows a weak, barely noticeable emission, which can be attributed to a slight autofluorescence. The positive control shows a clear and highly intense fluorescence of BCECF within the targeted cells.

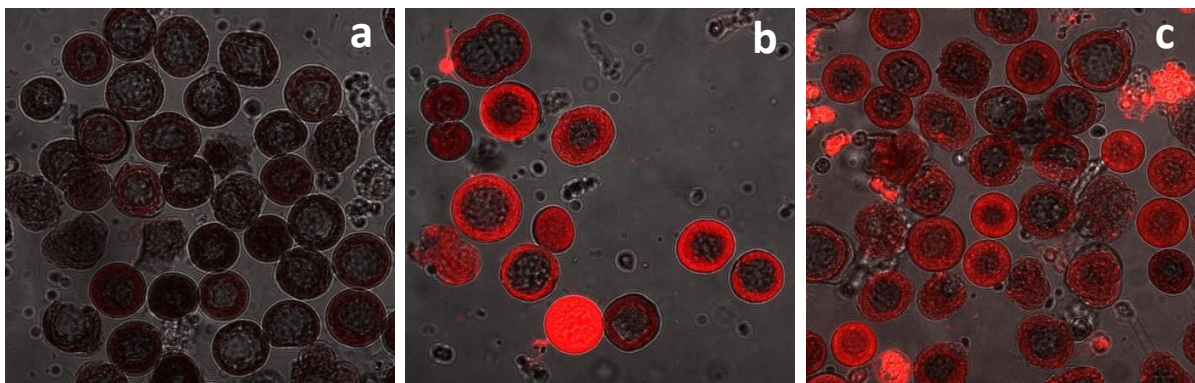


Figure 22: Confocal fluorescence images of *Prochloron didemni*. a: negative control (unloaded cells) b,c: Positive control (Cells loaded with 0.01mM BCECF/AM). A three-dimensional version of the confocal microscopic-scan can be found in the appendix (A-pH 3)



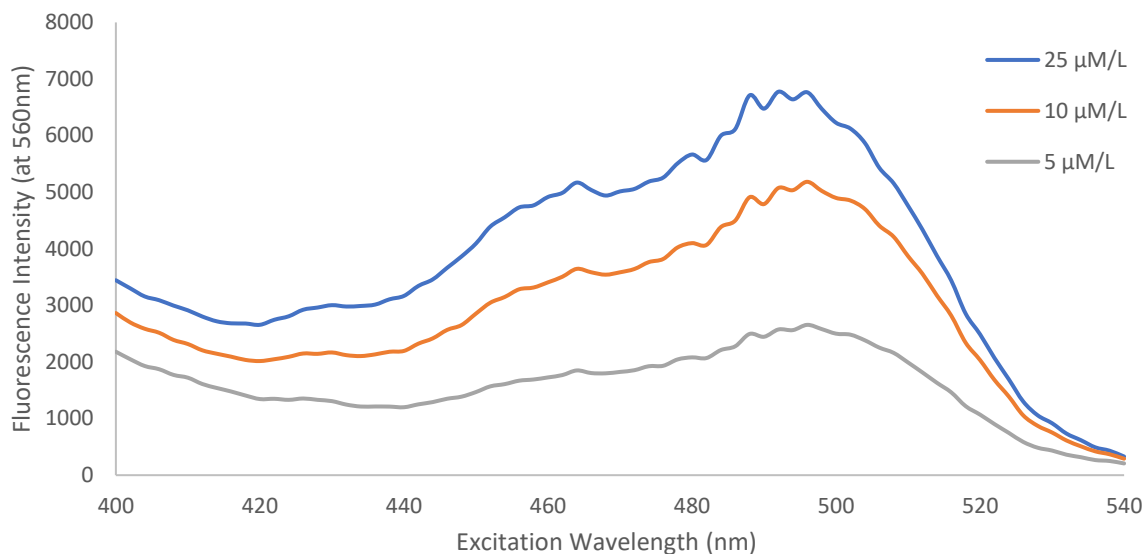


Figure 23: Excitation spectrum, measuring the emission intensity at 560 nm of *Prochloron didemni* incubated with three different concentrations of BCECF at variable excitation wavelengths. The shown spectra are averaged over 8 samples.

The loading was compared for a 1:40, 1:100, and 1:200 dilution of the 1 mM/L BCECF/AM stock solution, and the spectra show very similar features and ratios at all three dilutions (Figure 23). For further assays and for the microscopy the 10  $\mu\text{M}$  concentration was chosen, as the 1:200 dilution showed a worse signal-to-noise ratio than the higher concentrations with less pronounced excitation maxima, while the 1:40 dilution gave a very similar signal to the 1:100 dilution and thus the lower concentration was preferred. The ratios for the emission at 560 nm with the excitation at 504 nm to the excitation at 440 nm for all three dilutions were around 2.1 and the ratio for the emission at 560 nm with the excitation at 504 nm to the excitation at 460 nm was around 1.32 (Table 6). The ratios were determined for both excitation wavelengths, as the instrumentally preferred wavelength uses 440 nm for technical reasons, while the measured spectra showed the second maximum at 460 nm.

Table 6: Overview of the excitations ratios of the spectra shown in Figure 16.

Dilution	Concentration	Ratio F(504)/F(440nm)	Ratio F(504)/F(460nm)
1:40	25 $\mu\text{M}$	1.870531	1.194236
1:100	10 $\mu\text{M}$	2.142207	1.380411
1:200	5 $\mu\text{M}$	2.053777	1.379613
	<b>Average</b>	<b>2.097992</b>	<b>1.318087</b>

The pH-dependence of the fluorescence excitation ratios shows a nearly linear trend (Appendix A-pH 2). However, the accurate determination of the pH value was performed based on Equation 2 and 3, which describe the relationship between proton concentration and its logarithm and fluorescence ratios, with **R** being the ratio between the fluorescence emission at 560nm upon excitation at  $\lambda_1 = 504\text{nm}$  to the emission upon excitation at  $\lambda_2 = 460\text{nm}$  in the samples; **R<sub>A</sub>** and **R<sub>B</sub>** are the respective ratios at the acidic (**R<sub>A</sub>**) and basic (**R<sub>B</sub>**) end of the reference titration and  $F_{A(\lambda_2)}/F_{B(\lambda_2)}$  are the absolute values of the fluorescence at 560nm upon excitation at  $\lambda_2$ .

$$[H^+] = K_a \frac{(R - R_A)}{(R_B - R)} \times \frac{F_{A(\lambda_2)}}{F_{B(\lambda_2)}} \quad (2)$$

Equation 2: Relationship between H-concentration and the fluorescence ratios

$$pH = pK_a - \log \left( \frac{(R - R_A)}{(R_B - R)} \times \frac{F_{A(\lambda_2)}}{F_{B(\lambda_2)}} \right) \quad (3)$$

Equation 3: Relationship between the pH and the fluorescence Ratios

The resulting value for the pH, as determined by this method, is **6.9 (±0.1)**. Interestingly, this value is slightly lower than in most other cyanobacteria and lower than the intracellular pH for carbon-fixating cyanobacteria discussed by Mangan et al.<sup>[159]</sup>. The intracellular pH in cyanobacteria can vary depending on the surrounding light irradiation<sup>[159]</sup>, but as the cyanobacteria for this experiment were not dark-adapted, the pH should have been at the maximum level. This might indicate that *Prochloron* has an alternative way to ensure sufficient availability of carbon for its high levels of photosynthesis<sup>[29]</sup>.

## 5.2 Bioactivity of patellamides and their copper complexes on algae

As described in chapter **2.3.1 Medical properties**, the bioactivity of patellamides has been evaluated with several human cell lines, and its toxicity towards potential predators and infectious microorganisms was evaluated. In all published experiments, only the metal-free patellamide was used, and apart from some interactions with membrane proteins in human leukemia cell lines<sup>[16]</sup>, little activity was found. A possible positive or negative effect on the vitality of photosynthetic organisms such as algae or cyanobacteria has not yet been tested. To check these properties, a series of experiments was devised, where reference algae (*Nannochloropsis gaditana* or *Nannochloropsis salina*) were subjected to different concentrations of copper(II), to metal-free patellamides and to a combination of copper(II) and patellamides. The vitality of the algae was evaluated using a PAM chlorophyll fluorometer, as the fluorescence parameters of algae are known to be a good indicator of their vitality<sup>[161-163]</sup>.

Different parameters can be considered when testing the vitality of the algae. Firstly, the maximum photosynthesis rate  $F_m$  can be measured by saturating the chlorophyll excitation, closing all reaction centers of a dark-adapted sample (kept in complete darkness for at least 1 hour) sample. This parameter indicates the maximum level of excitable chlorophyll i.e., its content or the number of algae. Secondly, the current or variable chlorophyll fluorescence  $F_v$  can be observed (indication of the photosynthetic rate at a given moment). As third option, the minimum fluorescence  $F_0$  can be measured during the minima of the excitation pulses. This parameter gives an indication of the low-light or rest fluorescence in the absence of an excitation pulse with all reaction centers open and unexcited. Lastly, the photosynthesis yield  $Y = (F_v(F_m - F_0) / F_m)$  can be determined, which indicates the efficiency of the photochemical reactions in photosynthesis II.

To algae of the species *Nannochloropsis salina* patellamides either only patellamide (25  $\mu\text{M/L}$  or 50  $\mu\text{M/L}$ ) or copper(II) (1ppm or 2ppm) or both (25  $\mu\text{M/L}$  or 50  $\mu\text{M/L}$  asc + 1ppm copper) were added. Interestingly, when plotting the relative change of the maximum fluorescence ( $F_m$  of treatment compared to blank, see Figure 24), a significant increase in maximum fluorescence  $F_m$  can be observed, already within few hours after treatment. This may be caused by an increase in the number of algae or the effective number of reactive centers in

PS2 within the culture. As evident, there is hardly any difference between the samples with and without copper(II) added, which is most likely because copper(II) at these low concentrations is often already contained in the growth medium of marine algae.

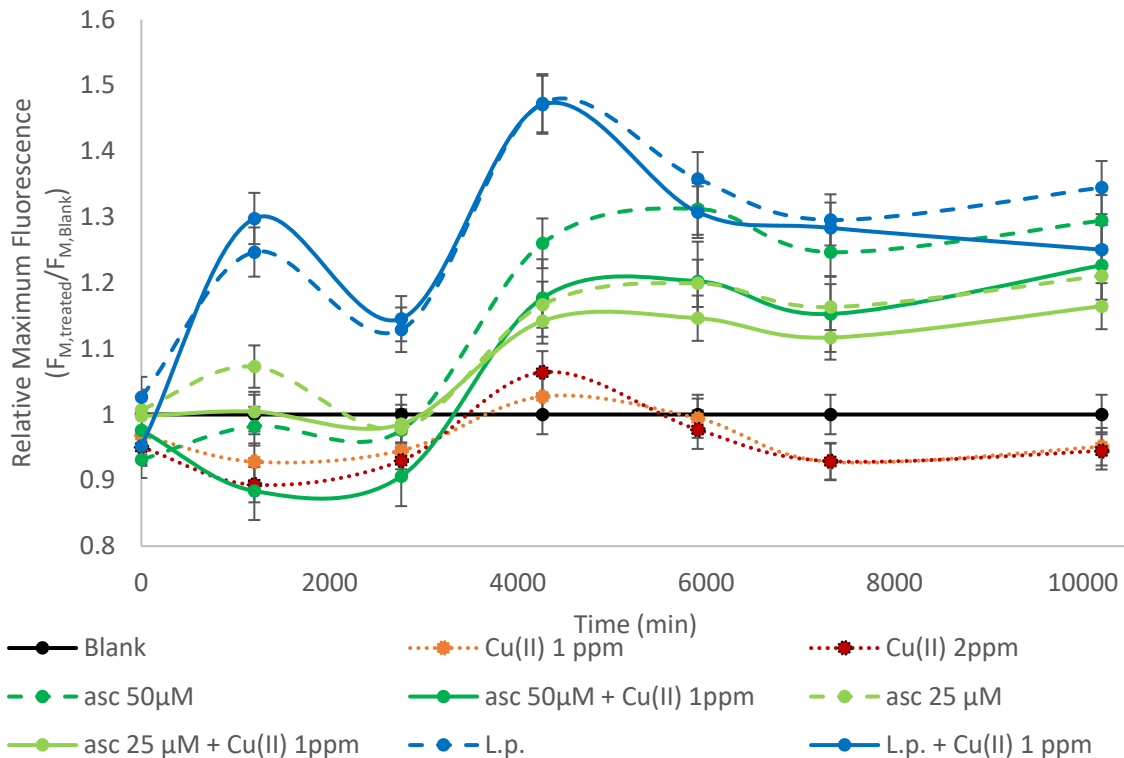


Figure 24: Change of the relative maximum chlorophyll fluorescence of the dark-adapted samples, shown relative to the values for the blanks. All measurements are averaged over 3 samples, the average standard deviation over all samples is ~3%. The two Asc series correspond to concentrations of 25 µM/L (Asc2, bright green) and 50 µM/L (dark green). In the samples labeled Pd, an extract from filtered cloacal water, collected from *Lissoclinum patella*, was directly added to the samples.

At these low concentrations of copper(II), no change between the treated cultures with and without copper(II) was noticeable. However, with algae of the same species at higher concentrations of copper(II) (50 - 100ppm), this was different (Figure 25). Algae of the same genus *Nannochloropsis* (this time the species *Nannochloropsis gaditana*) were treated with either copper (50 or 100 ppm), ascidiacyclamide, or PAO<sub>SS</sub> (53 µM), or both. At concentrations of 100 ppm, the algae died within 2 days, while at 50 ppm, they showed a decrease in fluorescence rate but recovered. While the metal-free patellamides did not show any negative effect, together with copper(II), the algae died as quickly as with the higher, lethal concentration of copper(II). The decrease in vitality is evident from the drop in variable chlorophyll fluorescence  $F_v$  measured using a PAM. In addition, the effect could usually be observed by the naked eye, as the deceasing samples changed their color from green to colorless-brown.

While the negative effects observed at this significantly higher concentration of copper(II) are most likely of little relevance for the biological system, they contradict one older hypothesis [20] on a possible biological function of the patellamides, to protect the cyanobacteria from the toxic effects of copper.

The experiments with the two different concentration ranges of copper(II) have shown, that at the physiological concentration of copper(II), patellamides do not decrease and eventually enhance the efficiency of the light reaction of PSII of an algae culture. In contrast, at excess concentrations of copper(II), a detrimental effect can be observed, enhanced by the patellamides. A possible explanation for this is that the patellamides as small cyclic peptides with short hydrophobic side chains pass the membranes in sufficient amounts. After binding copper(II), they can shield the charge of copper(II) and possibly enhance the transport of copper into the algae, explaining the detrimental effects observed in the first series of experiments. At lower copper(II) concentrations, the patellamides might be used to transport

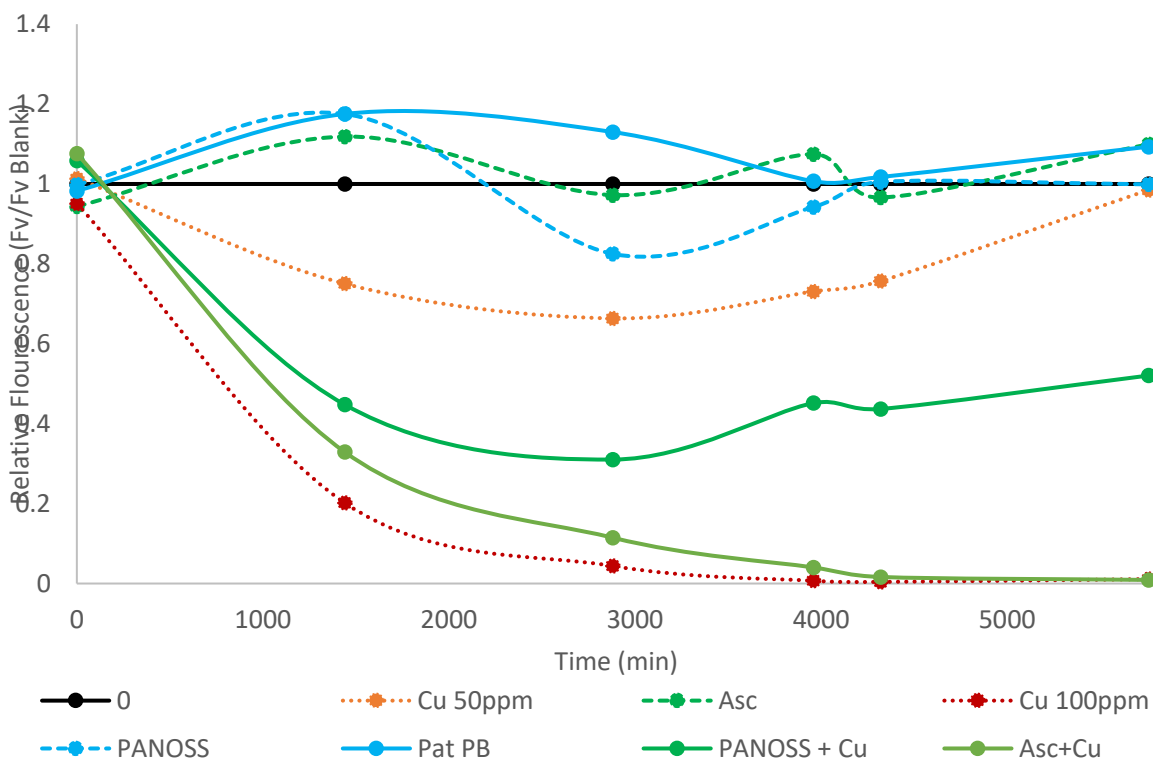


Figure 25: Comparison of the relative variable fluorescence ( $F_V/F_{V,Blank}$ ) of the samples under illumination (a lamp simulating light composition in the sea), relative to the control culture. All curves represent the average of 2-3 samples. Both asc (ascidiacyclamide) and PANOSS (patellamide analogue with oxazole heterocycles and S,S side chain stereochemistry) were added to concentrations of 53  $\mu\text{M/L}$ . The same concentration of copper the algae recovered from became lethal when added with the patellamides.

limited available carbonate through the membranes, thus increasing the carbon fixation activity of the algae as part of the photosynthesis cycle. However, it can not be excluded that the different results are in parts caused by the two different subspecies of the genus *Nannochloropsis* but due to the high similarity between the two cultures only a minor effect would be expected.

One possible way to test whether the positive effect on the algae, observed at physiological concentrations of copper(II), is related to an increase in the availability of assimilates for photosynthesis is by isotopic labeling experiments. When treating an algae culture with  $^{13}\text{C}$ -labeled carbonate with and without the addition of copper(II) and patellamides,  $^{13}\text{C}$  should be found in higher concentration in photosynthesis products from the cultures that have received both.

### 5.3 Catalytic activity of dicopper(II)-patellamide complexes

#### 5.3.1 Phosphoesterase activity with small molecules<sup>†</sup>

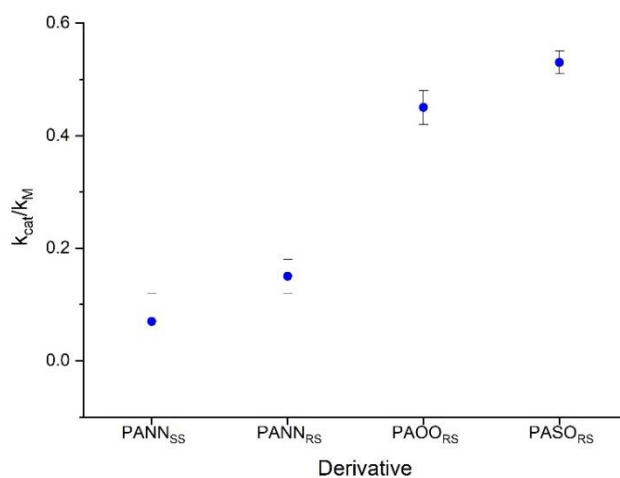


Figure 26: Comparison of the  $k_{\text{cat}}/k_{\text{M}}$  values for the BDNPP hydrolysis with different dicopper(II)-patellamide analogues (data from Appendix Table A-P1)<sup>[6]</sup>.

Previous studies have shown<sup>[2, 6, 23, 80-81, 164]</sup> that copper(II) complexes of various patellamide analogues have phosphodiesterase- and monoesterase activity. While this activity has been published for different patellamide analogues (PANN<sub>SS</sub>, PANN<sub>RS</sub>, PAOO<sub>RS</sub>, PASO<sub>RS</sub>)<sup>[2, 23, 80-81, 164]</sup>, the pH dependence for natural patellamides was not measured yet. Furthermore, it was observed, that the values of  $k_{\text{cat}}/k_{\text{M}}$  show higher values for the naturally occurring

<sup>†</sup> Main parts of this chapter have been published in [6] P. Baur, P. Comba, G. Velmurugan, Chem. Eur. J. 2022, 28, e20220024. The figures shown, and parts of the text are used as published.

heterocycles, than for the analogues (Figure 26). The key factors influencing the catalytic efficiency of the dicopper(II) patellamide complexes<sup>[79-80]</sup> like the kind of heterocycles (and the resulting electronic and structural differences) and structural properties resulting from the size and stereochemistry of the side chains have been discussed but the fundamental reasons are not qualitatively known. Only few crystal structures of the dicopper(II)-patellamide complexes are available<sup>[5, 94]</sup>, but the structural modeling data obtained in solution by EPR spectroscopy<sup>[2, 80, 83, 94, 118]</sup> allows a better understanding of the structural properties of these complexes. The mechanism of catalytic hydrolase activities, specifically carbonic anhydrase, and phosphatase have been studied experimentally<sup>[23, 79, 118, 164]</sup>. Based on this previously literature-reported data, DFT calculations were performed to better understand the observed differences in catalytic efficiencies. The proposed mechanism of the phosphodiesterase reaction, used for these calculations, is shown in Figure 27. Instead of the substrate used for the phosphoesterase experiments (BDNPP), the computationally less demanding phosphonic acid dimethyl ester was used in the calculations.

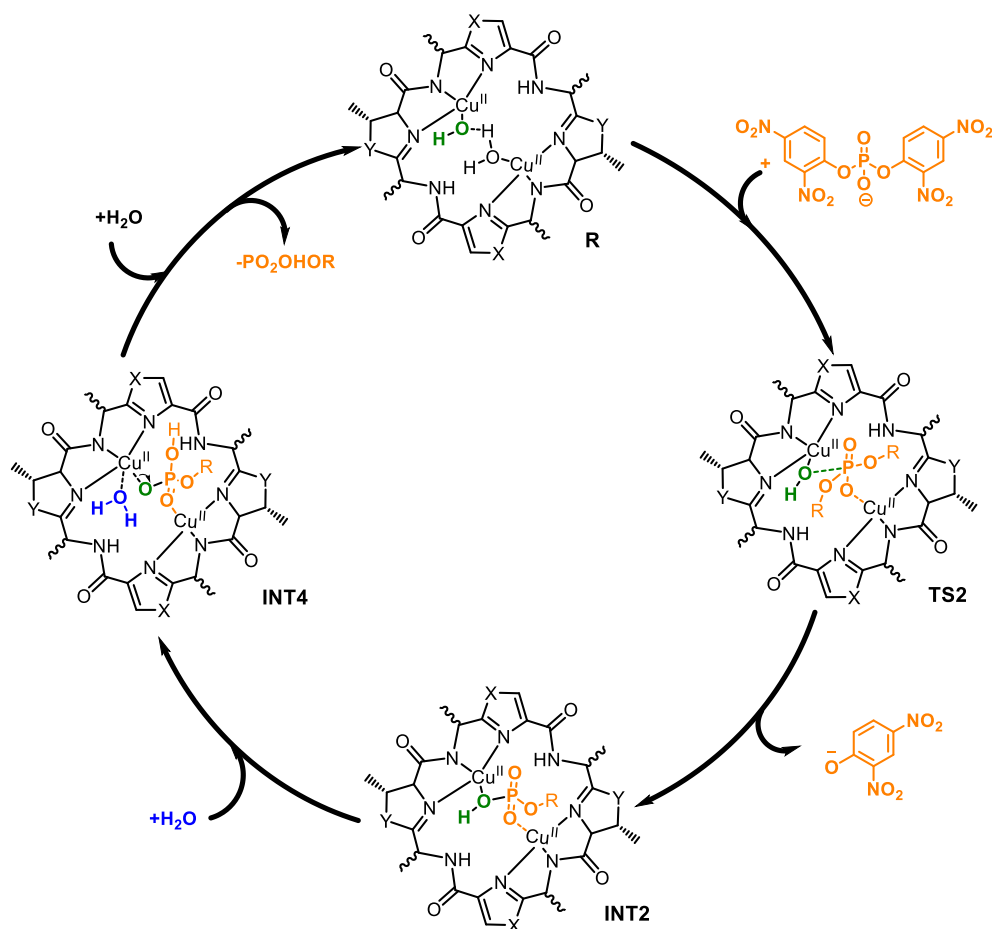


Figure 27: Proposed catalytic cycle for the phosphoester hydrolysis reaction. Additional water molecules in the copper center are omitted for clarity (taken from <sup>[6]</sup>).

For the evaluation of the reactivity of the different patellamide derivatives used, the energy barriers of the rate-limiting step (the step in the proposed mechanism with the highest energy barrier TS2 in Figure 27) were calculated. This is the attack of the  $\text{Cu}^{\text{II}}\text{-OH}$  nucleophile at the phosphorous center to yield the phosphate or phosphoester bridged dicopper(II) intermediate (INT2). The free energy profile of the catalytic cycle (Figure 28) suggests major differences between macrocycles with the natural heterocycles (thiazole and oxazoline) compared to the often-used imidazole-based analogues.

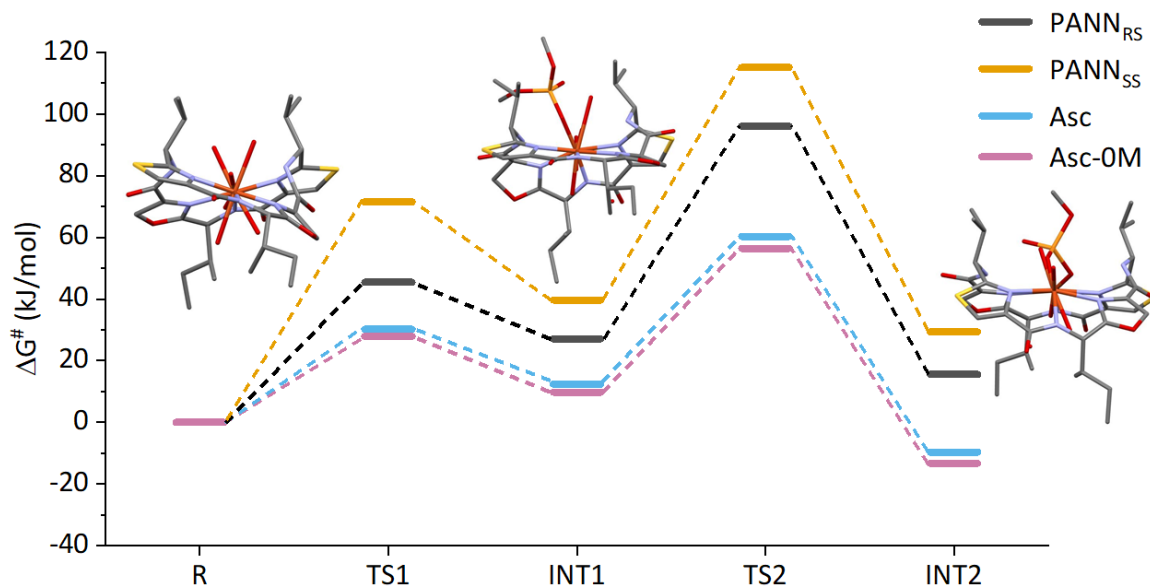


Figure 28: Free energy profile of the phosphodiester hydrolysis reaction, calculated by DFT/B3LYP-D3 (PCM; MeOH) for the dicopper(II) complexes of PANN<sub>SS</sub>, PANN<sub>RS</sub>, Asc and Asc-OM (taken from [6]).

The structures of the system at the rate-determining step are shown in the Appendix (Appendix Figure A-P2). Apparently, the stereochemistry of the side chains (PANN<sub>SS</sub>: 115.1 kJ/mol vs. PANN<sub>RS</sub>: 96.0 kJ/mol) affects the energy barrier at the rate-determining step less than the type of heterocycle used (PANN<sub>RS</sub>: 96.0 kJ/mol vs. Asc: 60.3 kJ/mol, Asc-OM: 56.4 kJ/mol). These computed predictions agree with the experimental results, i.e., that the rates depend both on the stereochemistry of the side chain and the nature of the heterocycle (Figure 26). This is in contrast to the carbonic anhydrase reaction of the dicopper(II)-patellamide complexes, where the two catalysts PANN<sub>RS</sub> and PASO<sub>RS</sub> with the natural RS stereochemistry are much more efficient than the analogues with the not naturally occurring S,S,S,S-sidechain configuration<sup>[79]</sup>. When comparing the calculated transition state structures of the derivatives PANN<sub>SS</sub> and Asc with large differences in the computed reactivity, it becomes evident, that these differences are most likely caused by the significantly larger flexibility of the  $\text{Cu}^{\text{II}}\text{-N}$  bonds in the natural macrocycles, compared to the symmetric and



aromatic imidazole-based macrocycles (see Appendix Figure/Table A-P3). Particularly during the coordination of the phosphoester substrate to one of the copper(II) ions and the attack of the  $\text{OH}^-$  nucleophile from the other copper(II) ion, the flexibility shown by natural systems allows an easier adjustment to the steric demands. This is most likely the reason for the higher catalytic efficiency observed for the patellamides. In contrast, for the carbonic anhydrase reaction, this is less important, as the sterically less demanding substrate  $\text{CO}_2$  and the hydrolysis product  $\text{CO}_3^{2-}$  are not expected to necessitate the same magnitude of structural changes to the system.

Besides the calculations, two experimental series of phosphoesterase reactions have been performed. Firstly, the pH dependence of the phosphodiesterase reaction with dicopper(II)-ascidiacyclamide was measured, which showed a similar optimum pH (6-7) on the reaction as the imidazole-based derivatives<sup>[23, 164]</sup>. It must be noted that due to inhibitory effects of phosphate impurities within BDNPP used for the measurements, the absolute values of  $v_0$  determined are most likely higher than experimentally determined, but this is not expected to affect the pH-dependence of the reaction.

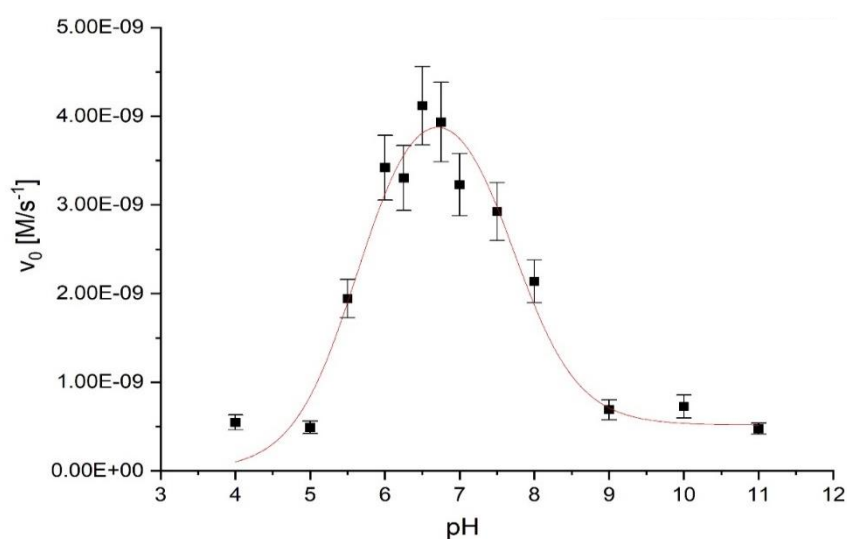


Figure 29: The pH dependence of the phosphodiesterase activity of  $[\text{Cu}^{\text{II}}_2(\text{Asc})(\text{OH})]^+$  with BDNPP. The concentration of the ascidiacyclamide complex in the cuvette was  $40 \mu\text{M}$ , the BDNPP substrate concentration was  $2.5 \text{ mM}$  and the solvent consisted of 45:50:5 (acetonitrile:buffer:MeOH with the buffer system AcONa/MES/HEPES/CHES/CAPS, see Experimental Section).

Furthermore, a fluorescence assay, based on 6,8-difluoro-7-hydroxy-4-methylumbelliferyl phosphate (DiFMUP) was used to evaluate the rate of the phosphomonoester hydrolysis. Unexpectedly, most of the tested patellamides and patellamide analogues, barely showed any reaction, only the imidazole-based PANN<sub>55</sub> seemed to have notable reactivity (see

Appendix Figure A-P4). This is attributed to two factors, firstly possible steric demands of the substrate, which most likely does not fit into the catalytic site proposed in the reactive cycle (see Appendix Figure-A2), and instead binds to the catalyst from the other side, which only in the non-natural *S,S,S,S* is sterically unhindered by side chains. The second and more important factor, however, is that phosphomonoesterase activity, particularly of patellamides, is slower because it has lower  $K_M$  values<sup>[23, 81]</sup>, and it generally involves an attack on the phosphorus followed by the cleavage of the bond between phosphorus to the metal-coordinated alkoxide<sup>[165-166]</sup>, which in case of DiFMUP might be further hindered by the electron-withdrawing effect of the two fluorine atoms. As the main reason for the measurements with DiFMUP was to evaluate the utility for *in vivo* measurements, this assay was not used further, as it appears not to be suitable for measurements with the natural patellamides.

Further details on the calculations as well as the XYZ-data used in the calculations can be found in the Experimental Section and the Supporting Information of the paper published on these results<sup>[6]</sup>.

### 5.3.2 Phosphodiesterase activity with DNA

In previous experiments, the phosphodiesterase properties of dicopper(II)-patellamide complexes have only been evaluated using phosphodiester model substrates such as BDNPP and DNPP<sup>[23, 164]</sup>. However, the reactivity with the most important phosphodiester in nature for which BDNPP is commonly used as a model substrate<sup>[167]</sup>, DNA (or RNA), has not yet been evaluated.

Preliminary experiments with supercoiled double-stranded DNA-plasmids (dsDNA<sub>scp</sub>) showed, that the dicopper(II)-patellamide complexes interact with the double-stranded DNA (Appendix Figure A-DNA1) as evident from an additional line in the sample containing the complexes. This was attributed to the hydrolysis of the DNA phosphodiester backbone of one of the strands (referred to as nicking). Due to the mechanism of the patellamide phosphodiesterase reaction, involving the hydrolysis of a single phosphodiester bond, this outcome would be expected - given that double-stranded DNA was used, making it statistically unlikely that the complexes cut both strands at the same time.

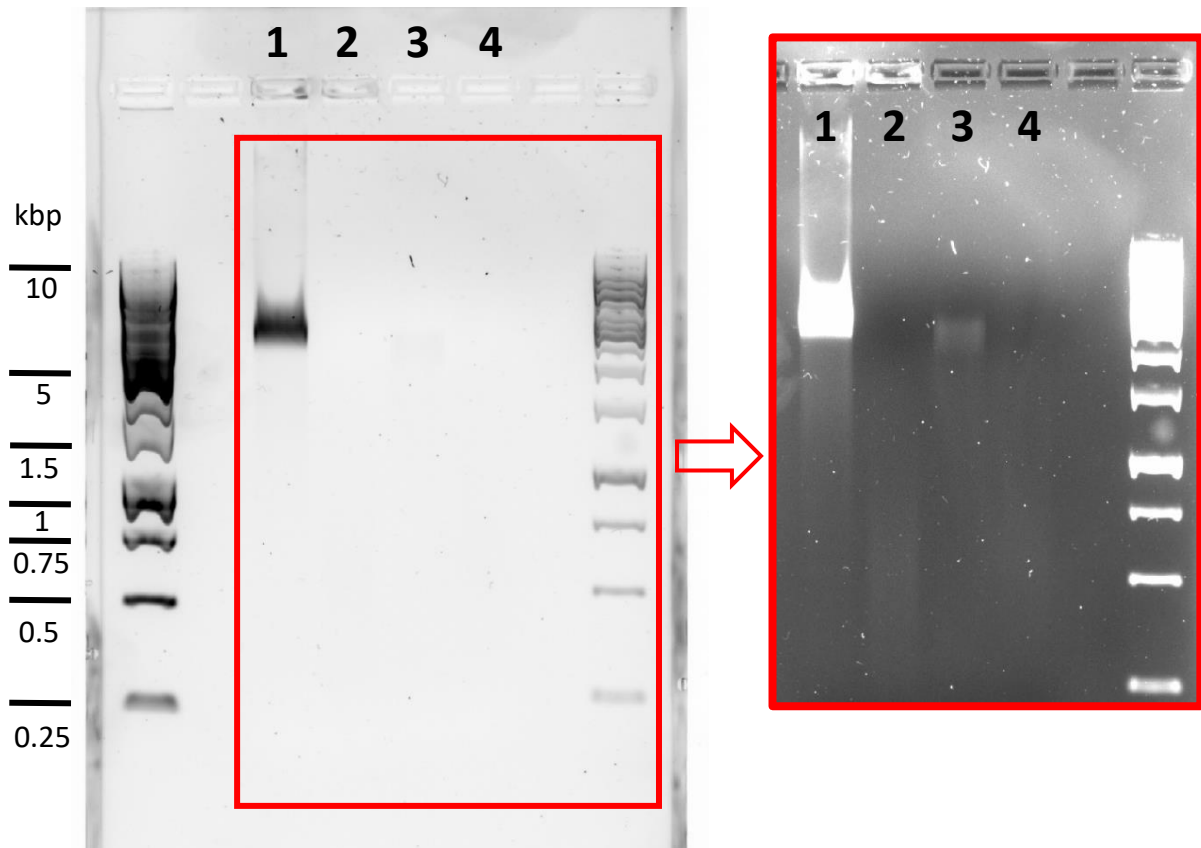


Figure 30: Gel electrophoresis of single-stranded DNA (ssDNA) from the bacteriophage M13mp18 was used. In all cases, only traces of DNA remain visible after incubation (1h, 37°C). The samples used were **1**: control, **2**: water from cloaca (denatured 30 minutes at 98°C), **3**: evaporated and redissolved (in 20% aqueous MeOH) DCM extract of *Lissoclinum patella* **4**: synthetically produced Cu<sub>2</sub>Asc. At the left and right well, the Generuler 1kb ladder was run. To remove excess NaCl from **2** and copper(II) from **4**, which were found to lead to agglomeration of DNA in the well, all four samples were purified using a Cytiva silica-binding kit. At maximum contrast (area marked in red), it can be seen that in samples **2** and **4**, instead of the original strand, multiple randomly distributed smaller fragments remain.

Based on this scenario, it is expected that with single-stranded DNA a decomposition of the polynucleotide should be visible. Therefore, follow-up experiments with different substrates were measured at the DWI and RWTH in Aachen, Germany. In this second series of experiments, synthetically produced ascidiacyclamide as well as biological samples of *Lissoclinum patella*, collected during the field trip to Heron Island were used. During the first separations, free metal ions in the synthetic samples and the high salt content in the biological aqueous samples led to agglomeration of the DNA in the loading wells, making it necessary to purify the DNA after incubation (using the Illustra GFX PCR DNA and Gel Band Purification Kit). The gel electrophoresis of single-stranded viral DNA from the bacteriophage M13mp18 shows that after incubation with the biological samples as well as with the

synthetic sample, the original ssDNA strand has mostly or completely been decomposed (Figure 30). The denatured cloaca (sample **2**) and the synthetic samples only faintly show randomly sized DNA fragments, indicating an actual deterioration of the original DNA. In addition, the redissolved DCM (sample **3**) shows a faint remainder of the original strand as well.

Since in Figure 30, most of the used ssDNA has been decomposed, the experiment was repeated under the same conditions as before with lower concentrations of the samples (samples **2-5**) and with double-stranded-DNA (samples 6-9)(see Figure 31). To ensure that the observed results emerge from the dicopper(II)-patellamide complexes and not from interaction with the copper(II) and base used for the complexation, the copper(II)-base mixture used for the complexation was run as a control as well (sample **1**), showing no deterioration of the DNA. At the lower concentrations of the previously used samples, the signal decrease as expected, is significantly weaker than before, with only sample **2** and **4** ( $1/10^{\text{th}}$  of the previous concentration) showing a reaction after 1 hour of incubation, as is evident from the decreased signal intensity of the ssDNA strand and the increase of the intensity of the smaller fragments. In the case of the dsDNA plasmid, even the control sample (sample **6**) has a very low intensity, making the further decreased intensity in the sample with  $\text{Cu}_2\text{Asc}$  (sample **7**) hard to interpret. In the case of the linear dsDNA not only does the  $\text{Cu}_2\text{Asc}$  sample (sample **9**) show a decrease of the signal with respect to the control (sample **8**), there clearly are more defined lines above and below the main line of the original strand, possibly indicative of the previously observed nicking behavior. The experiments suggest that the synthetically produced copper-patellamide complexes have a phosphodiesterase activity towards DNA. While the effects observed in the case of native cloaca aqueous solution (Appendix Figure A-DNA 2) may result from nucleases of one of the involved organisms, heating to temperatures of  $98^\circ\text{C}$  for 30 minutes should ensure that the corresponding enzymes are denatured. The samples where the homogenized cloaca and cyanobacteria are extracted with DCM, followed by solvent evaporation and redissolution of the residue in water (20% aqueous MeOH), should also not have any intact enzymes that would explain the observed reactions.

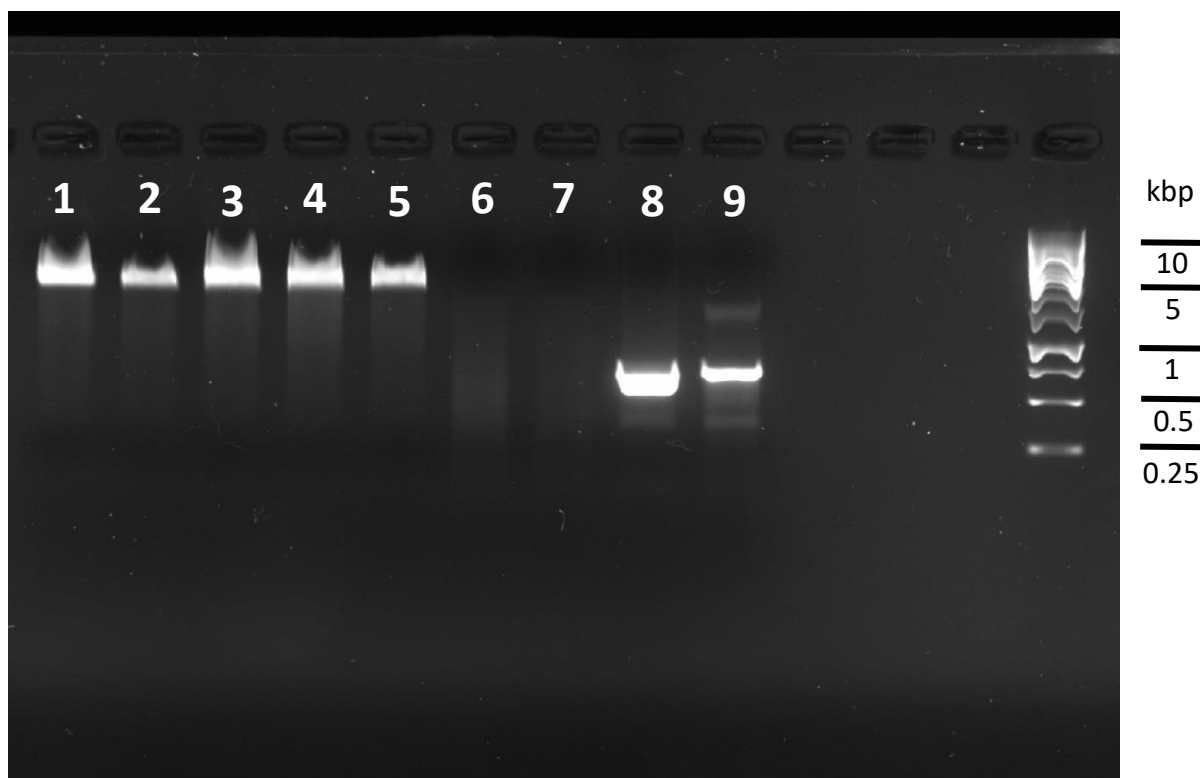


Figure 31: Gel electrophoresis of incubations with the previously used samples at lower concentrations: M13mp18 ssDNA (with: **1**: Control: Only the  $\text{Cu}^{2+}$  and the base  $\text{NEt}_3$  used for the  $\text{Cu}_2\text{Asc}$  samples, **2,3**  $\text{Cu}_2\text{Asc}$  at 1/10 and 1/100 of the concentrations used in Figure 23, **4,5**: the denatured water from the cloaca at 1/10 and 1/100 of the concentration used in Figure 23), a dsDNA plasmid (**6**: control,**7**: with  $\text{Cu}_2\text{Asc}$ ), and linear dsDNA (**8**: control,**9**:  $\text{Cu}_2\text{Asc}$ ). At the right well shown, the GeneRuler 1kb DNA ladder was run, the most prominent lines are indicated on the right.

However, both the denaturing step as well as the extraction should leave the naturally present dicopper(II)-patellamide complexes intact, explaining the effect on the DNA. Therefore, the deterioration of free DNA can be expected to occur in the biological system as well. As evident, while double-stranded DNA is not significantly affected by hydrolysis, single-stranded DNA is close to completely deteriorated. As many bacteriophages (like the one the DNA in the experiments was isolated from) have single-stranded DNA, it might be possible that this effect is advantageous for and intended by the producer of the patellamides, *Prochloron didemni*.

In general, the ability of the dicopper(II)-patellamide complexes to interact with DNA is likely, given that they are dinuclear and have shown the ability to hydrolyze BDNPP. The extent to which this reactivity occurs has been shown to depend on the structural and electronic properties of the complex [167-169]. While it is not uncommon for small dinuclear complexes to be able to hydrolyze DNA<sup>[167]</sup>, these biomimetic compounds are, in contrast to the dicopper(II)patellamide complexes, not naturally occurring.

#### 5.4 Discovery of a new species of parasite within *Lissoclinum patella*

While it is known that *Lissoclinum patella* shares its colony with multiple kinds of cyanobacteria and is in a symbiotic relationship with many of them, a specific parasite living in the ascidians has not been mentioned before. During the field expedition on Heron Island, Queensland, Australia, several of the collected ascidian specimens were observed under light-microscopes. In 3 of the 7 specimens, a total of 6 individuals of an unfamiliar round organism was found, apparently entrenched within the cloacal cavity of the ascidian (Figure 32).

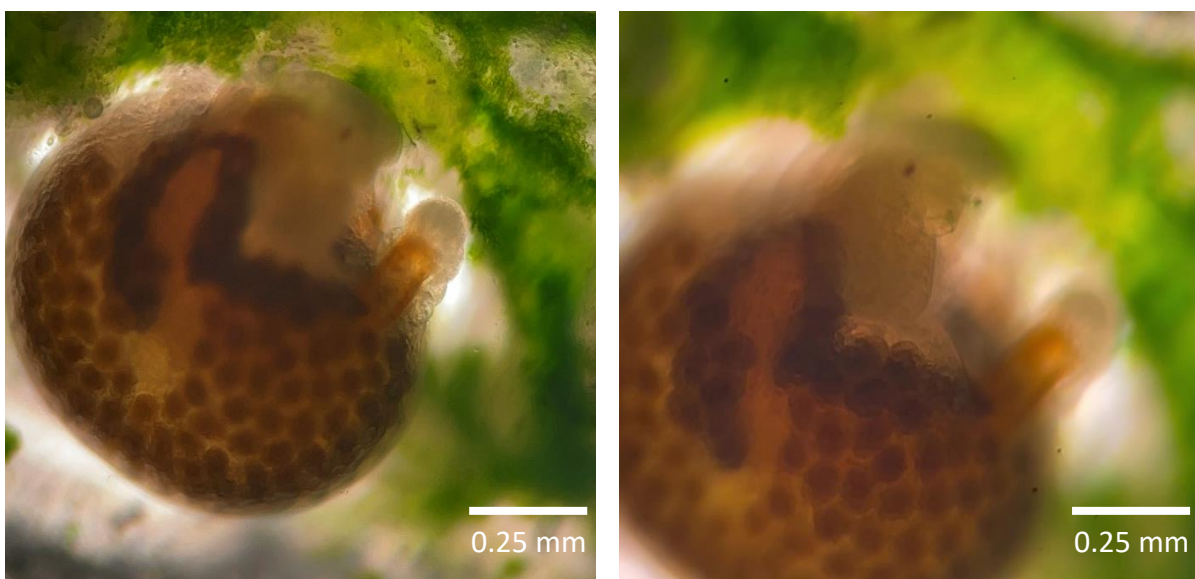


Figure 32: Unknown parasite species found in *Lissoclinum patella* on the Heron Island Reef. Right: Part of a video sequence showing the parasite using small mouthparts to ingest *Prochloron didemni* (Video in additional files, eating sequence at 00:27).

The organism has diameters between 0.5 and 0.8 mm and can be seen by the naked eye. It has an orange-brown color with 2-3 dark lines as well as several dark spots visible through its transparent skin. Unlike typical parasites, it does not appear to show high mobility with no extremities, other than a small, movable “tail”-like structure and mouthparts, that suggest that the parasite might be a member of the crustacean subclass of copepod. Opposite the tail, there is a head with a mouth-opening with at least three pairs of mouthparts and an apparent visual organ with a red color, which might be the red compound eye typical for copepods.

While none of the parasites seemed to possess the ability to move around inside the cloaca because the tail is too short and inflexible to allow targeted movements, The parasite repeatedly moved its head towards nearby cyanobacteria during the observation. It was also observed to sometimes move its tail, possibly to move cyanobacteria toward its mouth. The organism reacted quickly to changes in the irradiation level, stopping all movements.

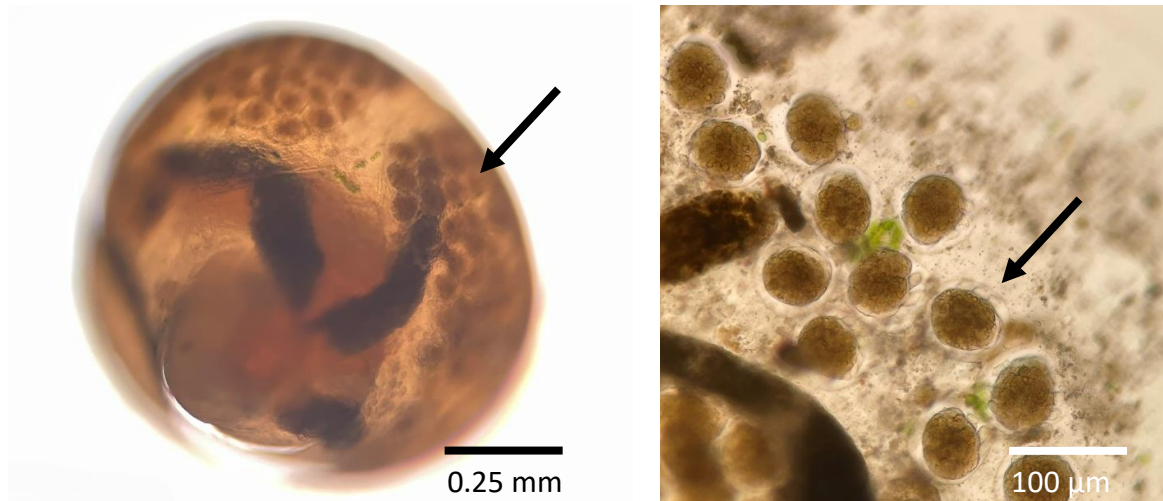


Figure 33: Left: Another perspective of an isolated organism with the three dark lines and the dots clearly visible. Right: Magnification of the dark dots (shown with arrows) after opening the organism.

Dissecting the organism has revealed that the dark spots seen within the organisms are embryos (Figure 33), suggesting that all found individuals might be in a late stage of their reproductive cycle. A magnification of the embryos shows that, unlike the adult specimen, the embryos have three pairs of legs. All found individuals of the organism have had the same appearance, being full of embryos.

It seems to be possible, that at the time of the collection of the samples in July - the coldest month of winter in Australia, the parasites are producing offspring, matching the ascidians to start their reproductive cycle. As the parasite does not have any extremities for movement or any tools to penetrate the ascidian mantle, the parasite embryos are possibly introduced into the larvae of the ascidian and grow with the new colony. However, further studies in the field on the life-cycle form of the parasite in other seasons are needed. The finding of this parasite is significant, as a new example of a highly specialized species, adapted to the complicated reproductive cycle and growth stages of the unique host, the colonial ascidian *L.p.*. The fact, that there is no reference to this or any other parasite in previous sample collections raises the question, whether this infestation is a rare event, indicative of a possible stress-related weakness of the local ascidian population or was just missed in past studies.

## 6. Conclusions and outlook

The foremost objective of this work was to gain an understanding of possible biological functions of the patellamides for its producer *Prochloron didemni* or the ascidians. The first phase of this work focused on the development of a new approach to the synthesis of patellamides, based on the contemporary, solid phase compatible Fmoc-strategy. The new, convergent synthetic route enables the synthesis of a wide range of natural patellamides and synthetic analogues. Patellamides produced using this method have been used as reference for measurements with biological samples and to study different properties of their dicopper(II) complexes, such as their bioactivity and their reactivity with DNA.

In a field excursion to Heron Island, multiple colonies of *Lissoclinum patella* have successfully been found, identified, and collected, allowing to test different hypotheses on the role of patellamides for the organisms *in situ* and obtaining various samples of the animal for later analyses. An initial important finding was that the copper concentration within *Lissoclinum patella* is significantly lower than previously described in literature, especially concerning the cloacal cavity of the ascidian, where the copper concentration is related to the formation and presence of dicopper(II)-patellamide complexes.

Injecting copper(II) into parts of a colony of *L.p.* has caused the cyanobacteria to synthesize significantly more patellamides, as indicated by TripleTOF MS experiments. The high level of patellamides even doubles the total protein content in the cloaca. The dependency of the patellamide production on the copper(II) concentration has not been described before. For a detailed understanding of this phenomenon, the experiments need to be performed with more specimens to determine the direct impact of the copper(II) concentration on the expression rate of the patG gene. Furthermore, the impact of other metal ions on patellamide production should also be studied.

It has been observed that, when subjecting algae of the genus *Nannochloropsis* to patellamides and copper(II), both in millimolar concentrations based on values previously reported in the literature, the patellamides themselves are not harmful but can significantly increase the toxicity of the present copper(II). However, subjecting the algae to patellamides (millimolar concentration) and copper(II) in the newly determined and realistic lower



copper(II) concentration (micromolar concentration) had the opposite effect. In all algae cultures where natural patellamides or even the aqueous extract from the cloaca of *L.p.* were added, the cultures showed significantly (25-40%) increased maximum chlorophyll fluorescence, indicating greater growth. Here investigations using  $^{13}\text{C}$ -labeled carbonate may help to evaluate the influence of dicopper(II)patellamide on the uptake of labeled carbonate. This might indicate that the observed growth effect is due to an increase in carbonate availability.

While it has been previously reported that copper complexation(II) to fluorescence-tagged patellamide analogues occurs *in vivo*, the presence of dicopper(II) complexes of natural patellamides has not been confirmed before. Samples of *Lissoclinum patella* and *Prochloron didemni* have been concentrated by freeze-drying and copper K-edge spectra have been measured without further treatment. Comparison to synthetically produced dicopper(II)-patellamide complexes and fitting to literature-reported crystal structures strongly suggests, that the majority of copper(II) present within the organism is bound to patellamides. While the presence of the complexes of interest can be concluded from the data, it remains open whether carbonate is bound to the dicopper(II) center as we so far lack suitable reference samples with and without a carbonate bridge.

Generally, the XAS data as well as the observed interdependence of the patellamide and copper(II) concentrations substantiate the conclusion, that the copper(II) binding behavior is not coincidental but indeed related to its biological function. The fact that the copper concentration in the organisms is lower than previously believed makes it even more likely that, despite the modest complex stability of dicopper(II)-patellamide complexes, most of the copper(II) inside the cloacal cavity is bound to the patellamides which might have over 100-fold higher concentrations.

Combining all observations and results obtained during this work together with the earlier reported properties of dicopper(II)-patellamide complexes such as their extraordinary carbonic anhydrase reactivity, the currently most relevant hypothesis is, that patellamides are made by *Prochloron didemni* for their own advantage: it is proposed that the dicopper(II) complexes formed in the cloaca, bind transport carbonate through the cell membrane of the cyanobacteria, thus maximizing the amount of  $\text{CO}_2$  available for photosynthesis. This possible biological function agrees with most of the observations made. The patellamides as small

macrocycles with hydrophobic side chains and a neutral charge as carbonato-bridged dicopper(II) complexes, may help to pass the cyanobacterial membranes. This transport of the carbonato-bridged dicopper(II) complexes has not yet been experimentally confirmed. However, copper(II) complexes of patellamides have been shown to be present in *P.d.* cells, and the doubly deprotonated dinuclear copper(II) complexes are known to be efficient carbonic anhydrases. A transmembrane carrier or channel, allowing facilitated or even active transport of the hydrophilic molecule in an aqueous phase is not yet known but appears possible. Additionally, it was reported<sup>[29, 170]</sup> that *P.d.* does not possess carbonate transporter molecules such as *NdhD3-F3* and the low-CO<sub>2</sub> inducible bicarbonate transporters *sbtA* and *CmpA-D*, commonly found in other cyanobacteria<sup>[170]</sup>.

The extremely high carbonic anhydrase activity of dicopper(II) complexes of patellamides<sup>[79]</sup> led previously to the hypothesis that the molecules might act as carbonic anhydrases. While it would be highly unusual for an organism to produce an efficient enzyme in these exorbitant amounts (at least 100-fold higher concentrations than the coordinated metal ion) and for an enzyme to only consist of eight amino acids, both properties would agree with the proposed role of carbonate transport. An additional indication is the fact that the patellamides appear to promote the growth of a higher algae species. Future experiments, comparing the <sup>13</sup>C-content of major assimilates or photosynthesis-dependent products, and intermediates of *Prochloron didemni* being cultivated in a <sup>13</sup>C-carbonate-rich sea water solution with and without added dicopper(II)-patellamides, may help to test this hypothesis.

If this hypothetical biological function of the patellamides can be further supported or confirmed, this would be the first example of a function of the family of marine small cyclic peptides related to metal-binding. Currently, many related compounds are considered to assume defensive functions, but it might be worth examining the metal binding properties of other cyclic peptides, unfolding further the versatility of these compounds.

## 7. Experimental Section

### 7.1 Materials and methods

#### **Synthetic Procedure**

Any reaction possibly affected by the presence of water or air was carried out under an inert atmosphere of argon or nitrogen using standard Schlenk techniques. In such cases, Glassware was heated and dried under vacuum before use. All chemicals were purchased from BLD Pharm, Fluorochem, TCI Chemicals, Carbosynth Biosynth, Sigma-Aldrich/Merck GmbH, ABCR GmbH & Co. KG and at the University Heidelberg central chemical vendor at the highest available purity (unless using a less expensive purity grade was sufficient and allowed for a more economic reaction). Dry solvents were purchased and used as delivered.

#### **Chromatography**

All chromatographic purifications were performed using a Interchem Puriflash PF-420 equipped with a 200-400nm UV-DAD Multi wavelength detector, using self-filled columns with sizes of 12, 40, 60, 80, 120, 220 or 330 grams of silica as appropriate for the amount of crude substance and the separability, filled with technical grade silica obtained from Sigma Aldrich Germany (40-60  $\mu\text{m}$  particle size, 230-400 mesh, 60 Å pore size). Highly polar products were in some cases purified using a reversed phase C- 18 column for the same chromatograph.

#### **Mass spectrometry**

Mass spectra (ESI-MS) were recorded with a Bruker micrOTOF II: ESI Mass Spectrometer by Claudia Dienemann at the mass spectrometry labs of the Krämer Group at the Department of Inorganic Chemistry of Heidelberg University. Atmospheric pressure chemical ionization mass spectra (APCI MS) were recorded on a Waters UPLC-SQD2 single quadrupole. High-Resolution-Triple-TOF mass spectra were recorded using a Sciex TripleTOF+ 5600 and a TripleTOF+ 6600 by Alun Jones at the mass spectrometry facility of the group of Prof. David Fairlie at the Institute of Molecular Biology of the University of Queensland, Brisbane,

Australia. These Triple-TOF files were interpreted using the Sciex OS package as well as the Open MS package.

### **NMR spectroscopy**

Nuclear magnetic resonance spectra were recorded with a Bruker Avance I (200 MHz) or a Bruker Avance III (600 MHz) spectrometer equipped with a cryoprobe. Chemical shifts  $\delta$  are given in ppm and coupling constants  $J$  in Hz and refer to the  $^3J_{\text{H-H}}$  couplings. All spectra were calibrated using the residual  $^1\text{H}$ - or  $^{13}\text{C}$ -signals of the deuterated solvents. Spectra were recorded at 295 K. The following abbreviations are used to describe the multiplicities of the signals: s (singlet), bs (broad singlet), d (doublet), t (triplet), qn (quintet), m (multiplet). Signals were assigned using DEPT, HSQC and HMBC spectra, using MestReNova 14.0.1.

### **EPR experiments**

All X-band (9.462 GHz) continuous wave (CW) EPR spectra at 30 K were recorded with an Elexsys E500 spectrometer fitted with an ER 4116 DM dual mode resonator. Temperatures of 20 K at the sample position were provided by an ER 4112HV-CF58uc In-Cavity Cryogen-Free VT System. All X-Band CW EPR spectra at 120-140 K were recorded with a Bruker Elex540 spectrometer using a Bruker super-high Q cavity. All Spin Hamilton parameters were provided by computer simulations of the experimental spectra with XSophe. For data treatment and visualization, the Bruker Xepr package was used.

### **Computational Methods**

All computations were performed in collaboration with Dr. Velmurugan Gunasekaran in the Group of Prof. Peter Comba at Heidelberg University. Gaussian 09<sup>[171]</sup> with B3LYP-D3 (LACVP basis set) was used for geometry optimizations and ef2-TZVP for single point calculations<sup>[172-175]</sup>. The solvation energies were computed by using the continuous polarizable continuum (CPCM) solvation model, with methanol as solvent. All reported energies are B3LYP-D3 solvent-phase energies incorporating free energy corrections at 298.15 K, unless otherwise mentioned. A Non-Covalent Interactions plot (NCI Plot)<sup>[176-177]</sup> has been used to distinguish the various non covalent interactions present in the complex (included in the supporting information of <sup>[6]</sup>).

### **Determination of intracellular pH**

The freshly harvested cyanobacteria were directly incubated with BCECF/AM, initially the ideal incubation conditions were tested by first incubating for 30 minutes at room temperature and by subjecting the cyanobacteria to an acidic shock (1 minute in 1M HCl), followed by 30 minutes incubation with BCECF/AM – and comparing different concentrations of BCECF/AM (25  $\mu\text{M/L}$ , 10  $\mu\text{M/L}$ , 5  $\mu\text{M/L}$ ). As the cyanobacteria did not survive the acid treatment, future cultures were directly incubated with BCECF/AM. While all concentrations gave a measurable signal, 10  $\mu\text{M/L}$  was considered the ideal concentration.

All plate reader measurements were performed in collaboration with Dr. James Lim (Fairlie Group, at the IMB of the University of Queensland, Brisbane), in 8-fold repetition on a 96-well plate. The measurements were performed using a Tecan Spark Multimode plate reader. All confocal microscopies were performed using the Zeiss Axiovert 200 Inverted Microscope Stand equipped with a LSM 710 Meta Confocal Scanner in cooperation with Dr. Kathy Wu in the IMB microscopy facility.

### **Determination of copper concentration in biological samples (as described in <sup>[131]</sup>)**

#### *Digestions*

The ICP-OES measurements were performed by Dipl.-Geol. Christian Scholz and Dipl.-Ing Stefan Rheinberger at the Institut für Geowissenschaften, Universität Heidelberg. For sample preparation, 2 ml of nitric acid (65 %, p.A., Neofroxx GmbH) and 125  $\mu\text{l}$  of hydrogen peroxide (30 %, p.A., Merck KGaA) were added to the previously dried (20 mg – 70 mg) and in 250  $\mu\text{l}$  redissolved liquid samples, respectively. All samples were prepared in duplicate. The resulting digestion suspensions were heated to 90 °C in a graphite block (Digiprep) for a period of one hour. Following complete digestion, samples were filled up to 10 ml with Milli-Q water.

For quality control, three different reference materials (CRM), BCR 060 Lagarosiphon Major, IAEA-336 Lichen and NCS ZC71001 Beef Liver (50 mg – 100 mg) were used, which were digested, like the samples, but in triplicates.

Because the samples of *Lissoclinum patella* were not completely dissolved after sample preparation, 3 ml of hydrochloric acid (32 %, p.A., Merck KGaA) were added to the suspensions and the samples again heated up 90 °C for a period of 0.5 h. Subsequent to the

described procedure gelatinous streaks could be observed in the solution, which flocculated after filling the solution up to 10 ml with Milli-Q water. For this reason, *Lissoclinum patella* digestion solutions were filtered (0.45  $\mu\text{m}$ ) in advance of analysis.

### Measurements

Copper concentrations were determined by ICP-OES (Agilent ICP-OES 720) at  $\lambda = 327.395 \text{ nm}$ . The relative standard deviation (RSD) of the measured digestion doublets ranges between 0.6 % and 7.4 %. The recovery rates of the certified values of copper for the used CRM (measured by ICP-OES) ranges between 92.0 % and 98.2 %. The RSD of the triple measurements ranges between 0.9 % and 6.2 %.

To verify the ICP-OES measurements, all samples were additionally measured by ICP-MS (Thermo Fisher iCAP TQ-e). All solutions were diluted ten times for analysis by adding Indium as internal standard. The RSD of the measured digestion doublets ranges between 0.6 % and 44.4 %.

The recovery rates of the certified values of copper for the used CRM (measured by ICP-MS) ranges between 79.8 % and 89.5 %. The RSD of the triple measurements ranges between 2.0 % and 6.5 %.

### Impact of patellamides and copper on algae

For the observations concerning the impact of the addition of copper, patellamides or both, the easily available and commonly used algae of the genus *Nannochloropsis spp.* were used. For the first set of measurements with the higher copper concentrations, *Nannochloropsis gaditana* and *Nannochloropsis oculata* were obtained from the lab of Prof. Annika Guse at the Center of Organismal studies, Universität Heidelberg. Due to lack of access to the former source, for the second series of measurements *Nannochloropsis salina* produced by NYOS Aquatics was purchased. The algae were stored in a darkened room under a lamp simulating the light composition at a water depth of 1 meter (SolarStinger LED SunStrip Marine).

For all PAM measurements, a Walz MINI-PAM-II chlorophyll fluorometer was used. The data analysis has been performed using Microsoft Excel 365.

In all measurements, 2 mL of the algae culture were filled into heat-sterilized screw-cap glasses. To these cultures, either 100  $\mu\text{L}$  of a patellamide-containing solution (1.32 mM/L in

DMSO for all synthetically produced patellamides, or the denatured, filtered aqueous cloaca extract), a copper solution (100  $\mu\text{L}$  of 15 mM/L  $\text{CuCl}_2 \cdot 2\text{H}_2\text{O}$  in the first series of measurements, 25  $\mu\text{L}$  of 1.2 mM/L  $\text{CuCl}_2$  in the second series of measurements) or both were added. In case of the control cultures 100  $\mu\text{L}$  of the solvent, DMSO or  $\text{H}_2\text{O}$ , was added instead.

All algae samples were measured simultaneously in regular intervals, always once light - and once dark-adapted.

### Phosphoesterase measurements

The phosphatase-like activity was determined by spectrophotometric measurement of the hydrolysis of BDNPP. The hydrolysis product 2,4-dinitrophenolate was detected by monitoring the increase of the absorbance at 400 nm ( $\epsilon = 12,100 \text{ M}^{-1} \text{ cm}^{-1}$ , 25 °C). UV-vis data were recorded on a Jasco V-570 spectrophotometer equipped with a Jasco ETC-505T cryostat (set to 25 °C) and in 45 : 50 : 5 MeCN : buffer : MeOH solutions. The pH dependence of the catalysis rates was measured in steps of 0.25 - 1 pH units from pH = 4 to pH = 11 using time-course measurements at the fixed wavelength of  $\lambda_{\text{max}} = 400 \text{ nm}$ . The stock solution concentrations of the copper(II) complexes of the cyclic pseudo-peptides was 0.8 mM (dry MeOH). The final concentrations of the dicopper(II) complexes of the ligands in the cuvette were 40  $\mu\text{M}$ . For the determination of pH-dependent reaction velocities a substrate concentration of 2.5 mM (MeCN) was chosen (while this is below the optimum substrate concentration, this concentration was necessary to ensure the reproduction of previously reported solvent compositions). The measurements with DiFMUP were performed at pH 6.75 with the same concentrations by following the increase of the fluorescent product hydrolysis product of the reaction, DiFMU (6,8-Difluoro-7-hydroxy-4-methylcoumarin) at its emission wavelength of  $\lambda = 455 \pm 10 \text{ nm}$  upon excitation at  $\lambda = 358 \text{ nm}$  using a Varian Cary Eclipse Fluorescence Spectrometer.

### Reactivity with DNA (only the experiments in 5.4)

The experiments with DNA were performed in collaboration with Johannes Hahmann at the Herrmann group at DWI and RWTH Aachen. The synthetically produced ascidiacyclamide (1.3mM/L in DMSO) was complexated freshly with an aqueous solution of  $\text{Cu}_2(\text{NO}_3)_2$  (2.5 eq) and  $\text{NEt}_3$  base (5 eq) and diluted to a final complex concentration of 0.65 mM/L. The biological cloaca samples used, were water extracts from the cloaca of a colony of *Lissoclinum patella*

and filtered using a cellulose acetate 0.45  $\mu\text{m}$  syringe filter. In case of the denatured sample, the same solution was heated for 30 minutes at 98°C to ensure full denaturing of any present nucleases. The DCM-extract sample was obtained by stirring homogenized ascidians (cloaca liquid, any present cyanobacteria, and parts of ascidian tissue) for 12 hours with DCM, separating the organic phase using a separating funnel and centrifuging and filtering off any solids. For the DNA-assays, the DCM was evaporated, and the residue was resuspended in 20% MeOH/H<sub>2</sub>O.

All DNA used was obtained from New England Biolabs. For all gel electrophoreses, a 1% agarose gel in 0.5x TBE buffer with 0.01 % GelRed was prepared, all gels (unless indicated otherwise) were run for 90 minutes at 90V, with the GeneRuler 1kb ladder run as mass reference. In the samples with M13mp18 ssDNA, 4  $\mu\text{L}$  of the stock solution (concentration: 250 ng/ $\mu\text{L}$ ) were diluted with 16  $\mu\text{L}$  of water, leading to a total of 1000ng DNA per sample. Aliquots of 778 ng from the double stranded DNA plasmid were used per sample. The double stranded linear DNA, pET-25b(+), was diluted to a final amount of 1036 ng in the 20  $\mu\text{L}$  samples. The DNA was then mixed 1:1 with the respective sample and incubated for 1h at 37°C and subsequently purified using an Illustra GFX PCR DNA and Gel Band Purification Kit. The samples were first diluted in the capture solution, loaded onto the separation frit, washed with the ethanolic washing buffer and subsequently the purified DNA was eluted off the column using 2x20  $\mu\text{L}$  heated (70°C) ultrapure water. After solvent addition and a wait time of 3 minutes, the filtrate was centrifuged off at 16000 rpm for 1 minute.

## 7.2 Field Experiments and Sample Collection

Intact specimens of *Lissoclinum patella* with sizes of 20-160 cm<sup>2</sup> and thicknesses of 5-15mm were collected in June and July 2022 (except for specimen 4 and 5, which were collected by Lars Behrendt in 2011), in and around the blue pools area at depths between 0.5m and 1.5m on Heron Island (23°26'04.4"S 151°55'21.1"E). Two examples of collected specimen are shown in Figure S1. All specimens were transported in fresh seawater as quickly as possible to the Heron Island Research Station, where they were kept in shaded outdoor aquaria (less than 200  $\mu\text{Mol Photons/m}^2\cdot\text{sec}$ ) with continuous supply of fresh reef water. The collected animals were handled using sterile or sterilized equipment. All samples collected were kept at dry ice temperature or below until they were processed.



For the finely minced samples, a freshly cut 4x4cm piece of specimen was frozen and kept frozen until it was finely cut to be freeze-dried. For the cyanobacterial samples, the cyanobacteria and the cloacal liquid were collected from the specimen by cutting the ascidian longitudinally with slight mechanical pressure, which causes the liquid with the cyanobacteria to flow out. For the homogenate, a glass/Teflon Potter Elvehjem homogenizer was used. To obtain only the water from the cloaca, the cyanobacteria were centrifuged off; for the filtered samples, a syringe filter (0.45  $\mu\text{m}$  CA) was used.

In the sample “copper added” (specimen 3), a solution of 3x2ml 14.2 mM  $\text{Cu}(\text{SO}_4) \cdot 6 \text{H}_2\text{O}$  was injected to one section of the living species, the other section was treated similarly with fresh water. The specimen was then kept in the aquarium before preparing it as described above (freezing, cutting, separating cloaca/Prochloron, homogenizing etc.).

For the measurements requiring living cyanobacteria e.g., for as the determination of the intracellular pH, it was necessary to transport living ascidians to the laboratories in Brisbane. As the cyanobacteria typically start to die within 1-3 days outside of their host, the properties might not be representative of healthy cells even though they might still be alive. Therefore, the cyanobacteria were transported inside healthy ascidian hosts. The ascidians were transported in plastic bags filled with fresh reef water inside an esky box, the water regularly being replaced by fresh reef water, separately transported.

For samples of the water within the cloaca, either a syringe or disposable pipette were used – or the organism was cut longitudinally, and the cloaca content carefully squeezed out, and subsequently any larger particles and cells were filtered off, using cellulose acetate filters. For measurements involving the DCM-extract, the sea squirt was cut into small pieces, homogenized using a glass Teflon homogenizer and the mixture (without the outer mantle tissue) was stirred with an equal volume of DCM for 8 hours in a covered Erlenmeyer-flask and the organic phase was separated, using a separating funnel. For samples using cyanobacteria, the sea squirt was cut longitudinally, and the cyanobacteria and water were gently squeezed out.

All samples were immediately stored in a  $-80^\circ \text{C}$  freezer and have continuously been transported in dry ice-cooled containers.

### 7.3 X-ray Absorption Spectroscopy

Initial X-ray absorption spectroscopy measurements were performed at the mini-undulator beamline P65 of DESY Hamburg in April 2021 after introduction by the beamline-scientist Edmund Welter. The samples were measured in self-designed sample holders made from PEEK, POM and polyimide and produced by the fine mechanic workshop of the department of inorganic chemistry at Heidelberg University. The sample environment used a He-cooled cryostat and a precision motorized sample holder. The fluorescence signal was measured using a PIPS-diode detector (due to the low concentration of copper in the samples an HPGe detector was asked for in the proposal, but it was not available at the time).

The main measurements were performed at the bending magnet beamline SuperXAS at the Paul Scherrer Institute in Villigen, Switzerland in January and August of 2022 and were set up by the beamline scientist Grigori Smoletsev. The samples were mostly measured in thin-walled (10 $\mu$ m) quartz glass capillaries made by Hampton Research, the freeze-dried biological samples were measured in 0.3 mm wall thickness Kapton tube capillaries made by DuPont. The sample environment used a liquid nitrogen-cooled cryojet (100K) and a sample holder for 1-3 capillaries mounted to a precision-engine block. The fluorescence signal was measured using a 5-element silicon drift detector.

After determining the optimal measurement coordinates of the sample table engines, ensuring correct alignment of the sample within the beam. For all samples, initially the photodamage was evaluated, by repeatedly measuring 5-minute XANES spectra at the same spot and looking for photodamage-related changes, to choose a measurement time at which the impact of photoreduction on the spectrum is minimal. For all samples, measurement times of 16 min and 55 seconds for EXAFS measurements and 5 minutes for XANES were chosen at PSI (at DESY, 20 minutes). For each EXAFS measurement, a successive XANES measurement was performed at the same spot, to be able to estimate whether the sample might have been photodamaged at this spot. For the more concentrated samples such as frozen liquid solutions of the synthetically produced ligands the quartz capillaries were used and measured at 4-6 positions. For the biological samples, Kapton capillaries leading to a stronger fluorescence signal were used, measuring as many points as possible (considering the filling height of the capillary, the beam size and a buffer around each spot), which in most

cases were 12-16 spots. The python scripts for the measurement were adapted from the ones provided by the beamline.

The measured spectra were initially opened using Athena from the Demeter Package<sup>[178]</sup> to view the data, identify faulty scans, remove glitches/Bragg reflections from the spectra and to average multiple XAS spectra into one. The averaged XAS spectra were then opened by PySpline<sup>[179]</sup>, to normalize, remove the spline, and obtain the weighted EXAFS spectrum and its Fourier-transform. This data set was imported by Microsoft Excel 365, to adjust the k-weighting of the respective column. The final data was then fitted in the software EXAFSPAK<sup>[180]</sup> using path files generated by FEFF10<sup>[138]</sup> based on reported crystal structures. In some cases, the fits were verified by fitting the same spectrum with the same parameters in Artemis.

Any XAS/EXAFS spectra shown in the text section were created using Microsoft Excel 365 or Origin Pro 2021b, spectra in the appendices were generally using the default export settings of the respective software.

## 7.4 Synthesis

### General Procedures:

**Workup:** Unless stated otherwise, the regular workup procedure involves subsequent washing with water, saturated NaHCO<sub>3</sub> solution, water and brine followed by drying over MgSO<sub>4</sub> and removal of the solvent.

**General Procedure A (Peptide Coupling):** For all Fmoc-based coupling reactions, the component with the free acid functionality (1 eq.) is dissolved in DMF or DCM (depending on solubility), 10 mL per g of reactant. HOBt•H<sub>2</sub>O (1.1 eq) and HBTU (1.1 eq) are added, and the solution is stirred for 10 minutes. Then the second component is subsequently added (1.1 eq. for free amines or 2.0 eq for allyl alcohol) as well as N,N-Diisopropylethylamine (DIEA) (2.1 eq.). The reaction mixture is stirred over night at room temperature under an inert atmosphere. After regular workup the resulting crude product is purified by flash chromatography (EtOAc/Petrol Ether, increasing gradient 15%→33%) to afford the clean product.

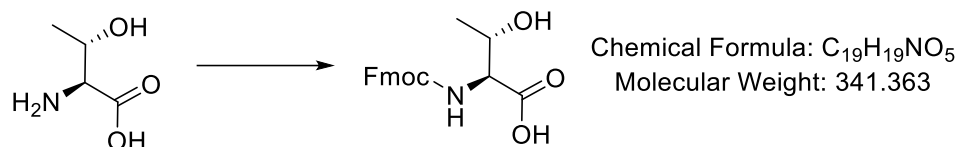
**General Procedure B (Fmoc deprotection - amino acid):** To deprotect the Fmoc-protected amino acid, the fully protected starting material is dissolved in a 50% diethylamine/acetonitrile (10 mL/ mmol) solution and stirred for one hour at room temperature. The solvent is removed *in vacuo* and remaining diethylamine is azeotropically removed with acetonitrile at least three times, until a thick suspension or solid is obtained.

**General Procedure C (Fmoc deprotection - building blocks):** To deprotect the Fmoc-protected peptide, the compound is dissolved in a 20% piperidine-DMF solution (20 mL/3 mmol) and stirred for 30 minutes at room temperature. After the solvent is removed *in vacuo* the resulting residue is purified using a short flash chromatography column and a gradient of 15% EtOAc/PE→33% EtOAc/PE→10% MeOH/DCM. After removing the solvent of the MeOH/DCM fraction, the product is obtained as an orange oil or solid.

**General Procedure D (heterocyclization):** Triphenylphosphine Oxide (3 eq.) is dissolved in dry DCM (10 mL/mM) and the solution is cooled down to 0°C followed by slow addition of trifluoromethane sulfonic anhydride (1.5 eq). After 10 minutes, the solution is cooled down to and kept at -20°C using a EtOH/dry ice bath. Then, a solution of the dipeptide (1eq - with the polar amino acid side chain protected by Trt or unprotected) is slowly added. The reaction progress is monitored by TLC and usually is completed after 2-3 hours. If the educt used is trityl protected, the reaction progress can also be evaluated by an increasingly intense dark red color of the reaction mixture. After regular workup, the resulting product is purified by flash chromatography (gradient 15% EtOAc/PE -> 33% EtOAc/PE -> 66% EtOAc/PE).

**General Procedure E (allyl deprotection):** To a solution of the allyl ester (1.0 eq.) in DCM (5 mL/mM) were added PhSiH<sub>3</sub> (2 eq.) and P.d.(PPh<sub>3</sub>) (0.025 eq) (or alternatively: P.d.(OAc)<sub>2</sub> (0.2 Eq) and PS-PPh<sub>3</sub> (0.2 Eq) are added resulting in a quickly darkening solution which is stirred for 6 hours. After removing the solvent, the resulting residue is purified using a short flash chromatography column and a gradient of 15% EtOAc/PE->33% EtOAc/PE->10% MeOH/DCM. After removing the solvent of the MeOH/DCM fraction, the product is obtained as a brown foam (light-brown to white in case of polymer-supported PPh<sub>3</sub> or if the remaining palladium is subsequently removed, using a metal scavenger).

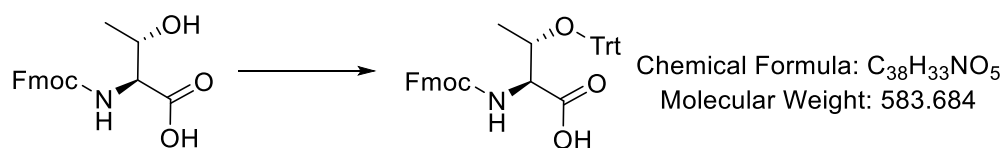
**General Procedure F (thiazoline oxidation):** The purified heterocyclic thiazoline building block is dissolved in dry DCM (10 mL per gram of starting material). MnO<sub>2</sub> with a maximum particle size of 10 µm is activated by heating up to at least 120 °C for 30 hours, followed by additional heating under vacuum. The activated MnO<sub>2</sub> (10 eq) is added to the thiazoline and the solution is stirred for at least 2 days (higher yield is obtained after 4 days), if desired the progress can be monitored via TLC or mass-spectrometric methods. After completion the MnO<sub>2</sub> is removed by filtration through a fritted glass filled with a thin layer of celite and silica gel. After concentration *in vacuo* the crude product is purified by flash chromatography (gradient 15% EE/PE -> 40% EE/PE) to afford the thiazole as a yellow oil, slowly solidifying to a white substance.

**Fmoc-L-*allo*-threonine:**

The unprotected amino acid H<sub>2</sub>N-*α*-Thr-OH (4.0 g, 33.6 mM) is dissolved in 75 mL of a 9% Na<sub>2</sub>CO<sub>3</sub> and the solution is cooled to 0°C using an ice bath. N-(9-Fluorenylmethoxycarbonyloxy) succinimide (10.2g, 30.2 mM) is dissolved in DMF (60 mL) and added dropwise to the amino acid solution. The mixture is stirred at room temperature for 2 hours and diluted with ice-cold water. The aqueous solution is washed with Et<sub>2</sub>O (60 mL), EtOAc (3 x 80 mL) and subsequently acidified to pH 2 at 0°C using conc. HCl and extracted with 5 x 100 mL EtOAc. The combined organic layers are washed (using brine, 1M HCl, water and brine), separated, dried with Na<sub>2</sub>SO<sub>4</sub> and concentrated *in vacuo* to provide Fmoc-*α*-Thr-OH (7.78 g, 22.8 mM, 68%) as a white solid, which is used without further purification.

<sup>1</sup>H NMR (200 MHz, RT, Chloroform-*d*) δ = 7.80 (d, *J*=7.2, 2H), 7.63 (d, *J*=7.2, 2H), 7.46 (d, *J*=7.3, 2H), 7.37 (d, *J*=7.1, 2H), 4.47 (s, 2H), 4.15 (q, *J*=7.2, 2H), 3.76 (q, *J*=7.0, 3H), 2.15 (s, 1H), 1.28 (d, *J*=7.1, 3H);

**ESI-MS:** calc. for C<sub>19</sub>H<sub>19</sub>NO<sub>5</sub>Na : 364.12 m/z (M+Na<sup>+</sup>), found: 364.13 m/z (M+Na<sup>+</sup>).

**Fmoc-L-*allo*-threonine(OTrt):**

**Fmoc-aThr-OH** (5.4 g, 15.82 mmol) and **AgOTf** (10.16 g, 39.6 mmol) are suspended in dry CH<sub>2</sub>Cl<sub>2</sub> (35 mL) and 2,4,6 collidine (3.14 mL, 7.5 mmol) are added at 0°C. Triphenylmethyl chloride (4.41 g, 15.82 mmol) is added, and the red solution is stirred vigorously at room temperature in a Schlenk-flask covered with aluminum foil. After 5 h, the insoluble salts are filtered through a short column of Celite, and the filtrate is washed with sat. aq. NaHCO<sub>3</sub>, 0.1 N aq. HCl and brine. After evaporation of the Solvent, the residue is dissolved in MeOH and stirred overnight to ensure complete deprotection of the trityl ester. Methanol is then removed and the product recrystallized from diethyl ether and hexanes. A final wash with 0.1 N HCl and evaporation of the solvent produced the trityl protected acid (2.4 g, 3.6 mmol, 76%) as a white solid, which is used without further purification.

**<sup>1</sup>H NMR (200 MHz, RT, Chloroform-*d*)** δ 7.77 (s, 2H), 7.56 (d, *J* = 7.2 Hz, 4H), 7.52 – 7.39 (m, 2H), 7.39 – 7.25 (m, 15H), 6.88 (s, 2H), 4.29 (s, 2H), 1.03 (s, 3H).

**ESI-MS:** calc for C<sub>38</sub>H<sub>33</sub>NO<sub>5</sub>: 606.22 m/z (M+Na<sup>+</sup>) found: 606.15 m/z (M+Na<sup>+</sup>)

*Dipeptides (Val-Cys, Ile-Ser, Ile- $\alpha$ Thr)*. For the synthesis of the dipeptides required for the synthesis of the heterocyclic building blocks, the polar amino acid (Cys/Ser/ $\alpha$ Thr) is first allyl protected using allyl alcohol as described in **GP-A** (Coupling). The purified protected peptide is then Fmoc-Deprotected as described in **GP-B** (Fmoc deprotection – amino acids) and used without further purification for a coupling to the desired amino acid as described in **GP-A**. After purification and upon concentration *in vacuo*, the dipeptides are obtained as white foams with yields between 60% and 80%, respective to the starting material and verified using ESI-MS and NMR.

Compound	Formula	Starting material	Yield	ESI-MS Calc.	ESI-MS found
Fmoc-Val-Cys(STrt)-Oallyl	C <sub>45</sub> H <sub>44</sub> NO <sub>5</sub> S	7.5 g (16.6 mMol)	80 %	747.28 m/z (M+Na <sup>+</sup> )	747.17 m/z (M+Na <sup>+</sup> )
Fmoc-Ile- $\alpha$ Thr(OTrt)-Oallyl	C <sub>47</sub> H <sub>48</sub> N <sub>2</sub> O <sub>6</sub>	4.0 g	75 %	759.341 m/z (M+Na <sup>+</sup> )	759.34 m/z (M+Na <sup>+</sup> )
Fmoc-Ile- $\alpha$ Thr-Oallyl	C <sub>28</sub> H <sub>34</sub> N <sub>2</sub> O <sub>6</sub>	4.0 g	55 %	517.231 m/z (M+Na <sup>+</sup> )	517.23 m/z (M+Na <sup>+</sup> ),
Fmoc-Ile-Ser(OTrt)-Oallyl	C <sub>46</sub> H <sub>46</sub> N <sub>2</sub> O <sub>6</sub>	6.0 g	68 %	745.325 m/z (M+Na <sup>+</sup> )	745.33 m/z (M+Na <sup>+</sup> )
Fmoc-Ala-Cys(STrt)-Oallyl	C <sub>43</sub> H <sub>40</sub> NO <sub>5</sub> S	5.0 g	66 %	719.256 m/z (M+Na <sup>+</sup> )	719.23 m/z (M+Na <sup>+</sup> )
Fmoc-Phe-Cys(STrt)-Oallyl	C <sub>49</sub> H <sub>44</sub> NO <sub>5</sub> S	6.0 g	69 %	795.287 m/z (M+Na <sup>+</sup> )	795.26 m/z (M+Na <sup>+</sup> )
Fmoc-Ala- $\alpha$ Thr(OtBu)-Oallyl	C <sub>28</sub> H <sub>34</sub> NO <sub>6</sub>	6.0 g	66 %	531.247 m/z (M+Na <sup>+</sup> )	m/z (M+Na <sup>+</sup> )

**Heterocyclic Building Blocks:** The heterocyclization of all dipeptides is performed following **GP-D** (heterocyclization). After purification the heterocyclic building blocks are obtained as oils with yields between 70% and 80% and characterized by NMR and ESI.



*Fmoc-Val-Thiazoline-Oallyl*. <sup>1</sup>H NMR (200 MHz, RT, Chloroform-d) δ 8.12 (s, 1H), δ 7.88 – 7.73 (d, J=7.4, 2H), 7.66 (d, J = 7.3 Hz, 2H), 7.53 – 7.20 (m, 4H), 6.07 – 5.79 (m, 1H), 5.51 – 5.18 (m, 3H), 4.73 (m, 2H), 4.54 – 4.04 (m, 5H), 3.69 (d, J = 8.3 Hz, 1H), 2.32 (s, 1H), 0.95(m, 6H).

*Fmoc-Ala-Thiazoline-Oallyl* (200 MHz, RT, CDCl<sub>3</sub>): δ = 7.77 (dd, J = 7.0, 1.7 Hz, 2H), 7.61 (d, J = 7.2 Hz, 2H), 7.46 – 7.22 (m, 5H), 6.04 – 5.83 (m, 1H), 5.43 – 5.21 (m, 2H), 4.76 – 4.65 (m, 2H), 4.47 – 4.35 (m, 2H), 4.29 – 4.19 (m, 1H), 3.68 – 3.56 (m, 1H), 1.51 (d, J = 6.9 Hz, 3H) ppm.

**ESI-MS:** calc for C<sub>24</sub>H<sub>24</sub>N<sub>2</sub>O<sub>4</sub>S: 459.135 m/z (M+Na<sup>+</sup>) found: 459.19 m/z (M+Na<sup>+</sup>)

*Fmoc-Phe-Thiazoline-Oallyl* <sup>1</sup>H NMR (200 MHz, RT, CDCl<sub>3</sub>): δ = 7.76 (d, J = 7.4 Hz, 2H), 7.57 – 7.47 (m, 2H), 7.48 – 7.15 (m, 10H), 5.88 – 5.76 (m, 1H), 5.38 – 5.17 (m, 0H), 4.74 – 4.31 (m, 5H), 3.06 (s, 2H), 2.56 (s, 1H) ppm.

*Fmoc-Ile-Thr-methyloxazoline-Oallyl*. <sup>1</sup>H NMR (600 MHz, RT, Chloroform-d) δ = 7.78 – 7.72 (m, 2H), 7.67 – 7.56 (m, 2H), 7.42 – 7.35 (m, 3H), 7.30 (tdd, J=7.4, 5.6, 3.7, 2H), 5.91 (ddt, J=16.5, 11.0, 5.9, 1H), 5.59 (d, J=9.2, 1H), 5.36 – 5.29 (m, 1H), 5.28 – 5.21 (m, 1H), 4.83 (p, J=6.4, 1H), 4.68 – 4.64 (m, 1H), 4.63 (s, 1H), 4.47 – 4.27 (m, 2H), 4.21 (t, J=7.1, 1H), 1.58 – 1.45 (m, 1H), 1.45 – 1.09 (m, 5H), 0.97 – 0.85 (m, 6H), 0.82 (s, 3H).

**ESI-MS:** calc for C<sub>28</sub>H<sub>32</sub>N<sub>2</sub>O<sub>5</sub>: 477.239 (M+H<sup>+</sup>), 499.221 m/z (M+Na<sup>+</sup>) found: 477.22 m/z (M+H<sup>+</sup>), 499.23 m/z (M+Na<sup>+</sup>)

*Fmoc-Ile-Ser-oxazoline-Oallyl*. <sup>1</sup>H NMR (200 MHz, RT, CDCl<sub>3</sub>): δ [ppm]= 7.81 (d, 2H), 7.78 (d, 2H), 7.62 (s, 1H), 7.43 (d, 1H), 7.34 (s, 2H), 5.94 (s, 1H), 5.37 (s, 1H), 5.34 (s, 1H), 4.77 (s, 1H), 4.42 (s, 2H), 4.17 (s, 2H), 4.14 (s, 1H), 3.53 (s, 2H), 2.08 (s, 1H), 1.58 (s, 1H), 1.29 (s, 2H), 1.20 (s, 3H), 0.97 (s, 3H),

**ESI-MS:** calc for C<sub>27</sub>H<sub>30</sub>N<sub>2</sub>O<sub>5</sub>: 485.205 m/z (M+Na<sup>+</sup>) found: 485.27 m/z (M+Na<sup>+</sup>)

*Fmoc-Ala-Thr-oxa-Oallyl*. <sup>1</sup>H NMR (600 MHz, RT, Chloroform-d) δ 7.77 – 7.68 (m, 1H), 7.64 (ddt, J = 12.0, 6.9, 1.4 Hz, 5H), 7.60 – 7.47 (m, 4H), 7.44 (td, J = 7.7, 2.9 Hz, 5H), 7.36 (q, J = 6.0, 4.4 Hz, 1H), 7.27 (t, J = 7.4 Hz, 1H), 4.65 – 4.54 (m, 1H), 4.38 – 4.28 (m, 1H), 2.81 (s, 1H), 2.02

(s, 1H), 1.35 (d, J = 7.0 Hz, 1H), 1.23 (t, J = 7.1 Hz, 1H), 1.20 (d, J = 6.4 Hz, 1H). <sup>13</sup>C NMR (151 MHz, RT, Chloroform-d) δ 171.21, 141.27, 132.56, 132.16, 132.09, 132.08, 132.06, 131.87, 131.56, 128.61, 128.53, 127.71, 127.08, 119.97, 118.75, 68.04, 67.06, 66.07, 60.43, 57.83, 50.54, 47.06, 47.05, 21.09, 20.20, 19.00, 14.23.

**ESI-MS:** calc for C<sub>25</sub>H<sub>26</sub>NO<sub>5</sub>: 457.174 m/z (M+Na<sup>+</sup>) found: 457.23 m/z (M+Na<sup>+</sup>)

*Fmoc-Ala-Ser-oxa-Oallyl*. <sup>1</sup>H NMR (600 MHz, RT, Chloroform-d) δ 7.73 (d, J = 7.6 Hz, 1H), 7.64 (dd, J = 12.0, 7.4 Hz, 7H), 7.53 (t, J = 7.4 Hz, 4H), 7.45 (td, J = 7.6, 2.5 Hz, 7H), 7.37 (q, J = 7.6, 5.6 Hz, 1H), 7.27 (q, J = 6.9 Hz, 1H), 4.64 (t, J = 7.1 Hz, 1H), 4.37 – 4.27 (m, 0H), 2.65 (s, 2H), 1.34 (d, J = 6.9 Hz, 1H). <sup>13</sup>C NMR (151 MHz, RT, Chloroform-d) δ 132.31 – 132.05 (m), 131.49, 129.69, 128.62 (d, J = 12.2 Hz), 127.94 (d, J = 2.2 Hz), 127.79, 127.73, 127.26, 127.10 (d, J = 1.8 Hz), 125.15 (d, J = 3.9 Hz), 120.01 (d, J = 6.0 Hz), 67.06 (d, J = 11.3 Hz), 66.22, 62.70, 18.75.

**ESI-MS:** calc for C<sub>24</sub>H<sub>24</sub>NO<sub>5</sub>: 443.158 m/z (M+Na<sup>+</sup>) found: 443.19 m/z (M+Na<sup>+</sup>)

**Thiazoles:** The thiazoline building blocks were further oxidized to the respective thiazoles as described in **GP-F**. After purification, the building blocks were characterized using NMR and ESI-MS.

*Fmoc-Val-Thiazole-Oallyl* <sup>1</sup>H NMR (200 MHz, RT, chloroform-d) δ = 8.14 (s, 1H), 7.80 (d, J=7.4, 2H), 7.63 (d, J=7.3, 2H), 7.52 – 7.29 (m, 4H), 6.23 – 5.93 (m, 1H), 5.59 (d, J=9.2, 1H), 5.45 (dd, J=17.2, 1.5, 1H), 5.34 (dd, J=10.3, 1.4, 1H), 4.89 (dt, J=5.8, 1.4, 2H), 4.49 (d, J=6.9, 2H), 4.27 (t, J=7.2, 1H), 2.54 – 2.37 (m, 1H), 1.38 – 1.12 (m, 1H), 0.98 (dd, J=6.7, 3.4, 6H).

**ESI-MS:** calc. for C<sub>26</sub>H<sub>26</sub>N<sub>2</sub>O<sub>4</sub>S: 485.151 m/z (M+Na<sup>+</sup>) found: 463.16 m/z (M+H<sup>+</sup>), 485.15 m/z (M+Na<sup>+</sup>)

*Fmoc-Ala-Thiazole-Oallyl* <sup>1</sup>H NMR (600 MHz, RT, Chloroform-d) δ 8.09 (s, 1H), 7.75 (d, J = 7.6 Hz, 2H), 7.58 (s, 2H), 7.38 (s, 2H), 7.30 (s, 2H), 6.02 (ddt, J = 16.5, 10.9, 5.9 Hz, 1H), 5.48 (d, J = 7.8 Hz, 1H), 5.39 (dd, J = 17.0, 1.7 Hz, 1H), 5.28 (dd, J = 10.4, 1.4 Hz, 1H), 5.16 (d, J = 7.9 Hz, 1H), 4.84 (d, J = 5.9 Hz, 2H), 4.47 (dd, J = 10.6, 6.7 Hz, 1H), 4.39 (s, 1H), 4.20 (s, 1H), 1.64 (d, J

= 7.0 Hz, 3H), 1.28 – 1.20 (m, 1H), 0.81 (s, 1H). <sup>13</sup>C NMR (151 MHz, RT, Chloroform-d) δ 160.89, 141.35, 131.84, 127.74, 120.03, 127.59, 127.10, 77.22, 66.96, 66.06.

**ESI-MS:** calc. for C<sub>24</sub>H<sub>22</sub>N<sub>2</sub>O<sub>4</sub>S: 457.120 m/z (M+Na<sup>+</sup>) found: 457.18 m/z (M+Na<sup>+</sup>)

*Fmoc-Phe-Thiazole-Oallyl* <sup>1</sup>H NMR (600 MHz, RT, Chloroform-d) δ 7.74 (d, J = 7.4 Hz, 1H), 7.50 (s, 0H), 7.49 (dd, J = 20.7, 7.5 Hz, 1H), 7.41 – 7.13 (m, 9H), 7.19 (s, 5H), 5.36 – 5.17 (m, 1H), 4.86 (d, J = 5.9 Hz, 0H), 4.61 – 4.49 (m, 1H), 4.42 (s, 1H), 4.37 (ddd, J = 29.6, 11.6, 6.8 Hz, 1H), 4.30 – 4.23 (m, 0H), 4.20 – 4.07 (m, 1H), 3.32 (s, 0H), 3.05 (s, 1H), 2.52 (s, 1H), 2.03 (s, 1H), 1.29 – 1.17 (m, 1H), 0.81 (s, 0H). <sup>13</sup>C NMR (151 MHz, RT, Chloroform-d) δ 170.47, 169.71, 141.33, 131.84, 131.34, 129.69, 129.46, 129.38, 128.75, 128.04, 128.03, 127.93, 127.79, 127.72, 127.07, 126.92, 120.02, 119.98, 118.86, 67.14, 66.31, 60.43, 51.48, 21.09.

**ESI-MS:** calc. for C<sub>30</sub>H<sub>26</sub>N<sub>2</sub>O<sub>4</sub>S: 533.151 m/z (M+Na<sup>+</sup>) found: 533.15 m/z (M+Na<sup>+</sup>)

***Tetrapeptides/Dimers of the building blocks.*** The heterocyclic building blocks are deprotected on one side (one N-terminally following **GP-C**, one O-terminally following **GP-E**) and after the described purification coupled to each other following **GP-A** (it is worth mentioning, that better easier purification and better yields were achieved when deprotecting the thiazole building block HC at the O-terminus to obtain the free acid and the respective oxazoline at the N-terminus). This yields the dimeric compounds as white foams in yields between 45% and 75%.

*Fmoc-Val-Thia-Ile-MeOxa-Oallyl (Ascidacyclamide Dimer):* Yield: 75%

**ESI-MS:** calc. for C<sub>36</sub>H<sub>42</sub>N<sub>4</sub>O<sub>6</sub>S: 681.272 m/z (M+Na<sup>+</sup>) found: 681.26 m/z (M+Na<sup>+</sup>)

*Fmoc-Val-Thia-Ile-Oxa-Oallyl (AscOM Dimer):* Yield: 45%

**ESI-MS:** calc. for C<sub>35</sub>H<sub>40</sub>N<sub>4</sub>O<sub>6</sub>S: 667.257 m/z (M+Na<sup>+</sup>) found: 667.24 m/z (M+Na<sup>+</sup>)

***Octapeptides/Tetramers.*** The di-heterocyclic dimers were deprotected on both sides, first the allyl group is removed following **GP-E**, then the Fmoc-group is removed following **GP-C**.

The dimer is dissolved in dry acetonitrile (10 mL per 100 mg educt), subsequently FDPP (2 Eq) and EDIPA (E eq) are added, and the solution is left stirring at room temperature for at least 3 days or until TLC shows completion of the reaction. The solvent is evaporated, and the residue dissolved in EtOAc, washed with water and brine, dried over  $\text{MgSO}_4$  and concentrated *in vacuo*. The crude product is purified by flash chromatography (gradient 20% EE/PE  $\rightarrow$  50% EE/PE, followed by DCM/EtOAc/MeOH 70/25/5) to yield the desired cyclodimerized octapeptide as an amorphous white solid with yields of 10-41 %.

*Ascidiacyclamide (Cyclotetramer)*. 328 mg (0.83 mMol) of the deprotected tetrapeptide were used. 132 mg (0.17 mMol, 41% yield) were obtained as white amorphous solid with a yellow hue which was characterized by NMR and ESI-MS.

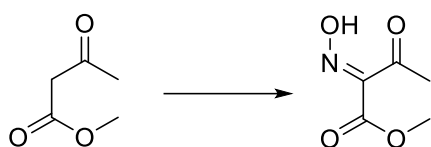
$^1\text{H-NMR}$  (600 MHz, RT, Chloroform- $d$ )  $\delta$  8.14 (s, 2H,  $\text{N}_{\text{Thia}}$ ), 7.71 (dd,  $J = 11.4, 6.5$  Hz, 2H), 7.64 – 7.50 (m, 1H), 5.28 – 5.12 (m, 1H), 5.11 (s, 1H), 4.54 (d,  $J = 6.0$  Hz, 1H), 4.47 (ttt,  $J = 20.4, 14.1, 6.1$  Hz, 1H), 4.26 (dt,  $J = 17.5, 6.6$  Hz, 1H), 3.51 – 3.37 (m, 2H), 2.99 – 2.79 (m, 2H), 2.64 – 2.44 (m, 2H), 1.37 – 1.04 (m, 12H), 0.97-0.70 (m, 24H).

$^{13}\text{C NMR}$  (151 MHz, RT, Chloroform- $d$ )  $\delta$  169.77, 169.22, 168.37, 160.75, 131.50, 131.32, 131.29, 131.26, 129.61, 129.60, 129.58, 129.55, 129.53, 129.49, 129.48, 129.46, 129.12, 128.21, 128.18, 128.15, 128.11, 128.10, 128.08, 128.07, 128.06, 128.03, 127.93, 127.26, 127.07, 126.95, 126.93, 126.91, 126.86, 126.83, 120.35, 119.98, 119.00, 118.95, 118.83, 118.74, 118.47, 118.37, 79.90, 70.61, 69.39, 51.42, 48.51, 31.05, 30.23, 29.98, 20.31, 19.86, 18.63.

**ESI-MS:** calc. for  $\text{C}_{36}\text{H}_{53}\text{N}_8\text{O}_6\text{S}_2$  757.353 (M+H); measured: 757.357 (M+H))

*Patellamide PB (Cyclotetramer)*. 110 mg (0.29 mMol) of the deprotected tetrapeptide were used. 29 mg (0.04 mMol, 28% yield) were obtained as a white, amorphous solid, which was characterized by ESI-MS.

**ESI-MS:** calc. for  $\text{C}_{36}\text{H}_{53}\text{N}_8\text{O}_6\text{S}_2$  747.332 (M+  $\text{H}_3\text{O}^+$ ), measured: 747.44 (M+  $\text{H}_3\text{O}^+$ ).

**(E)-methyl-2-(hydroxyamino)-3-oxobutanoate (NN1):**Chemical Formula: C<sub>5</sub>H<sub>7</sub>NO<sub>4</sub>

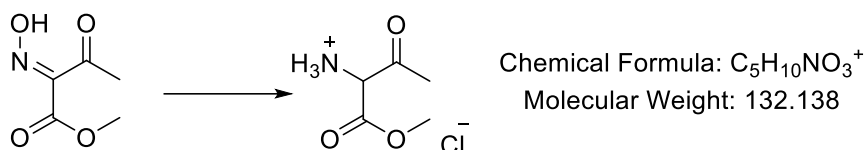
Molecular Weight: 145.114

A solution of 100 g methyl acetoacetate (0.86 mol, 1eq) and 140 mL glacial acetic acid is cooled in an ice bath to -5°C or below. An aqueous solution of 148.5g (2.15 mol, 2.5 eq) of sodium nitrate is slowly added to the solution using a dropping funnel, keeping the temperature below 0°C. The reaction mixture is stirred for three hours at 0-5°C and for 1.5 hours at room temperature\* and afterwards is poured on 800g ice. The aqueous phase is extracted 3-4 times with 400 mL of diethyl ether. The organic extract is washed with saturated NaHCO<sub>3</sub> solution until a neutral pH is reached. The organic phase is then dried over MgSO<sub>4</sub> and concentrated *in vacuo* to yield 88g (71% yield) of a viscous yellow oil which after azeotropic removal of remaining solvent can slowly solidify.

<sup>1</sup>H NMR (200 MHz, RT, Chloroform-*d*) δ 10.63 (bs, 1H, OH), 3.88 (s, 3H, OCCH<sub>3</sub>), 2.41 (s, 3H, OCH<sub>3</sub>). <sup>13</sup>C NMR (101 MHz, RT, Methanol-*d*<sub>4</sub>) δ 196.91, 54.55, 27.92.

---

\* It should be noted that in some cases after hours of reaction time the reaction mixture can start heating up while producing nitrous gasses. In this case the cooling and extraction step should start immediately.

**1-methoxy-1,3-dioxobutan-2-aminium chloride (NN2):**

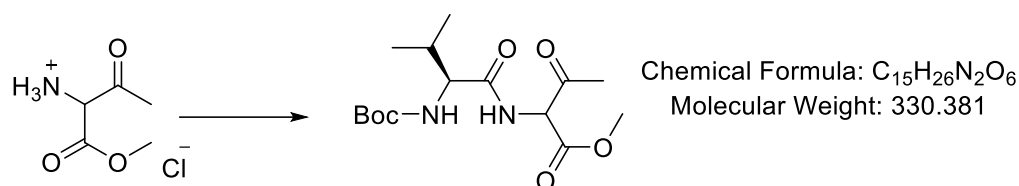
Due to limited availability of HCl dissolved in MeOH two different approaches were used<sup>†</sup> (the 1.8M solution of HCl is prepared by dissolving HCl gas in methanol and determining the molarity by titration):

- 38.5 g of **NN1** (0.27 mol, 1 eq) are dissolved in 500 mL of EtOH under Ar atmosphere. 20g of Palladium on active charcoal (10%) are added. Then 400 mL of 1.8 M HCl in methanol are added dropwise.
- 40 g of **NN1** (0.28 mol, 1 eq) are dissolved in 500 mL of MeOH under Ar atmosphere. 20g of Palladium on active charcoal (10%) are added. Then 210 mL 2.5 M HCl in ethanol are added dropwise.

The black suspension is stirred rapidly with a large stirrer fish under H<sub>2</sub> atmosphere for at least 48 h (until TLC shows complete reaction). The reaction mixture is filtered over celite and evaporation of the solvent a bright yellow crude product is obtained which is recrystallized at low temperatures in ethyl acetate and subsequently washed with cold DCM. In a) 35.1g (78% yield), in b) 36 g (75% yield) were obtained as a pure white, crystalline solid, which needs to be stored under Ar atmosphere.

<sup>1</sup>H NMR (400 MHz, RT, DMSO-*d*<sub>6</sub>) δ 9.06 (s, 3H, NH<sub>3</sub>), 5.30 (s, 2H, CH<sub>2</sub>N), 3.81 (s, 3H, OCH<sub>3</sub>), 2.40 (s, 3H, OCCH<sub>3</sub>). <sup>13</sup>C NMR (101 MHz, RT, DMSO-*d*<sub>6</sub>) δ 197.25, 166.28, 61.72, 54.15, 28.65.

<sup>†</sup> MeOH as major solvent component is important for the kinetics of the reaction, otherwise EtOH would be easier.

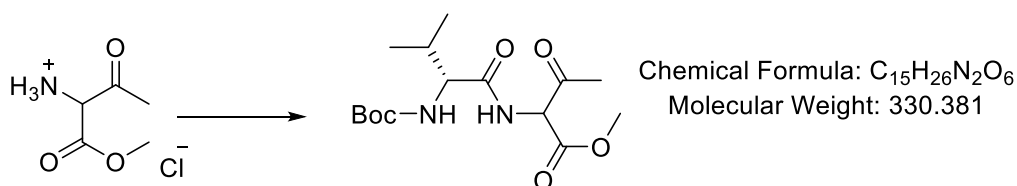
**Methyl-2((S)-tert-butoxycarbonylamino)-3-methylbutanamido)-3-oxobutanone (NN3s)**

20 g of (S)-Boc-Val-OH (92 mmol, 1 eq) are dissolved in 500 mL THF and after addition of one equivalent of NMM (6.52g, 92 mmol, 1.0 eq) the solution is cooled to -25°C using an ethanol cooling bath. Isobutyl chloroformate (13.06 g, 92 mmol, 1 eq) is added while maintaining the solution at -25°C and after 35 min **NN2** is added (15.36 g, 92 mmol, 1eq) followed by another equivalent of NMM (6.52g, 92 mmol, 1.0 eq). The solution is stirred for another 20 hours, while the solution is allowed to warm up to room temperature. After evaporation of the solvent *in vacuo* the residue is dissolved in ethyl acetate and washed with water and brine. The organic phase is dried over MgSO<sub>4</sub> and concentrated *in vacuo*. The crude product is recrystallized in ethyl acetate leading to 19.91 g (65% yield) of **NN3s** is obtained as white crystals.

**<sup>1</sup>H NMR: (200 MHz, RT, CDCl<sub>3</sub>):** δ = 0.91 (d, 3H, CH(CH<sub>3</sub>)<sub>2</sub>, <sub>3</sub>J<sub>H-H</sub> = 6.8 Hz); 0.98 (d, 3H, CH(CH<sub>3</sub>)<sub>2</sub>, <sub>3</sub>J<sub>H-H</sub> = 6.8 Hz); 1.46 (s, 9H, C(CH<sub>3</sub>)<sub>3</sub>), 2.18 – 2.28 (m, 1H, CH(CH<sub>3</sub>)<sub>2</sub>), 2.39 (s, 3H, COCH<sub>3</sub>), 3.82 (s, 3H, CO<sub>2</sub>CH<sub>3</sub>), 4.06 (m, 1H, NHCHCO), 4.95 - 4.99 (m, 1H, CO<sub>2</sub>NH), 5.24 (d, 1H, BocNHCHCO), 7.09-7.12, (m, 1H, NH) ppm.,

**ESI-MS:** calc for C<sub>15</sub>H<sub>26</sub>N<sub>2</sub>O<sub>6</sub>: 353.169 m/z (M+Na<sup>+</sup>) found: 353.16 m/z (M+Na<sup>+</sup>)

### Methyl-2((R)-tert-butoxycarbonylamino)-3-methylbutanamido)-3-oxobutanone (NN3r)

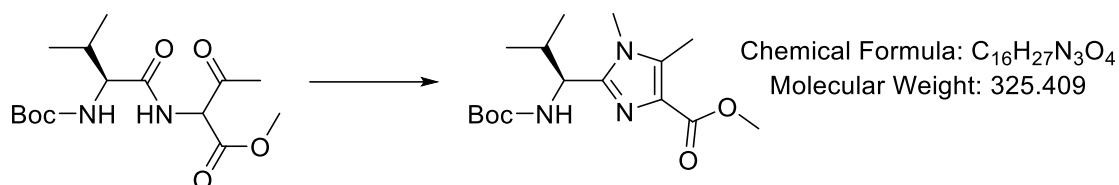


8.54 g of (*R*)-Boc-Val-OH (39.3 mmol, 1 eq) are dissolved in 250 mL THF and after addition of one equivalent of NMM (4.1, 40 mmol, 1.0 eq) the solution is cooled to -25°C using an ethanol cooling bath. Isobutyl chloroformate (5.46 g, 40 mmol, 1 eq) is added while maintaining the solution at -25°C and after 35 min **NN2** is added (6.46 g, 39 mmol, 1eq) followed by another equivalent of NMM (4.1 g, 40 mmol, 1.0 eq). The solution is stirred for another 20 hours, while the solution is allowed to warm up to room temperature. After evaporation of the solvent *in vacuo* the residue is dissolved in ethyl acetate and washed with water and brine. The organic phase is dried over MgSO<sub>4</sub> and concentrated *in vacuo*. The crude product is recrystallized in ethyl acetate leading to 9.38 g (71% yield) of **NN3r** is obtained as white crystals.

**<sup>1</sup>H NMR: (200 MHz, RT, CDCl<sub>3</sub>):** δ = 0.92 (d, 3H, CH(CH<sub>3</sub>)<sub>2</sub>, 3JH-H = 6.9 Hz); 0.98 (d, 3H, CH(CH<sub>3</sub>)<sub>2</sub>, 3JH-H = 6.8 Hz); 1.45 (s, 9H, C(CH<sub>3</sub>)<sub>3</sub>), 2.13 – 2.27 (m, 1H, CH(CH<sub>3</sub>)<sub>2</sub>), 2.39 (s, 3H, COCH<sub>3</sub>), 3.82 (s, 3H, CO<sub>2</sub>CH<sub>3</sub>), 4.0 - 4.12 (m, 1H, NHCHCO), 4.89 – 5.10 (m, 1H, CO<sub>2</sub>NH), 5.23 (d, 1H, BocNHCHCO), 6.98-7.13, (m, 1H, NH) ppm.,

**ESI-MS:** calc for C<sub>15</sub>H<sub>26</sub>N<sub>2</sub>O<sub>6</sub>: 353.169 m/z (M+Na<sup>+</sup>) found: 353.17 m/z (M+Na<sup>+</sup>)



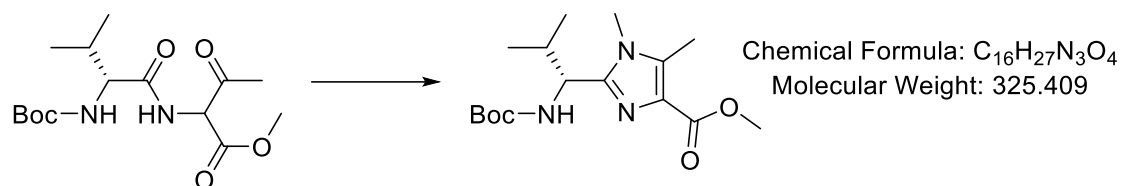
**Methyl-(S)-2-(1-((tert-butoxycarbonyl)amino)-2-methylpropyl)-1,5-dimethyl-1H-imidazole-4-carboxylate (NN4s):**

**NN3s** (13.32g, 39.6 mmol, 1eq) is dissolved in xylenes (400 mL) at room temperature. Glacial acetic acid (25mL, 432 mmol) and NH<sub>2</sub>Me 8M in MeOH (17 mL, 137.7 mMol, 3 eq) are added. The solution is stirred at 165°C with azeotropic removal of water, using a Dean-Stark-apparatus for at least 8 hours (until TLC shows completion of the reaction). The reaction mixture is cooled to room temperature and the solvent evaporated *in vacuo*. The residue is dissolved in ethyl acetate, washed with saturated NaHCO<sub>3</sub> and brine and dried over MgSO<sub>4</sub>. After evaporation of the solvent *in vacuo* the crude product is purified using column chromatography (gradient PE/EE 25%→40%) providing 7.1g (56%) of **NN4s** as a white solid.

**<sup>1</sup>H NMR: (200 MHz, RT, CDCl<sub>3</sub>):** δ = 0.81 (d, 3H, CH(CH<sub>3</sub>)<sub>2</sub>, <sub>3</sub>J<sub>H-H</sub> = 6.6 Hz); 1.00 (d, 3H, CH(CH<sub>3</sub>)<sub>2</sub>, <sub>3</sub>J<sub>H-H</sub> = 6.5 Hz); 1.38 (s, 9H, C(CH<sub>3</sub>)<sub>3</sub>), 2.12 – 2.30 (m, 1H, CH(CH<sub>3</sub>)<sub>2</sub>), 2.51 (s, 3H, imiCH<sub>3</sub>), 3.55 (s, 3H, CO<sub>2</sub>CH<sub>3</sub>), 3.86 (s, 3H, NCH<sub>3</sub>), 4.51 (t, 1H, NHCH, <sub>3</sub>J<sub>H-H</sub> = 9.4Hz), 5.30 (bs, 1H, NH) ppm.,

**ESI-MS:** calc for C<sub>16</sub>H<sub>27</sub>N<sub>3</sub>O<sub>4</sub>: 326.208 m/z (M+H<sup>+</sup>) found: 326.25 m/z (M+H<sup>+</sup>)

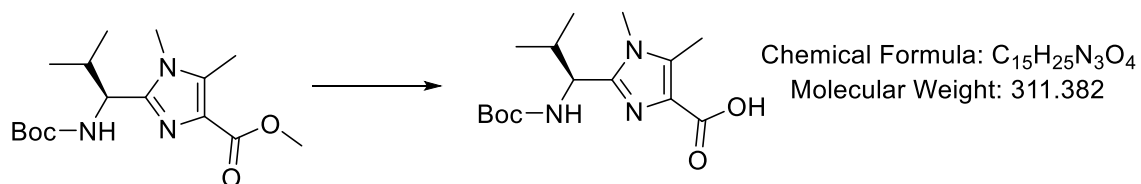
**Methyl-(R)-2-(1-((tert-butoxycarbonyl)amino)-2-methylpropyl)-1,5-dimethyl-1H-imidazole-4-carboxylate (NN4r):**



**NN3e** (11g, 33.3 mmol, 1eq) is dissolved in xylenes (400 mL) at room temperature. Glacial acetic acid (21.5mL, 375 mmol) and NH<sub>2</sub>Me 9.8 M in MeOH (15 mL, 120 mMol, 3 eq) are added. The solution is stirred at 165°C with azeotropic removal of water, using a Dean-Stark-apparatus for at least 8 hours (until TLC shows completion of the reaction). The reaction mixture is cooled to room temperature and the solvent evaporated *in vacuo*. The residue is dissolved in ethyl acetate, washed with saturated NaHCO<sub>3</sub> and brine and dried over MgSO<sub>4</sub>. After evaporation of the solvent *in vacuo* the crude product is purified using column chromatography (gradient PE/EE 25%→40%) providing 6.0g (54%) of **NN4s** as a white solid.

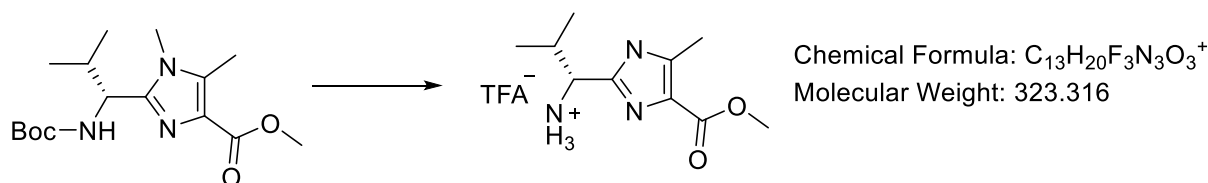
**<sup>1</sup>H NMR: (200 MHz, RT, CDCl<sub>3</sub>):** δ = 0.83 (d, 3H, CH(CH<sub>3</sub>)<sub>2</sub>, <sup>3</sup>J<sub>H-H</sub> = 6.6 Hz); 1.01 (d, 3H, CH(CH<sub>3</sub>)<sub>2</sub>, <sup>3</sup>J<sub>H-H</sub> = 6.5 Hz); 1.40 (s, 9H, C(CH<sub>3</sub>)<sub>3</sub>), 2.11 – 2.32 (m, 1H, CH(CH<sub>3</sub>)<sub>2</sub>), 2.53 (s, 3H, imiCH<sub>3</sub>), 3.56 (s, 3H, CO<sub>2</sub>CH<sub>3</sub>), 3.88 (s, 3H, NCH<sub>3</sub>), 4.53 (t, 1H, NHCH, <sup>3</sup>J<sub>H-H</sub> = 9.4Hz), 5.34 (bs, 1H, NH) ppm.

**ESI-MS:** calc for C<sub>16</sub>H<sub>27</sub>N<sub>3</sub>O<sub>4</sub>: 326.208 m/z (M+H<sup>+</sup>) found: 326.25 m/z (M+H<sup>+</sup>)

**(S)-2-(1-(tert-butoxycarbonylamino)-2-methylpropyl)-1,5-dimethyl-imidazole-4-carboxylic acid (NN4sOH):**

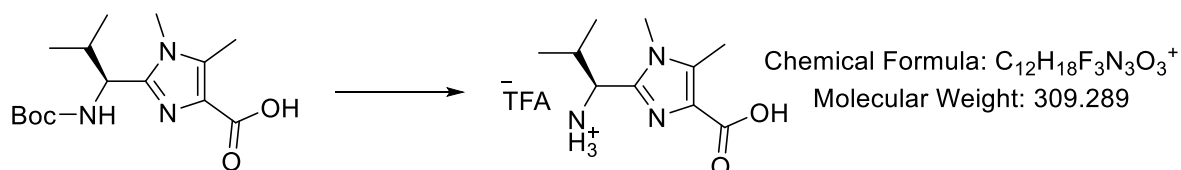
The protected acid **NN4s** (7.1g, 21.8 mmol, 1eq) is dissolved in a mixture of methanol and dioxane (10/7) to a concentration of 0.08 M. The solution is cooled down to 0°C and 2M NaOH (218mmol, 10 eq) are added slowly. The reaction is stirred until the reaction control by TLC/MS shows a completed reaction. Brine and 1M HCl are added until a pH of 1 is reached). The reaction mixture is extracted repeatedly with DCM, the organic layers are combined, dried with MgSO<sub>4</sub>, and concentrated *in vacuo*. After repeated azeotropic removal of the remaining dioxane with EtOAc the acid is obtained as a white solid in quantitative yield (6.6g, 97% yield).

**1-(4-methoxycarbonyl-1,5-dimethyl-imidazole-2-yl)-(R)-2-methylpropan-1-aminium trifluoro acetate (NNr04NH):**



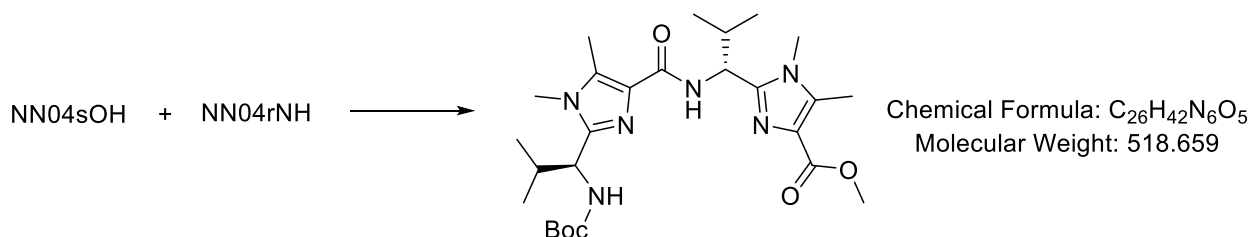
The Boc-protected building block **NN04r** (3.0g, 9.25 mmol, 1.0 eq) is dissolved in 100mL DCM to obtain a 0.1M solution, which is cooled to 0°C. TFA (25 mL) is added and the solution is stirred for 30 minutes at 0° C and for at another 4 hours at room temperature. The mixture is concentrated *in vacuo* and the remaining TFA is azeotropically removed with EtOAc. The resulting salt is washed with cold DCM (-28°C) to obtain the solid product (2.85 g, 95% yield).

**(S)-1-(4-carboxy-1,5-dimethyl-1H-imidazol-2-yl)-2-methylpropan-1-aminium trifluoro acetate (NN04sdp):**



The Boc-protected building block **NN04sOH** (3.0g, 9.25 mmol, 1.0 eq) is dissolved in 100mL DCM to obtain a 0.1M solution, which is cooled to 0°C. TFA (25 mL) is added and the solution is stirred for 30 minutes at 0° C and for at another 4 hours at room temperature. The mixture is concentrated *in vacuo* and the remaining TFA is azeotropically removed with EtOAc. The resulting salt is washed with cold DCM (-28°C used) to obtain the solid product (2.88 g, 96% yield).

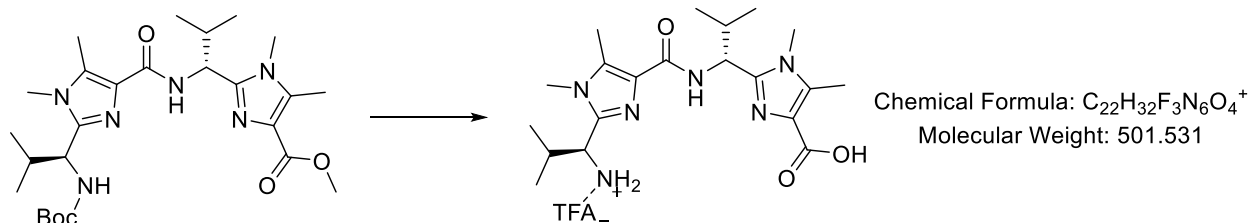
**Methyl-2-((R)-1-(2-((S)-1-((tert-butoxycarbonyl)amino)-2-methylpropyl)-1,5-dimethyl-1H-imidazole-4-carboxamido)-2-methylpropyl)-1,5-dimethyl-1H-imidazole-4-carboxylate (NNrsdi):**



**NN04rOH** (1.5 g, 4.82 mmol, 1.0 eq.) and **NN04sNH** (2.2 g, 8.25 mmol, 1.7 eq.), are dissolved in MeCN (70 mL) and cooled to 0°C and FDPP (1.92 g, 4.9 mmol, 1.1 eq.) is added. To the stirring solution DIPEA (5,03 mL, 29.0 mmol, 6.0 eq.) is added and the reaction mixture is stirred at room temperature for 24 h. After evaporation of the solvent *in vacuo* the crude product is redissolved in EtOAc (100mL) and washed with water and brine, dried over MgSO<sub>4</sub> and concentrated *in vacuo*. The product is purified by column chromatography (PE:EtOAc:DCM:MeOH). Das Dimer (12) (800 mg, 1.5 mmol, 31%) and is obtained as a bright yellow solid.

**ESI-MS:** calc for C<sub>26</sub>H<sub>42</sub>N<sub>6</sub>O<sub>5</sub>: 541.311 m/z (M+H<sup>+</sup>) found: 541.32 m/z (M+Na<sup>+</sup>)

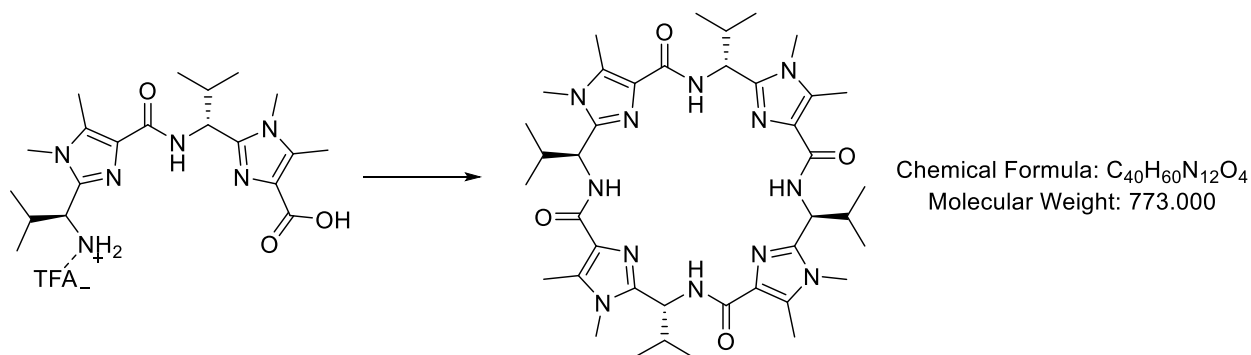
**(S)-1-(4-(((R)-1-(4-carboxy-1,5-dimethyl-1H-imidazol-2-yl)-2-methylpropyl)carbamoyl)-1,5-dimethyl-1H-imidazol-2-yl)-2-methylpropan-1-aminium (NNrsdidp):**



The Dimer **NNrsdidp** (800 mg, 1.54 mmol, 1.0 eq.) is dissolved in MeOH/Dioxane (10/7, 23.7mL) and the stirring solution is cooled to 0°C. A solution of NaOH (5M, 6.3mL, 15 eq) is slowly added, the solution is then stirred under reflux at 80°C for 15 hours. Brine and HCl (1M) are added until a pH of 2 is reached. The reaction mixture is extracted with DCM (3x 50mL) and the organic phase is washed with brine (3x50 mL), dried over MgSO<sub>4</sub>, and concentrated *in vacuo*. The remaining dioxane is removed azeotropically with EtOAc, leading to the free acid with a mediocre yield of 48% as a white foam. The product is confirmed via mass spectrometry (ESI-MS: [M+H<sup>+</sup>] 505.379 m/z) and Boc-protected without further purification.

The free acid is dissolved in dry DCM (5 mL) and cooled to 0 °C. TFA (2.0 mL) is slowly added. After stirring for 30 min at 0 °C and for 4 h at RT, the solvent and TFA is removed under vacuum into a cooling trap. Remaining TFA is azeotropically removed with EtOAc until the product is obtained as a lightly yellow solid with a yield of 82%.

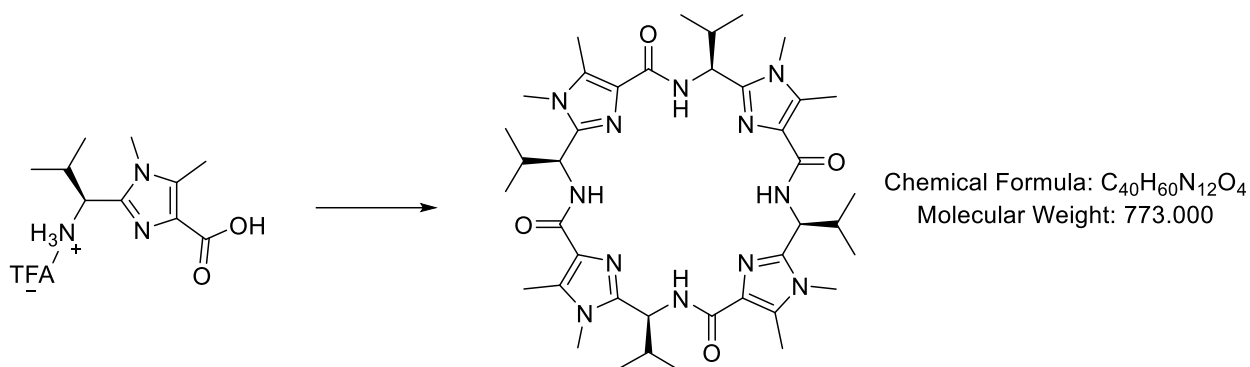
**3,6,10,13,17,20,24,27,29,30,31,32-Dodecaazapentacyclo-[24.2.1.15,8.112,15.119,22]-dotriaconta-5(32),7,12(31),14,19(30),21,26(29),28-octaene-2,9,16,23-tetrone-6,7,13,14,20,21,27,28-octamethyl-4,11,18,25-tetrakis(1-methylethyl)-,(4R,11S,18R,25S) (PANN<sub>RS</sub>):**



To the deprotected Dimer **NNrsdidp** (253 mg, 0.49 mmol, 1.0 eq), dissolved in acetonitrile (10 mL), FDPP (413 mg, 0.98 mmol, 2.0 eq) is added and DIEA (0.5 mL, 2.94 mmol, 6.0 eq) are added at 0°C and the reaction is stirred at room temperature for 5 days. The solvent is removed under vacuum and the residue is dissolved in EtOAc (50 mL) and washed twice with water and brine. The organic layer is dried over MgSO<sub>4</sub> and concentrated onto celite. The crude product is purified by column chromatography (PE:DCM:MeOH) to obtain the product **PANN<sub>RS</sub>** (87 mg, 0.11 mmol, 45%) as a bright foam with an orange hue.

**ESI-MS:** calc for C<sub>40</sub>H<sub>60</sub>N<sub>12</sub>O<sub>4</sub>: 795.476 m/z (M+Na<sup>+</sup>) found: 795.35 m/z (M+Na<sup>+</sup>)

**<sup>1</sup>H NMR** (400 MHz, RT, Chloroform-*d*) δ 7.92 – 7.72 (m, 3H, NH), 5.03 – 4.90 (m, 4H, HCNpept), 3.67 – 3.47 (m, 12H, NCH<sub>3</sub>), 2.59 – 2.37 (m, 12H), 2.20 – 2.11 (m, 4H, CHCH<sub>3</sub>), 1.36 – 1.20 (m, 12H), 1.24 – 1.11 (m, 6H), 0.91 (s, 6H), 0.85 (s, *J* = 6.7 Hz, 6H).

**3,6,10,13,17,20,24,27,29,30,31,32-Dodecaazapentacyclo-[24.2.1.15,8.112,15.119,22]****dotriaconta-5(32),7,12(31),14,19(30),21,26(29),28-octaene-2,9,16,23-tetrone-****,6,7,13,14,20,21,27,28-octamethyl-4,11,18,25-tetrakis(1-methylethyl)-,-(4R,11S,18R,25S)****(PANN<sub>SS</sub>)**

The deprotected building block **NN04ssdp** (600mg, 2mmol) is dissolved in dry acetonitrile together and DIEA (2 mL, 12mmol, 6.0 eq) and FDPP (1.69 g, 4.2 mmol, 2.1 eq) are added to the stirring solution. The mixture is stirred at room temperature for 4 days. Subsequently the solvent is evaporated, the residue redissolved in EtOAc, washed with water and brine, dried over MgSO<sub>4</sub>, and concentrated *in vacuo*. The crude product is purified by column chromatography (EE/PE 15:85) to obtain 135 mg (35% yield) of the desired tetramer, as well as 165 mg of the trimeric byproduct.

**ESI-MS:** calc for C<sub>40</sub>H<sub>60</sub>N<sub>12</sub>O<sub>4</sub>: 773.494 m/z (M+H<sup>+</sup>) found: 773.3529 m/z (M+H<sup>+</sup>)

**<sup>1</sup>H NMR** (600 MHz, RT, Chloroform-*d*) δ 7.80 (dd, *J* = 11.8, 7.6 Hz, 4H, NH<sub>pept</sub>), 4.99 (s, 4H, HCN<sub>pept</sub>), 3.95 – 3.78 (m, 12H, NCH<sub>3</sub>), 2.66-2.53 (m, 12H, ImiCH<sub>3</sub>), 2.4 – 2.20 (m, 4H, CHCH<sub>3</sub>), 1.10-0.99 (m, 12 H), 0.97 – 0.75 (m, 12H).

**<sup>13</sup>C NMR (151 MHz, RT, CDCl<sub>3</sub>):** **<sup>13</sup>C NMR (151 MHz, CDCl<sub>3</sub>) δ 172.40, 143.79, 131.52, 129.49, 96.50, 77.22, 77.02, 76.81, 53.07, 30.57, 19.90, 18.81.**



## 8. References

- [1] P. Baur, M. Kühl, P. Comba, L. Behrendt, *Mar. Drugs*. **2022**, *20*.
- [2] P. Comba, N. Dovalil, L. R. Gahan, G. Haberhauer, G. R. Hanson, C. J. Noble, B. Seibold, P. Vadivelu, *Chem. Eur. J.* **2012**, *18*, 2578-2590.
- [3] J. Koehnke, A. Bent, W. E. Houssen, D. Zollman, F. Morawitz, S. Shirran, J. Vendome, A. F. Nneoyiegbe, L. Trembleau, C. H. Botting, M. C. Smith, M. Jaspars, J. H. Naismith, *Nat. Struct. Mol. Biol.* **2012**, *19*, 767-772.
- [4] R. Lewin, *Prochloron: A Microbial Enigma*, Springer, Boston, MA, USA, **1989**.
- [5] A. L. van den Brenk, K. A. Byriel, D. P. Fairlie, L. R. Gahan, G. R. Hanson, C. J. Hawkins, A. Jones, C. H. L. Kennard, B. Moubaraki, K. S. Murray, *Inorg. Chem.* **1994**, *33*, 3549-3557.
- [6] P. Baur, P. Comba, G. Velmurugan, *Chem. Eur. J.* **2022**, *28*, e202200249.
- [7] W. E. Houssen, M. Jaspars, *ChemBioChem* **2010**, *11*, 1803-1815.
- [8] M. Heinrich, H. Jiang, F. Scotti, A. Booker, H. Walt, C. Weckerle, C. Maake, *J Pharm Pharmacol* **2021**, *73*, 956-967.
- [9] P. Russo, A. D. Bufalo, M. Fini, *EXCLI Journal* **2015**, 228-237.
- [10] J. Li, C. A. Larregieu, L. Z. Benet, *Chin. J. Nat. Med.* **2016**, *14*, 888-897.
- [11] S. Mathur, C. Hoskins, *Biomed. Rep.* **2017**, *6*, 612-614.
- [12] M. S. Butler, *J. Nat. Prod.* **2004**, *67*, 2141-2153.
- [13] A. R. D. Chris M. Ireland, Jr., Robert A. Newman, and Miles P. Hacker, *J. Org. Chem.* **1981**, 1807-1811.
- [14] N. Lindquist, M. E. Hay, W. Fenical, *Ecol. Monogr.* **1992**, *62*, 547-568.
- [15] B. M. Degnan, C. J. Hawkins, M. F. Lavin, E. J. McCaffrey, D. L. Parry, A. L. van den Brenk, D. J. Watters, *J. Med. Chem.* **1989**, *32*, 1349-1354.
- [16] R. S. J. Allen B. Williams, *Cancer Lett.* **1993**, 97-102.
- [17] E. W. Schmidt, J. T. Nelson, D. A. Rasko, S. Sudek, J. A. Eisen, M. G. Haygood, J. Ravel, *Proc. Natl. Acad. Sci. USA* **2005**, *102*, 7315-7320.
- [18] D. J. F. Christine E. Salomon, *J. Nat. Prod.* **2002**, 689-692.
- [19] E. W. Schmidt, M. S. Donia, *Curr. Opin. Biotechnol.* **2010**, *21*, 827-833.
- [20] L. A. Morris, M. Jaspars, in *Biodivers.*, **2000**, pp. 140-166.
- [21] L. A. Morris, M. Jaspars, J. J. Kettenes-van den Bosch, K. Versluis, A. J. R. Heck, S. M. Kelly, N. C. Price, *Tetrahedron* **2001**, *57*, 3185-3197.
- [22] C. J. Hawkins, *Pure Appl. Chem.* **1988**, *60*, 1267-1270.
- [23] P. Comba, L. R. Gahan, G. R. Hanson, M. Westphal, *Chem. Commun. (Camb)* **2012**, *48*, 9364-9366.
- [24] P. Comba, A. Eisenschmidt, N. Kipper, J. Schiessl, *J. Inorg. Biochem.* **2016**, *159*, 70-75.
- [25] P. Comba, A. Eisenschmidt, L. R. Gahan, D. P. Herten, G. Nette, G. Schenk, M. Seefeld, *Chem. Eur. J.* **2017**, *23*, 12264-12274.

- [26] P. Kott, *Mem. Qd Mus.* **1980**, *20*, 1-47.
- [27] E. Hirose, *Genesis* **2015**, *53*, 121-131.
- [28] E. Hirose, Y. Nozawa, *Zool. Stud.* **2020**, *59*, e19.
- [29] M. Kühl, L. Behrendt, E. Trampe, K. Qvortrup, U. Schreiber, S. M. Borisov, I. Klimant, A. W. Larkum, *Front. Microbiol.* **2012**, *3*, 402.
- [30] I. Koike, M. Yamamuro, P. C. Pollard, *Mar. Freshw. Res.* **1993**, *44*.
- [31] J. C. Kwan, M. S. Donia, A. W. Han, E. Hirose, M. G. Haygood, E. W. Schmidt, *Proc. Natl. Acad. Sci. USA* **2012**, *109*, 20655-20660.
- [32] R. R. Olson, *Mar. Biol.* **1986**, *93*, 437-442.
- [33] P. Kott, *J. Nat. Hist* **2004**, *38*, 2455-2526.
- [34] G. Cox, *New Phytol.* **1986**, *104*, 429-445.
- [35] P. Kott, *Mar. Freshw. Res.* **1962**, *13*.
- [36] R. Gottschaldt, *Abh. Senckenb. Naturforsch. Ges.* **1898**, *24*, 641-660.
- [37] L. Behrendt, A. W. Larkum, E. Trampe, A. Norman, S. J. Sorensen, M. Kühl, *ISME J* **2012**, *6*, 1222-1237.
- [38] D. B. Carlisle, *Proc. Roy. Soc. B* **1968**, *171*, 31-42.
- [39] R. Tzafiri-Milo, T. Benaltabet, A. Torfstein, N. Shenkar, *Front. Mar. Sci.* **2019**, *6*.
- [40] N. Holmes, *J. Exp. Mar. Biol. Ecol.* **1973**, *11*, 1-13.
- [41] E. Hirose, R. Adachi, K. Kuze, *J. Mar. Biolog. Assoc.* **2006**, *86*, 175-179.
- [42] R. R. Olson, R. McPherson, *J. Exp. Mar. Biol. Ecol.* **1987**, *110*, 245-256.
- [43] R. L. Pardy, in *Prochloron: A Microbial Enigma*, **1989**, pp. 19-29.
- [44] N. B. FRAZER, *Herpetol.* **1986**, *42*.
- [45] V. Erb, J. Wyneken, *Front. Mar. Sci.* **2019**, *6*.
- [46] J. W. Schopf, B. M. Packer, *Science* **1987**, *237*, 70-73.
- [47] A. R. Grossman, M. R. Schaefer, G. G. Chiang, J. L. Collier, *Microbiol Rev* **1993**, *57*, 725-749.
- [48] R. Lewin, *Nature* **1976**.
- [49] R. A. Lewin, L. Cheng, *Phycologia* **1975**, *14*, 149-152.
- [50] R. A. Lewin, *Phycologia* **1977**, *16*, 217-217.
- [51] R. A. Lewin, *Phycologia* **1984**, *23*, 203-208.
- [52] J. La Roche, G. W. van der Staay, F. Partensky, A. Ducret, R. Aebbersold, R. Li, S. S. Golden, R. G. Hiller, P. M. Wrench, A. W. Larkum, B. R. Green, *Proc. Natl. Acad. Sci. USA* **1996**, *93*, 15244-15248.
- [53] S. Turner, in *Origins of Algae and their Plastids*, **1997**, pp. 13-52.
- [54] R. A. Lewin, *Ann. N. Y. Acad. Sci.* **1981**, *361*, 325-329.
- [55] E. Stackebrandt, E. Seewaldt, V. J. Fowler, K.-H. Schleifer, *Arch Microbiol* **1982**, *132*, 216-217.
- [56] R. A. Lewin, N. W. Withers, *Nature* **1975**, *256*, 735-737.
- [57] R. A. Lewin, *Nature* **1976**, *261*, 697-698.

- [58] I. F. M. Rumengan, T. M. Kubelaborbir, T. E. Tallei, *Data Brief* **2020**, *29*, 105241.
- [59] H. Swift, G. P. Leser, *J. Phycol.* **1989**, *25*, 751-761.
- [60] M. R. Badger, G. D. Price, *J. Exp. Bot.* **2003**, *54*, 609-622.
- [61] B. P. Kremer, R. Pardy, R. A. Lewin, *Phycologia* **1981**, *21*, 258-263.
- [62] I. Koike, T. Suzuki, *Ecol. Res.* **1996**, *11*, 381-386.
- [63] M. S. Donia, W. F. Fricke, F. Partensky, J. Cox, S. I. Elshahawi, J. R. White, A. M. Phillippy, M. C. Schatz, J. Piel, M. G. Haygood, J. Ravel, E. W. Schmidt, *Proc. Natl. Acad. Sci. USA* **2011**, *108*, E1423-1432.
- [64] V. S. Odintsov, *Endocyt. C. Res.* **1991**, *7*, 253-258.
- [65] T. C. KLINE, R. A. LEWIN, *Symbiosis* **1999**, *26*, 193-198.
- [66] E. W. Schmidt, *Nat. Chem. Biol.* **2008**, *4*, 466-473.
- [67] T. Stokes, *Trends Plant Sci.* **2000**, *5*.
- [68] B. F. Milne, L. A. Morris, M. Jaspars, G. S. Thompson, *J. Chem. Soc., Perkin trans. II* **2002**, 1076-1080.
- [69] Y. I. Toshimasa Ishida, Mitsunobu Doi, Masatoshi Inoue, Yasumasa Hamada, Takayuki Shiori, *Biopolymers* **1992**, *32*, 131-143.
- [70] M. B. K. Francis J. Schmitz, James S. Chang, J. L. Wang, M. Bilayet Hossain, and Dick van der Helm, *J. Org. Chem.* **1989**, *54*, 3463-3472.
- [71] G. Abbenante, D. P. Fairlie, L. R. Gahan, G. R. Hanson, G. K. Pierens, A. L. van den Brenk, *J. Am. Chem. Soc.* **1996**, *118*, 10384-10388.
- [72] T. Ishida, Y. In, F. Shinozaki, M. Doi, D. Yamamoto, Y. Hamada, T. Shioiri, M. Kamigauchi, M. Sugiura, *J. Org. Chem.* **1995**, *60*, 3944-3952.
- [73] Y. In, M. Doi, M. Inoue, T. Ishida, Y. Hamada, T. Shioiri, *Acta Crystallogr C* **1994**, *50 ( Pt 3)*, 432-434.
- [74] A. L. van den Brenk, D. P. Fairlie, G. R. Hanson, L. R. Gahan, C. J. Hawkins, A. Jones, *Inorg. Chem.* **1994**, *33*, 2280-2289.
- [75] M. Gaye, O. Sarr, A. S. Sall, O. Diouf, S. Hadabere, *Bull. Chem. Soc. Ethiop.* **1997**, *11*.
- [76] A. L. van den Brenk, D. P. Fairlie, G. R. Hanson, L. R. Gahan, C. J. Hawkins, A. Jones, *Inorg Chem.* **2002**, *33*, 2280-2289.
- [77] R. Latifi, M. Bagherzadeh, B. F. Milne, M. Jaspars, S. P. de Visser, *J. Inorg. Biochem.* **2008**, *102*, 2171-2178.
- [78] N. Dovalil, Copper(II) Coordination Chemistry of Cyclic Pseudo Hexa- and Octapeptide, PhD thesis, Universität Heidelberg **2010**.
- [79] P. Comba, L. R. Gahan, G. R. Hanson, M. Maeder, M. Westphal, *Dalton Trans.* **2014**, *43*, 3144-3152.
- [80] P. Comba, A. Eisenschmidt, in *Future Directions in Metalloprotein and Metalloenzyme Research* (Eds.: G. Hanson, L. Berliner), Springer International Publishing, Cham, **2017**, pp. 13-32.
- [81] M. Westphal, Cu(II) Complexes of Cyclic Pseudo-Peptides: Carbonic Anhydrase and Phosphatase Activity as Possible Metabolic Functions of Patellamides, PhD thesis, Universität Heidelberg **2013**.

- [82] P. V. Bernhardt, P. Comba, D. P. Fairlie, L. R. Gahan, G. R. Hanson, L. Lötzbeyer, *Chem. Eur. J.* **2002**, *8*, 1527-1536.
- [83] P. Comba, N. Dovalil, G. Haberhauer, K. Kowski, N. Mehrkens, M. Westphal, *Z. anorg. allg. Chem.* **2013**, *639*, 1395-1400.
- [84] C. J. Hawkins, M. F. Lavin, K. A. Marshall, A. L. van den Brenk, D. J. Watters, *J. Med. Chem.* **1990**, *33*, 1634-1638.
- [85] D. E. Williams, R. E. Moore, V. J. Paul, *J. Nat. Prod.* **1989**, *52*, 732-739.
- [86] M. S. Donia, J. Ravel, E. W. Schmidt, *Nat. Chem. Biol.* **2008**, *4*, 341-343.
- [87] M. R. Prinsep, R. E. Moore, I. A. Levine, G. M. Patterson, *J. Nat. Prod.* **1992**, *55*, 140-142.
- [88] S. C. Ronny Banker, *J. Nat. Prod.* **1998**, *61*, 1248-1251.
- [89] F. Jüttner, A. K. Todorova, N. Walch, W. von Philipsborn, *Phytochem.* **2001**, *57*, 613-619.
- [90] U. A. Vered Admi, Shmuel Carmeli, *J. Nat. Prod.* **1996**, *59*, 396-399.
- [91] C. Portmann, J. F. Blom, K. Gademann, F. Juttner, *J. Nat. Prod.* **2008**, *71*, 1193-1196.
- [92] J. Ogino, R. E. Moore, G. M. Patterson, C. D. Smith, *J. Nat. Prod.* **1996**, *59*, 581-586.
- [93] A. v. d. Brenk, An Investigation into the Metal Complexes of Cyclic Peptides Isolated from the Ascidians, *Lissoclinum bistratum* and *Lissoclinum patella*, PhD thesis, University of Queensland, Brisbane **1994**.
- [94] P. Comba, N. Dovalil, G. R. Hanson, G. Linti, *Inorg. Chem.* **2011**, *50*, 5165-5174.
- [95] S. Xie, A. I. Savchenko, M. Kerscher, R. L. Grange, E. H. Krenske, J. R. Harmer, M. J. Bauer, N. Broit, D. J. Watters, G. M. Boyle, P. V. Bernhardt, P. G. Parsons, P. Comba, L. R. Gahan, C. M. Williams, *Eur. J. Org. Chem.* **2018**, *2018*, 1465-1476.
- [96] P. M. Dewick, *Essentials of Organic Chemistry – For Students of Pharmacy, Medicinal Chemistry and Biological Chemistry*, John Wiley & Sons Inc., **2006**.
- [97] S. K. Yasumasa Hamada, and Takayuki Shioiri, *Tetrahedron Lett.* **1985**, *Vol.26*, 3223-3226.
- [98] M. S. Yasumasa Hamada, and Takayuki Shioiri\*, *Tetrahedron Lett.* **1985**, *26*, 5155-5158.
- [99] G. Haberhauer, F. Rominger, *Eur. J. Org. Chem.* **2003**, *2003*, 3209-3218.
- [100] P. García-Reynaga, M. S. VanNieuwenhze\*, *Organic Letters* **2008**, *10*, 4621-4623.
- [101] J. Koehnke, A. F. Bent, W. E. Houssen, G. Mann, M. Jaspars, J. H. Naismith, *Curr. Opin. Struct. Biol.* **2014**, *29*, 112-121.
- [102] E. Oueis, H. Stevenson, M. Jaspars, N. J. Westwood, J. H. Naismith, *Chem. Commun. (Camb)* **2017**, *53*, 12274-12277.
- [103] J. A. McIntosh, M. S. Donia, E. W. Schmidt, *J. Am. Chem. Soc.* **2010**, *132*, 4089-4091.
- [104] J. A. McIntosh, E. W. Schmidt, *ChemBioChem* **2010**, *11*, 1413-1421.
- [105] B. F. Milne, P. F. Long, A. Starcevic, D. Hranueli, M. Jaspars, *Org. Biomol. Chem.* **2006**, *4*, 631-638.
- [106] K. Sivonen, N. Leikoski, D. P. Fewer, J. Jokela, *Appl. Microbiol. Biotechnol.* **2010**, *86*, 1213-1225.
- [107] N. B. Lopanik, K. Clay, *Funct. Ecol.* **2014**, *28*, 328-340.
- [108] S. A. Dyshlovoy, F. Honecker, *Mar. Drugs* **2015**, *13*, 5657-5665.

- [109] M. Jaspars, D. De Pascale, J. H. Andersen, F. Reyes, A. D. Crawford, A. Ianora, *J. Mar. Biolog. Assoc.* **2016**, *96*, 151-158.
- [110] M. S. Butler, A. A. Robertson, M. A. Cooper, *Nat. Prod. Rep.* **2014**, *31*, 1612-1661.
- [111] R. K. Singh, S. P. Tiwari, A. K. Rai, T. M. Mohapatra, *J. Antibiot. (Tokyo)* **2011**, *64*, 401-412.
- [112] A. Shahid, M. Khurshid, B. Aslam, S. Muzammil, H. M. Mehwish, M. S. R. Rajoka, H. F. Hayat, M. H. Sarfraz, M. K. Razzaq, M. A. Nisar, M. Waseem, *J. Basic. Microbiol.* **2022**, *62*, 1125-1142.
- [113] P. Comba, N. Dovalil, L. R. Gahan, G. R. Hanson, M. Westphal, *Dalton Trans.* **2014**, *43*, 1935-1956.
- [114] N. Mehrkens, Phosphatase Activity of Homo- and Heterodinuclear Transition Metal Complexes of Patellamide Derivatives, PhD thesis, Universität Heidelberg **2015**.
- [115] W. Kaim, B. Schwederski, A. Klein, *Bioinorganic Chemistry -- Inorganic Elements in the Chemistry of Life: An Introduction and Guide*, Wiley, **2013**.
- [116] J. S. Lopez, L. Lee, K. R. M. Mackey, *Front. Mar. Sci.* **2019**, *5*.
- [117] L. R. Gahan, R. M. Cusack, *Polyhedron* **2018**, *153*, 1-23.
- [118] P. Comba, R. Cusack, D. P. Fairlie, L. R. Gahan, G. R. Hanson, U. Kazmaier, A. Ramlow, *Inorg. Chem.* **1998**, *37*, 6721-6727.
- [119] W. P., *Chem. Rev.* **1995**, *95*, 2115-2134.
- [120] P. W. a. C. P. Miller, *Tetrahedron Letters* **1992**, *33*, pp. 6267-6270.
- [121] S.-L. Y. a. J. W. Kelly\*, *J. Org. Chem.* **2003**, *68*, 9506-9509.
- [122] S. L. You, H. Razavi, J. W. Kelly, *Angew. Chem. Int. Ed. Engl.* **2003**, *42*, 83-85.
- [123] U. Schmidt, R. Utz, A. Lieberknecht, H. Griesser, B. Potzolli, J. Bahr, K. Wagner, P. Fischer, *Synthesis* **1987**, *1987*, 233-236.
- [124] J. B. H. a. M. S. Hussoin, *J. Org. Chem.* **1989**, *54*, 1144-1149.
- [125] Z. Moussa, *ARKIVOC* **2012**.
- [126] S. M. Mali, M. Ganesh Kumar, M. M. Katariya, H. N. Gopi, *Org. Biomol. Chem.* **2014**, *12*, 8462-8472.
- [127] E. Peterse, N. Meeuwenoord, H. Elst, G. A. Marel, H. S. Overkleeft, D. V. Filippov, *Eur. J. Org. Chem.* **2022**, *2022*.
- [128] R. Sarangi, *Coord. Chem. Rev.* **2013**, *257*, 459-472.
- [129] J. P. Osborne, N. J. Cosper, C. M. Stalhandske, R. A. Scott, J. O. Alben, R. B. Gennis, *Biochem.* **1999**, *38*, 4526-4532.
- [130] J. L. DuBois, P. Mukherjee, T. D. P. Stack, B. Hedman, E. I. Solomon, K. O. Hodgson, *J. Am. Chem. Soc.* **2000**, *122*, 5775-5787.
- [131] P. Baur, P. Comba, L. R. Gahan, C. Scholz, *Aust. J. Chem.* **2022**.
- [132] D. J. Freeman, G. Pattenden, A. F. Drake, G. Siligardi, *J. Chem. Soc., Perkin trans. II* **1998**, 129-136.
- [133] F. T. Edward I. Solomon, \* David E. Root, and Carl A. Brown, *Chem. Rev.* **1994**, 827-856.
- [134] J. K. Kowalska, F. A. Lima, C. J. Pollock, J. A. Rees, S. DeBeer, *Isr. J. Chem.* **2016**, *56*, 803-815.

- [135] E. I. Solomon, *Inorg. Chem.* **2006**, *45*, 8012-8025.
- [136] S. C. Kunene, K. S. Lin, N. V. Mdlovu, W. C. Shih, *Chemosphere* **2021**, *265*, 129067.
- [137] A. Trampczynska, H. Kupper, W. Meyer-Klaucke, H. Schmidt, S. Clemens, *Metallomics* **2010**, *2*, 57-66.
- [138] F. D. V. J. J. Kas, J. J. Rehr, C. D. Pemmaraju, T. S. Tan, *J. Synchrotron Rad.* **2021**.
- [139] S. H. Wright, A. Raab, J. Feldmann, E. Krupp, M. Jaspars, in *Handbook of Marine Natural Products* (Eds.: E. Fattorusso, W. H. Gerwick, O. Tagliatela-Scafati), Springer Netherlands, Dordrecht, **2012**, pp. 861-892.
- [140] C. Urda, R. Fernandez, J. Rodriguez, M. Perez, C. Jimenez, C. Cuevas, *Mar. Drugs* **2017**, *15*.
- [141] G. R. W. Denton, C. Burdon-Jones, *Mar. Pollut. Bull.* **1986**, *17*, 96-98.
- [142] J. O. Nriagu, *Vol. ICA no. N-045*, John Wiley & Sons, New York, NY, USA, **1979**.
- [143] P. A. Yeats, J. A. Campbell, *Mar. Chem.* **1983**, *17*, 43-58.
- [144] L. G. Danielsson, B. Magnusson, S. Westerlund, *Mar. Chem.* **1985**, *17*, 23-41.
- [145] K. H. Coale, K. W. Bruland, *Limnol. Oceanogr.* **1988**, *33*, 1084-1101.
- [146] A. L. van den Brenk, D. P. Fairlie, G. R. Hanson, L. R. Gahan, C. J. Hawkins, A. Jones, *Inorg. Chem.* **1994**, *33*, 2280-2289.
- [147] B. J. Harrison, *Copper Information Sourcebook*, University of British Columbia, Vancouver, BC, Canada, **1998**.
- [148] N. Blossom, *Copper in the ocean environment*, American Chemet Corporation, **2001**.
- [149] A.-H. A. M. Ali, M. A. Hamed, H. A. El-Azim, *Mar. Res.* **2011**, *65*, 67-80.
- [150] S. Takano, M. Tanimizu, T. Hirata, Y. Sohrin, *Nature Comm.* **2014**, *5*, 5663.
- [151] P. Leal, C. L. Hurd, S. G. Sander, E. Armstrong, P. A. Fernandez, T. J. Suhrhoff, M. Y. Roleda, *Sci. Rep.* **2018**, 14763.
- [152] G. R. W. Denton, C. Burdon-Jones, *Mar. Pollut. Bull.* **1986**, *17*, 201-209.
- [153] J. E. Noble, M. J. Bailey, *Methods Enzymol* **2009**, *463*, 73-95.
- [154] M. M. Bradford, *Anal. Biochem.* **1976**, *72*, 248-254.
- [155] L. Behrendt, J. B. Raina, A. Lutz, W. Kot, M. Albertsen, P. Halkjaer-Nielsen, S. J. Sorensen, A. W. Larkum, M. Kühl, *ISME J* **2017**.
- [156] V. Herve, J. Derr, S. Douady, M. Quinet, L. Moisan, P. J. Lopez, *PLoS One* **2012**, *7*, e46722.
- [157] S. K. Apte, J. Thomas, *Eur. J. Biochem.* **1986**, *154*, 395-401.
- [158] B. A. Lawrence, J. Polse, A. DePina, M. M. Allen, N. H. Kolodny, *Curr. Microbiol.* **1997**, *34*, 280-283.
- [159] N. M. Mangan, A. Flamholz, R. D. Hood, R. Milo, D. F. Savage, *Proc. Natl. Acad. Sci. USA* **2016**, *113*, E5354-5362.
- [160] (Ed.: L. Invitrogen), <https://tools.thermofisher.com/content/sfs/manuals/mp01150.pdf>, **2006**.
- [161] K. S. Kumar, Y.-S. Han, K.-S. Choo, J.-A. Kong, T. Han, *J. Toxicol.* **2009**, *1*, 17-23.
- [162] H. A. Baumann, L. Morrison, D. B. Stengel, *Ecotoxicol Environ Saf* **2009**, *72*, 1063-1075.
- [163] A. J. Miao, W. X. Wang, P. Juneau, *Environ. Toxicol. Chem.* **2005**, *24*, 2603-2611.

- [164] P. Comba, A. Eisenschmidt, L. R. Gahan, G. R. Hanson, N. Mehrkens, M. Westphal, *Dalton Trans* **2016**, *45*, 18931-18945.
- [165] J. E. Coleman, *Annu. Rev. Biophys. Biomol. Struct.* **1992**, *21*, 441-483.
- [166] E. Kimura, *Bull. Jap. Soc. Coord. Chem.* **2012**, *59*, 26-47.
- [167] C. Liu, M. Wang, T. Zhang, H. Sun, *Coord. Chem. Rev.* **2004**, *248*, 147-168.
- [168] Z. Molphy, D. Montagner, S. S. Bhat, C. Slator, C. Long, A. Erxleben, A. Kellett, *Nucleic Acids Res.* **2018**, *46*, 9918-9931.
- [169] R. A. Peralta, A. J. Bortoluzzi, B. de Souza, R. Jovito, F. R. Xavier, R. A. Couto, A. Casellato, F. Nome, A. Dick, L. R. Gahan, G. Schenk, G. R. Hanson, F. C. de Paula, E. C. Pereira-Maia, P. M. S. de, P. C. Severino, C. Pich, T. Bortolotto, H. Terenzi, E. E. Castellano, A. Neves, M. J. Riley, *Inorg. Chem.* **2010**, *49*, 11421-11438.
- [170] M. R. Badger, D. Hanson, G. D. Price, *Funct. Plant Biol.* **2002**, *29*, 161-173.
- [171] M. J. Frisch, G. W. Trucks, H. B. Schlegel, G. E. Scuseria, M. A. Robb, J. R. Cheeseman, G. Scalmani, V. Barone, G. A. Petersson, H. Nakatsuji, X. Li, M. Caricato, A. V. Marenich, J. Bloino, B. G. Janesko, R. Gomperts, B. Mennucci, H. P. Hratchian, J. V. Ortiz, A. F. Izmaylov, J. L. Sonnenberg, Williams, F. Ding, F. Lipparini, F. Egidi, J. Goings, B. Peng, A. Petrone, T. Henderson, D. Ranasinghe, V. G. Zakrzewski, J. Gao, N. Rega, G. Zheng, W. Liang, M. Hada, M. Ehara, K. Toyota, R. Fukuda, J. Hasegawa, M. Ishida, T. Nakajima, Y. Honda, O. Kitao, H. Nakai, T. Vreven, K. Throssell, J. A. Montgomery Jr., J. E. Peralta, F. Ogliaro, M. J. Bearpark, J. J. Heyd, E. N. Brothers, K. N. Kudin, V. N. Staroverov, T. A. Keith, R. Kobayashi, J. Normand, K. Raghavachari, A. P. Rendell, J. C. Burant, S. S. Iyengar, J. Tomasi, M. Cossi, J. M. Millam, M. Klene, C. Adamo, R. Cammi, J. W. Ochterski, R. L. Martin, K. Morokuma, O. Farkas, J. B. Foresman, D. J. Fox, Wallingford, CT, **2016**.
- [172] P. J. Hay, W. R. Wadt, *J. Chem. Phys.* **1985**, *82*, 299-310.
- [173] W. R. Wadt, P. J. Hay, *J. Chem. Phys.* **1985**, *82*, 284-298.
- [174] J. Zheng, X. Xu, D. G. Truhlar, *Theor. Chem. Acc.* **2010**, *128*, 295-305.
- [175] I. Shimizu, Y. Morimoto, G. Velmurugan, T. Gupta, S. Paria, T. Ohta, H. Sugimoto, T. Ogura, P. Comba, S. Itoh, *Chem. Eur. J.* **2019**, *25*, 11157-11165.
- [176] J. Contreras-Garcia, E. R. Johnson, S. Keinan, R. Chaudret, J. P. Piquemal, D. N. Beratan, W. Yang, *J. Chem. Theory. Comput.* **2011**, *7*, 625-632.
- [177] E. R. Johnson, S. Keinan, P. Mori-Sanchez, J. Contreras-Garcia, A. J. Cohen, W. Yang, *J. Am. Chem. Soc.* **2010**, *132*, 6498-6506.
- [178] B. Ravel, M. Newville, *J. Synchrotron Rad.* **2005**, *12*, 537-541.
- [179] A. Tenderholt, B. Hedman, K. O. Hodgson, in *AIP Conference Proceedings*, **2007**, pp. 105-107.
- [180] G. N. George, I. J. Pickering, Stanford Synchrotron Radiation Laboratory, Stanford, CA, USA, **1995**.

## Appendices

The data of most measurements and analytical data of the syntheses presented in this work as well as some additional data that cannot be published in print can be found on the USB stick that comes with the evaluators' version of the thesis (and will be made available online upon publication of the results).

Synthesis – Maldi-MS spectra of linear peptides made by SPPS

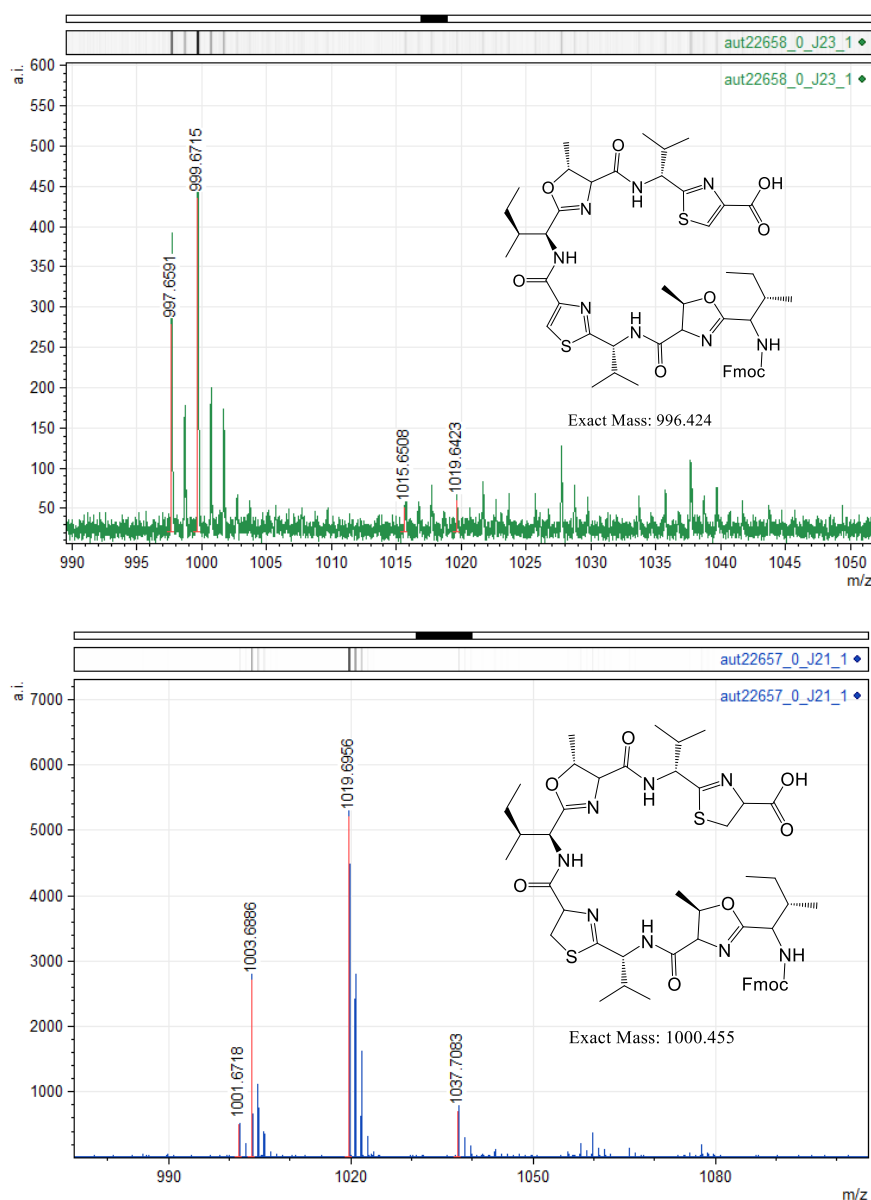


Figure A-S1: Mass spectra of the heterocyclizations on-resin following the automated SPPS. Top: Using thiazole building blocks, Bottom: using only amino acids. In both the reaction occurred on-resin as evident by the signals corresponding to the mass of the Fmoc-protected linear peptide with thiazoles (calc. 996.424 m/z for  $C_{51}H_{68}N_8O_9S_2$ ) or with thiazolines (calc. 1000.455 m/z for  $C_{51}H_{68}N_8O_9S_2$ ). In both cases, apart from the desired fully heterocyclized linear peptide, side products with opened heterocycles can be seen at higher masses (+18m/z), indicating that the reaction conditions were not optimal yet.



## XAS Data

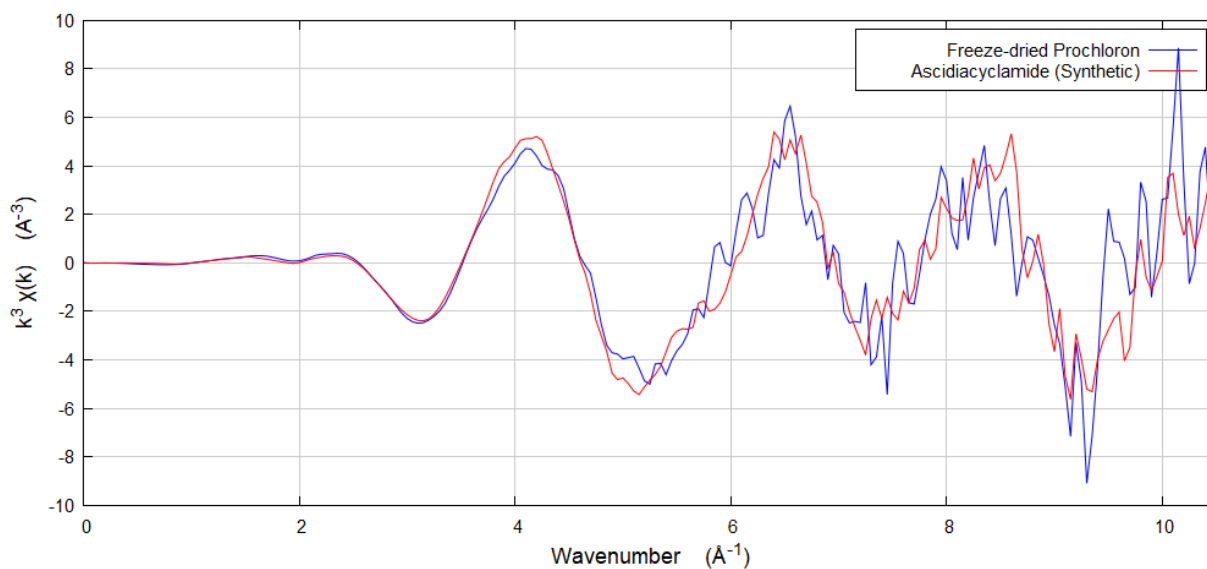


Figure A-XA1: Overlay of the EXAFS-Spectra of freeze-dried prochloron (blue) and synthetic ascidiacyclamide (red) with a k-weighting of 3. The full data can be found in the measurement data files.

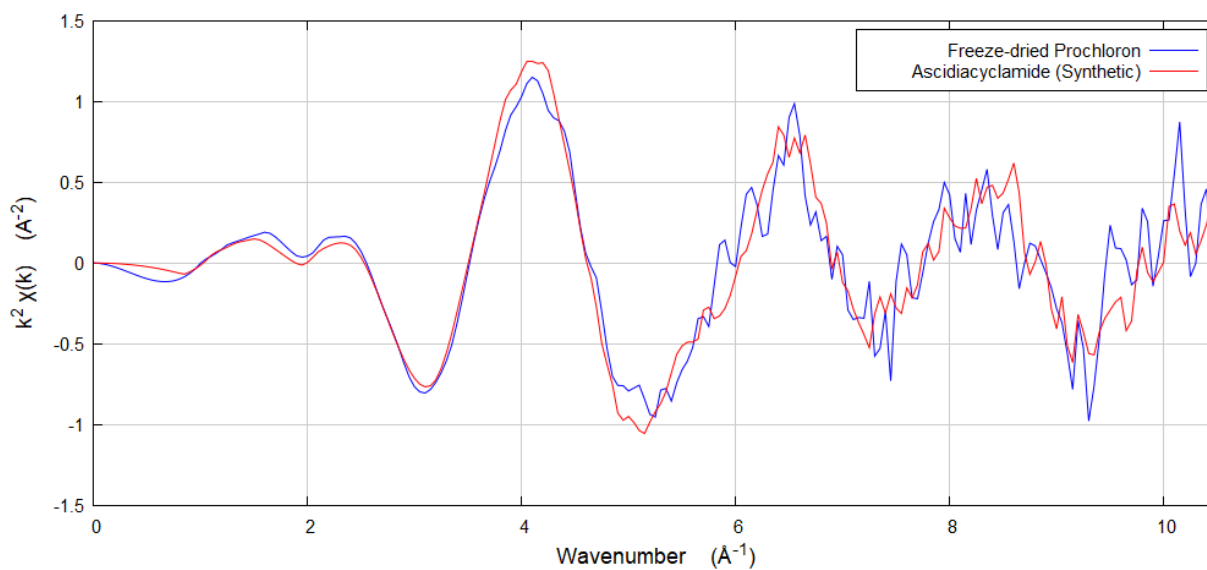


Figure A-XA2: Overlay of the EXAFS-Spectra of freeze-dried prochloron (blue) and synthetic ascidiacyclamide (red) with a k-weighting of 2.

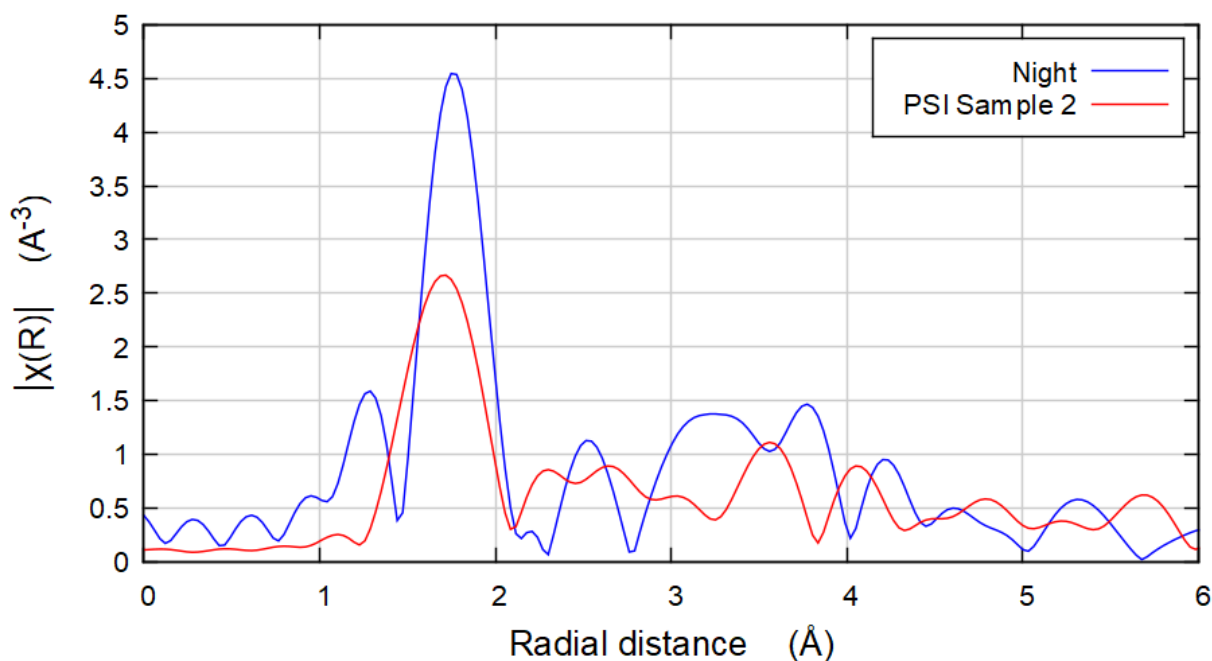


Figure A-XA3: Overlay of the EXAFS-Spectra of prochloron collected during the day (red), and of prochloron collected at night (blue) with a k-weighting of 3. As the samples for these spectra were not freeze-dried and only averaged over 5 spots rather than 20 due to time-limitations, the quality of the EXAFS does not make reliable fitting possible. However, clearly the sample measured at night, at significantly lower pH inside the cloaca is dominated by a low-k signal, which due to free copper present due to partial protonation of the patellamides.

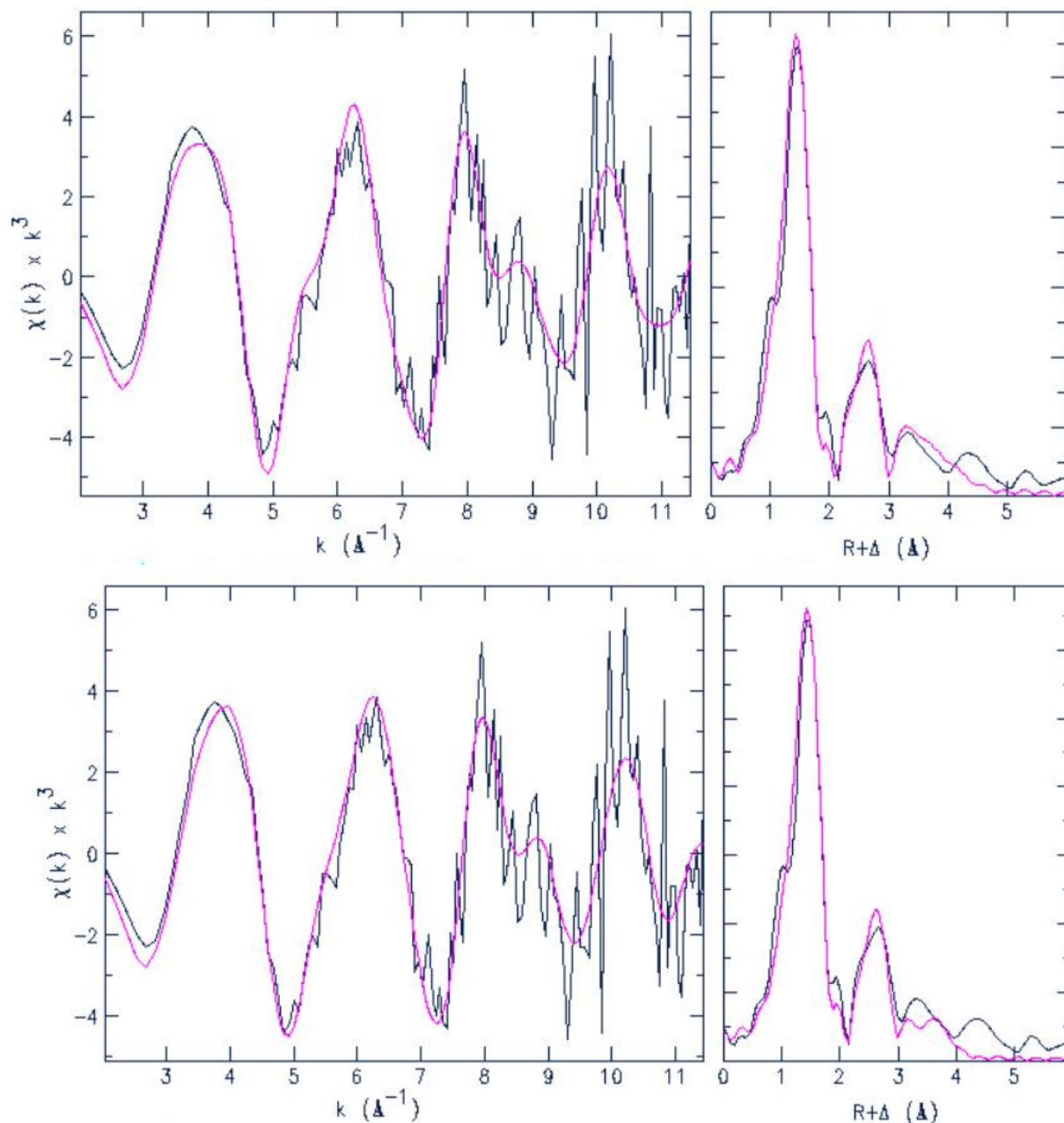


Figure A-XA4: The fits of the EXAFS-spectrum of the biological sample with (top) and without (bottom) inclusion of the copper-copper path. While the noise in the high- $k$  ( $>7$ ) region makes a clear interpretation of long paths difficult, it is evident, that without the copper-copper path, the fit lacks intensity between 3-4  $\text{\AA}$ . It must be noted that the distances in the Fourier-transformed spectra on the right are not drawn phase-corrected and thus the distances on the X-axis correspond to longer real distances.

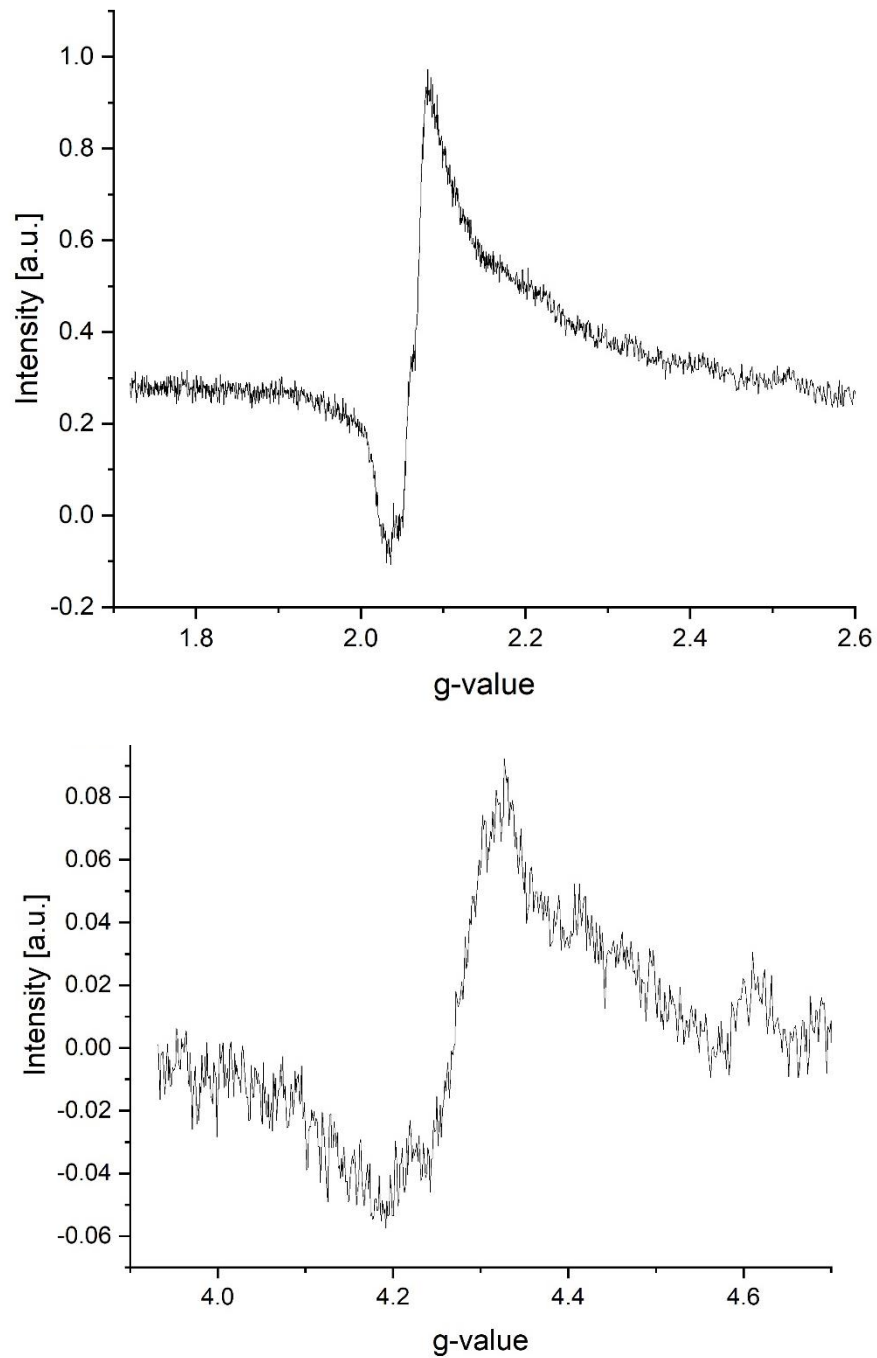


Figure A-XA5: EPR spectra of the 10x concentrated extracted DCM phase (both measured at 10° K, Top: Main signal at  $g \approx 2$ ,  $\nu = 9.62903$  MHz, Bottom: half-field signal at  $g \approx 4$ ,  $\nu = 9.63145$  MHz).

## Copper Concentration Measurements

**Table A-Cu1.** Metal ion concentrations with ICP-OES or ICP-MS, given in mg/kg (ppm) or mg/l for aqueous samples. Shown in this table are the water-loss corrected data before averaging. The specimen numbers refer to the different colonies used for the experiment, the samples 1,2 are the two duplicate measurements.

specimen		specimen 1	specimen 2	specimen 3		specimen 4	
				no copper added	copper added		
whole specimen	OES	sample 1	0.27	0.94	-	-	0.34
		sample 2	0.26	0.84	-	-	0.27
	MS	sample 1	0.31	0.95	-	-	0.24
		sample 2	0.30	0.85	-	-	0.29
cyanobacteria (homogenized)	OES	sample 1	0.11	0.51	0.55	3.76	0.79
		sample 2	0.12	0.47	0.48	3.51	0.69
	MS	sample 1	0.14	0.52	0.60	3.68	- <sup>a</sup>
		sample 2	0.12	0.50	0.54	3.63	- <sup>a</sup>
water inside cloaca	OES	sample 1	0.05	0.06	0.13	0.53	-
		sample 2	0.05	0.06	0.13	0.50	-
	MS	sample 1	0.05	0.10	0.06	0.55	-
		sample 2	0.06	0.12	0.16	0.52	-

<sup>a</sup>Not sufficient substance was left for the comparison with ICP-MS

**Table A-Cu2.** Metal concentrations determined by ICP-OES, measured as mg/kg of the dissolved dry substance (DS) except for the aqueous samples (highlighted in blue), where it corresponds to the wet concentration in mg/l. For the reference materials used, the determined reference values are given to verify the reliability of the method. The specimen numbers refer to the different colonies used for the experiment, the samples 1,2 are the two duplicate measurements.

	Ca g/kg DS	Cu mg/kg DS	Fe mg/kg DS	Mn mg/kg DS	Zn mg/kg DS
1 Specimen 1, whole, Sample 1	180	2.21	19.3	1.78	6.02
2 Specimen 1, whole, Sample 2	136	2.03	22.7	1.54	6.75
3 Specimen 2, whole, Sample 1	213	5.57	28.5	1.82	5.69
4 Specimen 2, whole, Sample 2 Specimen	201	4.99	41.5	2.35	6.54
5 Specimen 1, cyano, Sample 1	27.0	2.33	70.0	9.42	22.1
6 Specimen 1, cyano, Sample 2	26.0	2.43	75.0	9.43	21.8
7 Specimen 2, cyano, Sample 1	13.1	12.4	85.5	2.90	34.0
8 Specimen 2, cyano, Sample 2	12.9	11.3	73.7	2.72	31.3
9 Specimen 3, cyano, no Cu, Sample	18.7	13.1	106	3.47	34.1
10 Specimen 3, cyano, no Cu, Sample	20.3	11.3	88.4	3.26	30.2
11 Specimen 3, cyano, +Cu, Sample 1	17.5	81.8	183	5.45	48.3
12 Specimen 3, cyano, +Cu, Sample	21.2	76.4	181	5.36	46.8
13 Specimen 3, cloaca, +Cu, Sample	0.61	0.53	3.08	0.09	1.55
14 Specimen 3, cloaca, +Cu, Sample	0.61	0.50	2.08	0.09	1.54
15 Specimen 3, cloaca, no Cu, Sample 1	0.54	0.13	1.14	0.05	1.01
16 Specimen 3, cloaca, no Cu, Sample 2	0.56	0.13	1.43	0.05	1.03
17 Specimen 2, cloaca, Sample 1	0.72	0.06	0.82	0.10	1.13
18 Specimen 2, cloaca, Sample 2	0.72	0.06	1.29	0.11	1.14
19 Specimen 1, cloaca, Sample 1	0.62	0.05	1.34	0.05	0.46
20 Specimen 1, cloaca, Sample 2	0.66	0.05	1.02	0.06	0.43
21 Specimen 4, cyano, Sample1	30.5	8.7	433	54.5	36.1
22 Specimen 4, whole, Sample 1	241	1.5	36.1	2.35	5.58
23 Specimen 4, whole, Sample 2	240	1.2	31.0	2.30	5.01
1 Specimen 1, whole, Sample 1					
<b>Reference materials</b>					
BCR 060 Lagarosiphon Major	31.4	46.3	1908	187	311.0
BCR 060 Lagarosiphon Major	32.3	47.0	1638	1625	310.4
BCR 060 Lagarosiphon Major	33.8	53.0	1760	1737	334.0
IAEA-336 Lichen	2.66	3.29	300	68.4	31.2
IAEA-336 Lichen	2.56	3.35	321	70.4	31.5
IAEA-336 Lichen	2.49	3.29	306	68.4	31.0
NCS ZC71001 Beef Liver	0.19	90.2	348	9.67	201
NCS ZC71001 Beef Liver	0.20	93.1	380	10.2	207
NCS ZC71001 Beef Liver	0.19	86.6	373	9.77	199

Reference values for the used reference materials					
reference values BCR 060	30.9	51.2	1190	1759	313
±		1.9		51	8
mean	32.5	48.8	1769	1183	318
SD	0.99	3.02	111	706	11.0
RSD %	3.03	6.19	6.25	59.7	3.44
recovery %	105	95.3	149	67.2	102
reference values IAEA 336	2.49	3.6	430	63	30.4
±	0.039	0.5	50	7	3.4
mean	2.57	3.31	309	69.1	31.26
SD	0.07	0.03	8.87	0.95	0.21
RSD %	2.64	0.86	2.87	1.37	0.68
recovery %	103	92.0	71.9	110	103
reference values NCS ZC71001	0.189	91.6	346	8.92	192
±	0.005	3.8	31	0.84	12
mean	0.19	89.95	367	9.87	203
SD	0.00	2.67	13.9	0.21	3.46
RSD %	2.28	2.97	3.78	2.15	1.71
recovery %	101	98.2	106	111	105

**Table A-Cu3.** Metal concentrations determined by ICP-MS, measured as mg/kg of the dissolved dry substance (DS), except for the aqueous samples (highlighted in blue), where it corresponds to the wet concentration in mg/l. For the reference materials used, the determined reference values are given to verify the reliability of the method. For some samples measured with ICP-MS, the deviation between the two samples was unusually high, thus the ICP-OES data seem to be more reliable. The specimen numbers refer to the different colonies used for the experiment, the samples 1,2 are the two duplicate measurements.

	Cu mg/kg DS
1 Specimen 1, whole, Sample 1	2.42
2 Specimen 1, whole, Sample 2	2.35
3 Specimen 2, whole, Sample 1	5.67
4 Specimen 2, whole, Sample 2	5.25
5 Specimen 1, cyano, Sample 1	2.92
6 Specimen 1, cyano, Sample 2	2.43
7 Specimen 2, cyano, Sample 1	12.6
8 Specimen 2, cyano, Sample 2	12.1
9 Specimen 3, cyano, no Cu, Sample 1	14.3
10 Specimen 3, cyano, no Cu, Sample 2	12.7
11 Specimen 3, cyano, +Cu, Sample 1	80.1
12 Specimen 3, cyano, +Cu, Sample 2	79.1
13 Specimen 3, cloaca, +Cu, Sample 1	0.55
14 Specimen 3, cloaca, +Cu, Sample 2	0.52
15 Specimen 3, cloaca, no Cu, Sample 1	0.06
16 Specimen 3, cloaca, no Cu, Sample 2	0.16
17 Specimen 2, cloaca, Sample 1	0.10
18 Specimen 2, cloaca, Sample 2	0.12
19 Specimen 1, cloaca, Sample 1	0.05
20 Specimen 1, cloaca, Sample 2	0.08
21 Specimen 4, cyano, Sample1	7.6
22 Specimen 4, whole, Sample 1	1.1
23 Specimen 4, whole, Sample 2	1.3
<b>reference Materials</b>	
BCR 060 Lagarosiphon Major	44.0
BCR 060 Lagarosiphon Major	44.0
BCR 060 Lagarosiphon Major	49.4
IAEA-336 Lichen	2.62
IAEA-336 Lichen	3.08
IAEA-336 Lichen	2.91
NCS ZC71001 Beef Liver	79.8
NCS ZC71001 Beef Liver	83.2
NCS ZC71001 Beef Liver	79.7



reference values for the used reference materials	
reference value BCR 060	51.2
±	1.9
mean	45.8
SD	2.57
RSD %	5.62
recovery %	89.5
reference value IAEA 336	3.6
±	0.5
mean	2.87
SD	0.19
RSD %	6.54
recovery %	79.8
reference value NCS ZC71001	91.6
±	3.8
mean	80.9
SD	1.62
RSD %	2.00
recovery %	88.4

**Table A-Cu4.** Calculation of the copper content for the ICP-OES measurements (DS=dry substance, WS=wet substance). The specimen numbers refer to the different colonies used for the experiment, the samples 1,2 are the two duplicate measurements.

Sample Type	Cu mg/kg DS	wet			remaining weight	factor	Cu mg/kg WS
		mass	mass	mass			
1 Specimen 1 (finely minced)	<b>2.21</b>	3.686	0.466		12.63%	7.916	0.28
2 Specimen 1 (finely minced)	<b>2.03</b>	3.686	0.466		12.63%	7.916	0.26
3 Specimen 2 (big slices)	<b>5.57</b>	1.289	0.217		16.82%	5.944	0.94
4 Specimen 2 (big slices)	<b>4.99</b>	1.289	0.217		16.82%	5.944	0.84
5 Prochloron Homogenate Specimen 1	<b>2.33</b>	1.375	0.067		4.85%	20.621	0.11
6 Prochloron Homogenate Specimen 1	<b>2.43</b>	1.375	0.067		4.85%	20.621	0.12
7 Prochloron Homogenate Specimen 2	<b>12.4</b>	2.066	0.086		4.15%	24.084	0.51
8 Prochloron Homogenate Specimen 2	<b>11.3</b>	2.066	0.086		4.15%	24.084	0.47
9 Prochloron Homogenate Specimen 3 No Copper Added	<b>13.1</b>	1.708	0.072		4.23%	23.624	0.55
10 Prochloron Homogenate Specimen 3 No Copper Added	<b>11.3</b>	1.708	0.072		4.23%	23.624	0.48
11 Prochloron Homogenate Specimen 3 Copper Added (3x 2mL of 14.2mM CuSO <sub>4</sub> x6H <sub>2</sub> O)	<b>81.8</b>	1.883	0.087		4.59%	21.772	3.76
12 Prochloron Homogenate Specimen 3 Copper Added (3x 2mL of 14.2mM CuSO <sub>4</sub> x6H <sub>2</sub> O)	<b>76.4</b>	1.883	0.087		4.59%	21.772	3.51
13 Water from Cloaca Specimen 3 Copper Added (3x 2mL of 14.2mM CuSO <sub>4</sub> x6H <sub>2</sub> O)	<b>0.53</b>	0.600	0.600		100.00%	1.000	0.53
14 Water from Cloaca Specimen 3 Copper Added (3x 2mL of 14.2mM CuSO <sub>4</sub> x6H <sub>2</sub> O)	<b>0.50</b>	0.600	0.600		100.00%	1.000	0.50
15 Water from Cloaca Specimen 3 No Copper Added	<b>0.13</b>	0.600	0.600		100.00%	1.000	0.13
16 Water from Cloaca Specimen 3 No Copper Added	<b>0.13</b>	0.600	0.600		100.00%	1.000	0.13
17 Water from Cloaca Specimen 1/2 Filtered	<b>0.06</b>	0.600	0.600		100.00%	1.000	0.06
18 Water from Cloaca Specimen 1/2 Filtered	<b>0.06</b>	0.600	0.600		100.00%	1.000	0.06
19 Water from Cloaca Specimen 1/2 Unfiltered	<b>0.05</b>	0.600	0.600		100.00%	1.000	0.05
20 Water from Cloaca Specimen 1/2 Unfiltered	<b>0.05</b>	0.600	0.600		100.00%	1.000	0.05
21 Prochloron Homogenate Specimen 5	<b>8.7</b>	0.321	0.029		9.10%	10.993	0.79
22 Specimen 4, whole	<b>1.5</b>	0.281	0.063		22.55%	4.435	0.34
23 Specimen 4, whole	<b>1.2</b>	0.281	0.063		22.55%	4.435	0.27

**Table A-Cu5.** Calculation of the Copper Content for the ICP-MS measurements (DS=dry substance, WS=wet substance). The specimen numbers refer to the different colonies used for the experiment, the samples 1,2 are the two duplicate measurements.

Sample Type	Cu				Cu	
	mg/kg DS	wet mass	dry mass	remaining weight	factor	mg/kg WS
1 Specimen 1 (finely minced)	<b>2.42</b>	3.686	0.466	12.63%	7.916	<b>0.31</b>
2 Specimen 1 (finely minced)	<b>2.35</b>	3.686	0.466	12.63%	7.916	<b>0.30</b>
3 Specimen 2 (big slices)	<b>5.67</b>	1.289	0.217	16.82%	5.944	<b>0.95</b>
4 Specimen 2 (big slices)	<b>5.25</b>	1.289	0.217	16.82%	5.944	<b>0.88</b>
5 Prochloron Homogenate Specimen 1	<b>2.92</b>	1.375	0.067	4.85%	20.621	<b>0.14</b>
6 Prochloron Homogenate Specimen 1	<b>2.43</b>	1.375	0.067	4.85%	20.621	<b>0.12</b>
7 Prochloron Homogenate Specimen 2	<b>12.6</b>	2.066	0.086	4.15%	24.084	<b>0.52</b>
8 Prochloron Homogenate Specimen 2	<b>12.1</b>	2.066	0.086	4.15%	24.084	<b>0.50</b>
9 Prochloron Homogenate Specimen 3 No Copper Added	<b>14.3</b>	1.708	0.072	4.23%	23.624	<b>0.60</b>
10 Prochloron Homogenate Specimen 3 No Copper Added	<b>12.7</b>	1.708	0.072	4.23%	23.624	<b>0.54</b>
11 Prochloron Homogenate Specimen 3 Copper Added (3x 2mL of 14.2mM CuSO <sub>4</sub> x6H <sub>2</sub> O)	<b>80.1</b>	1.883	0.087	4.59%	21.772	<b>3.68</b>
12 Prochloron Homogenate Specimen 3 Copper Added (3x 2mL of 14.2mM CuSO <sub>4</sub> x6H <sub>2</sub> O)	<b>79.1</b>	1.883	0.087	4.59%	21.772	<b>3.63</b>
13 Water from Cloaca Specimen 3 Copper Added (3x 2mL of 14.2mM CuSO <sub>4</sub> x6H <sub>2</sub> O)Specimen	<b>0.55</b>	0.600	0.600	100.00%	1.000	<b>0.55</b>
14 Water from Cloaca Specimen 3 Copper Added (3x 2mL of 14.2mM CuSO <sub>4</sub> x6H <sub>2</sub> O)Specimen	<b>0.52</b>	0.600	0.600	100.00%	1.000	<b>0.52</b>
15 Water from Cloaca Specimen 3 No Copper AddedSpecimen	<b>0.06</b>	0.600	0.600	100.00%	1.000	<b>0.06</b>
16 Water from Cloaca Specimen 3 No Copper AddedSpecimen	<b>0.16</b>	0.600	0.600	100.00%	1.000	<b>0.16</b>
17 Water from Cloaca Specimen 1/2 FilteredSpecimen	<b>0.10</b>	0.600	0.600	100.00%	1.000	<b>0.10</b>
18 Water from Cloaca Specimen 1/2 FilteredSpecimen	<b>0.12</b>	0.600	0.600	100.00%	1.000	<b>0.12</b>
19 Water from Cloaca Specimen 1/2 UnfilteredSpecimen	<b>0.05</b>	0.600	0.600	100.00%	1.000	<b>0.05</b>
20 Water from Cloaca Specimen 1/2 UnfilteredSpecimen	<b>0.08</b>	0.600	0.600	100.00%	1.000	<b>0.08</b>
21 Prochloron Homogenate Lars Specimen	<b>7.6</b>	0.321	0.029	9.10%	10.993	<b>0.69</b>
22 Specimen LarsSpecimen	<b>1.1</b>	0.281	0.063	22.55%	4.435	<b>0.24</b>
23 Specimen LarsSpecimen	<b>1.3</b>	0.281	0.063	22.55%	4.435	<b>0.29</b>

## Patellamide concentration dynamics dependent on copper

The following images were created using TOPPview of the mass spectra files, measured at the Sciex TripleTOF 5600 and 6600. Each image consists of the chromatogram spectrum at the top (Y: Counts X: time [min]) and the mass distribution on the right (Y: m/z X: relative quantity), leading to the 2D figure at the bottom left (X: time [min], Y: m/z, the color shows the relative quantity). Raw data and the full resolution images can be found in the measurement data.

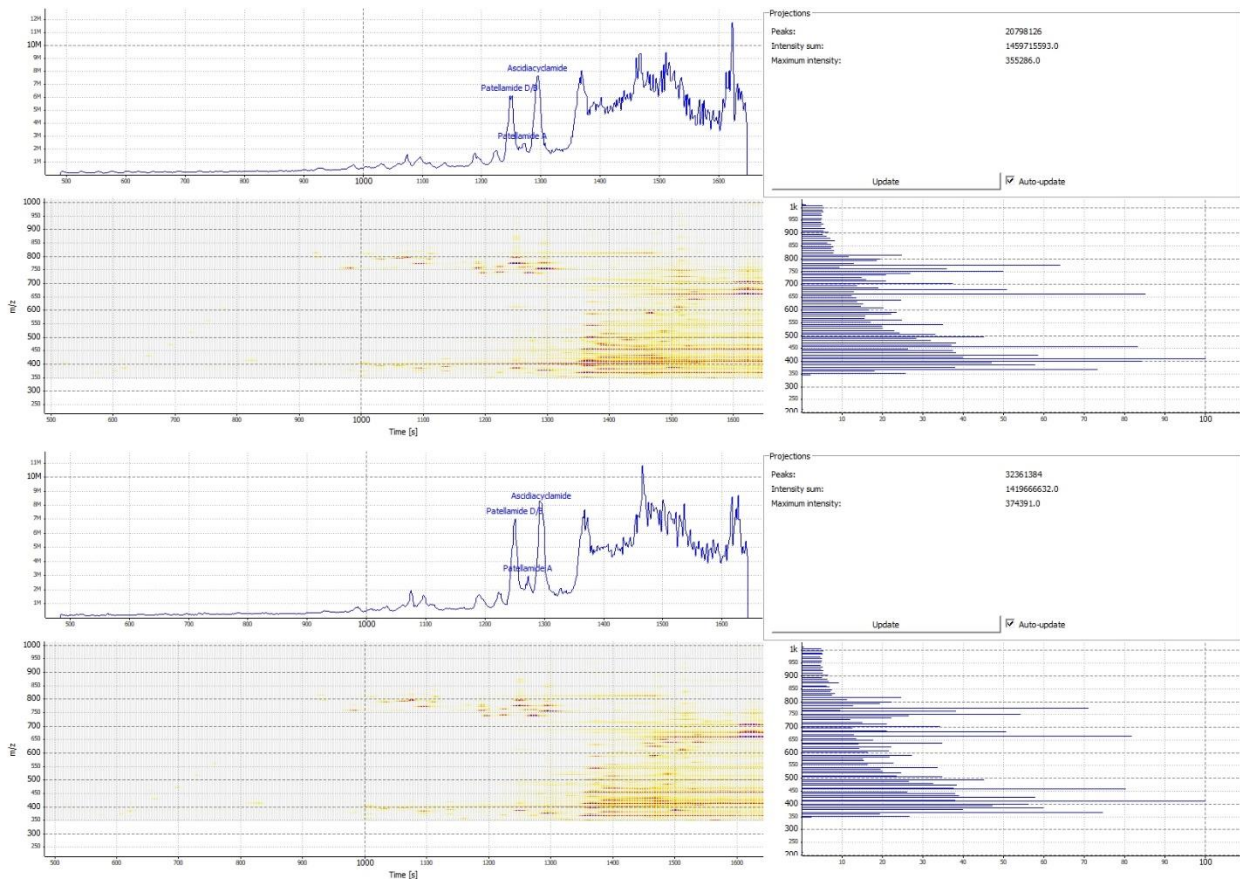


Figure A-CC1: HPLC-MS data of two samples of the water extracted from the cloacal cavity without addition of copper, measured at the Sciex TripleTOF 5600 system.

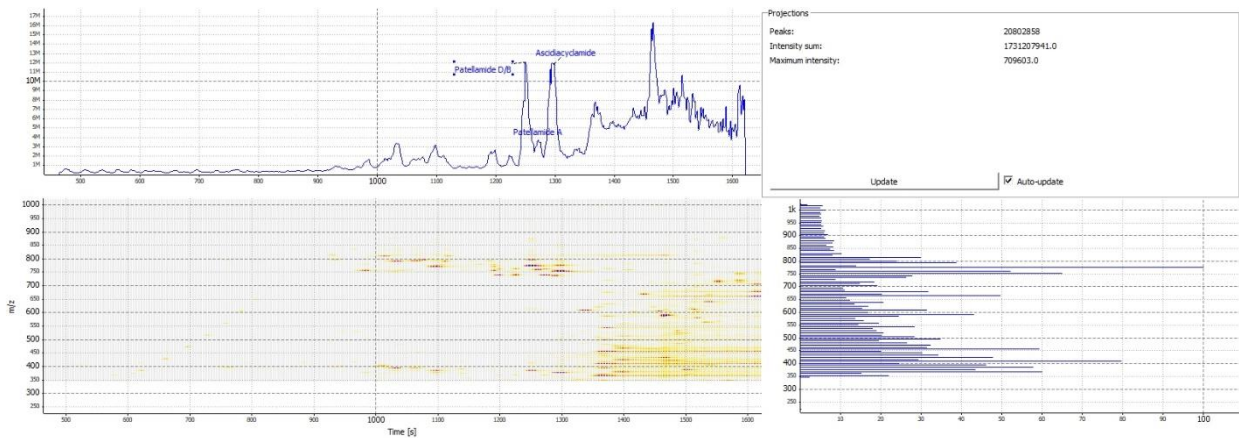


Figure A-CC2: HPLC-MS data of the water extracted from the cloacal cavity with addition of copper, measured at the Sciex TripleTOF 5600 system.

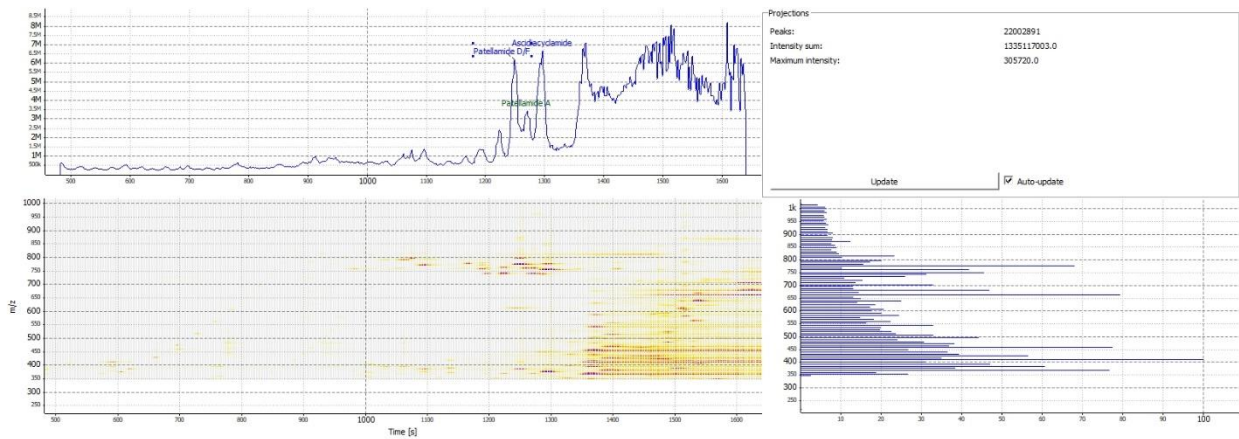


Figure A-CC3: HPLC-MS data of the filtered cyanobacteria homogenate extracted from the cloacal cavity without addition of copper, measured at the Sciex TripleTOF 5600 system.

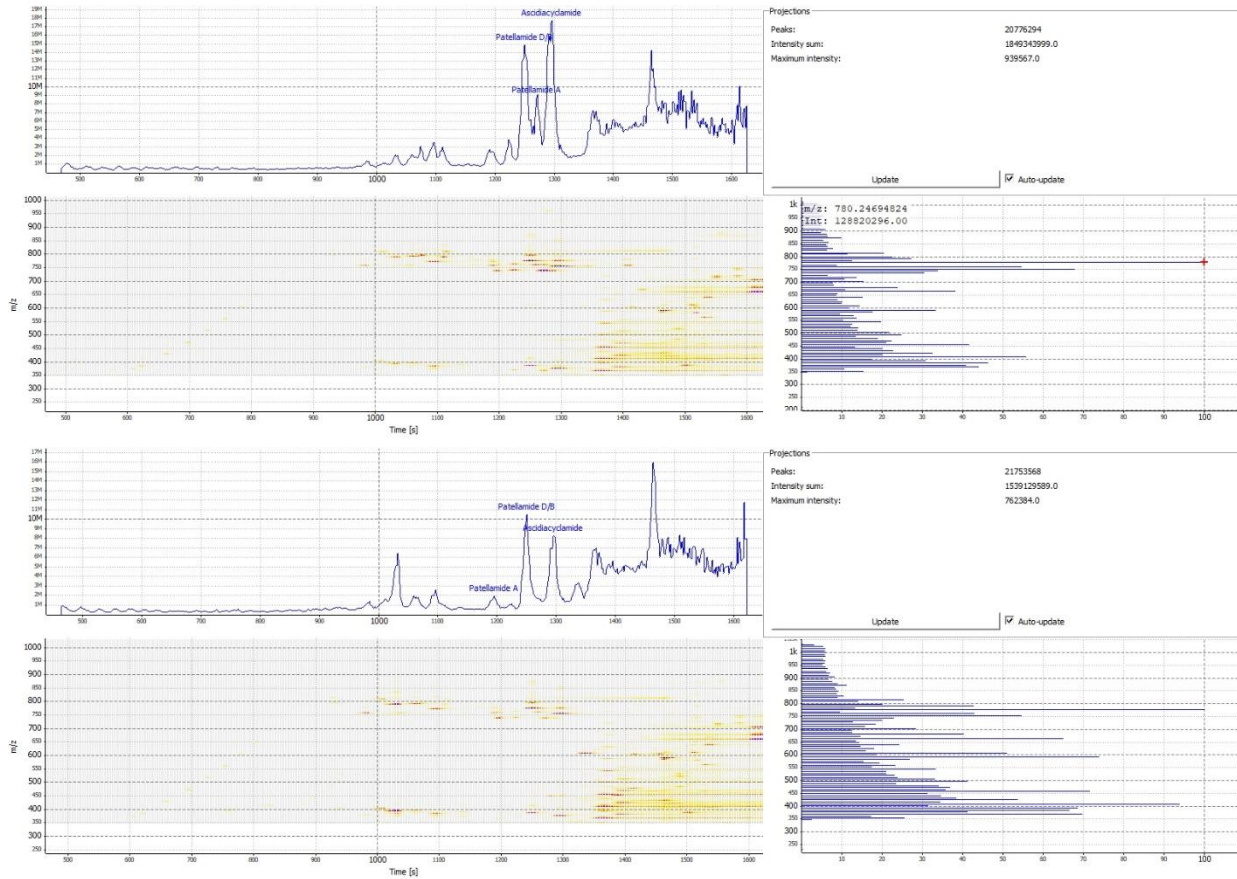


Figure A-CC4: HPLC-MS data of two samples of the filtered cyanobacteria homogenate extracted from the cloacal cavity with addition of copper, measured at the Sciex TripleTOF 5600 system.

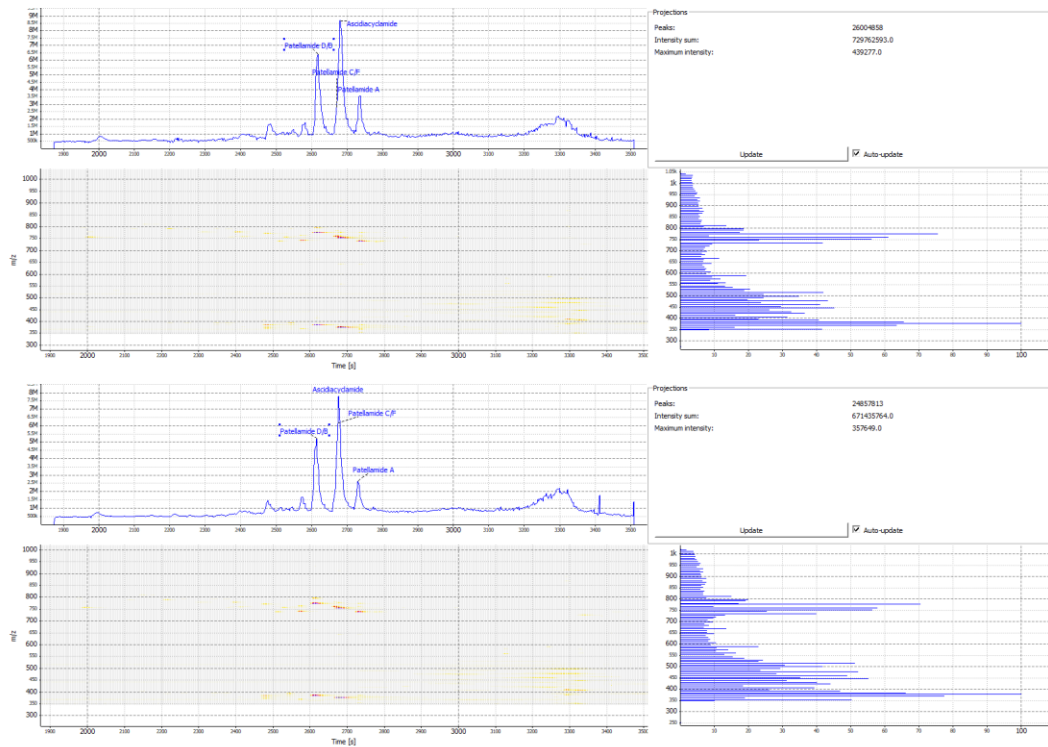


Figure A-CC5: HPLC-MS data of two samples of the water extracted from the cloacal cavity without addition of copper, measured at the Sciex TripleTOF 6600 system.

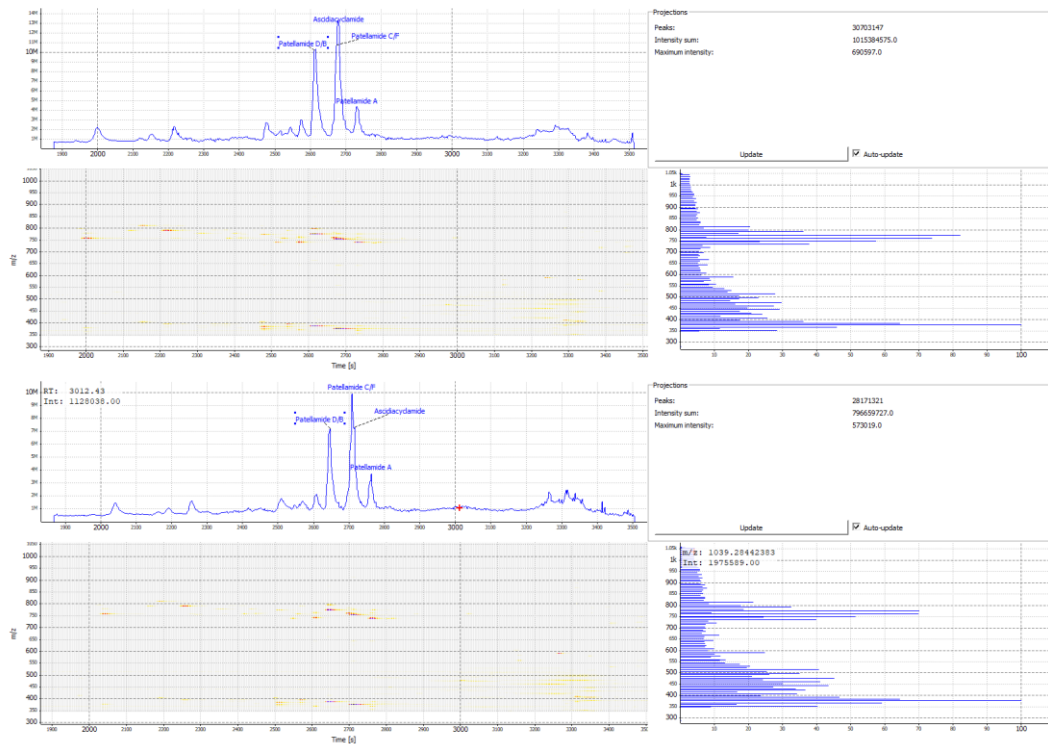


Figure A-CC6: HPLC-MS data of two samples of the water extracted from the cloacal cavity with addition of copper, measured at the Sciex TripleTOF 6600 system.

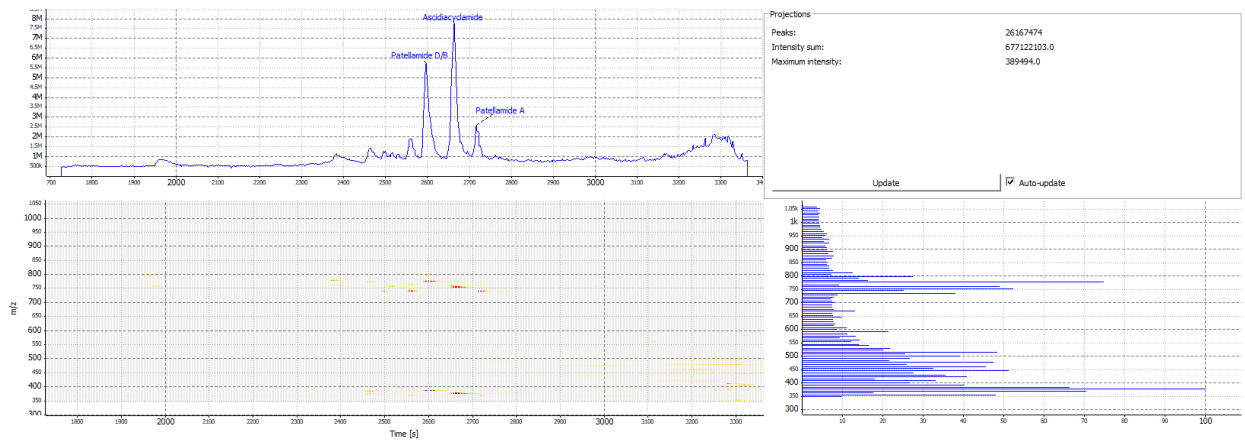


Figure A-CC7: HPLC-MS data of the filtered cyanobacteria homogenate extracted from the cloacal cavity without addition of copper, measured at the Sciex TripleTOF 6600 system.

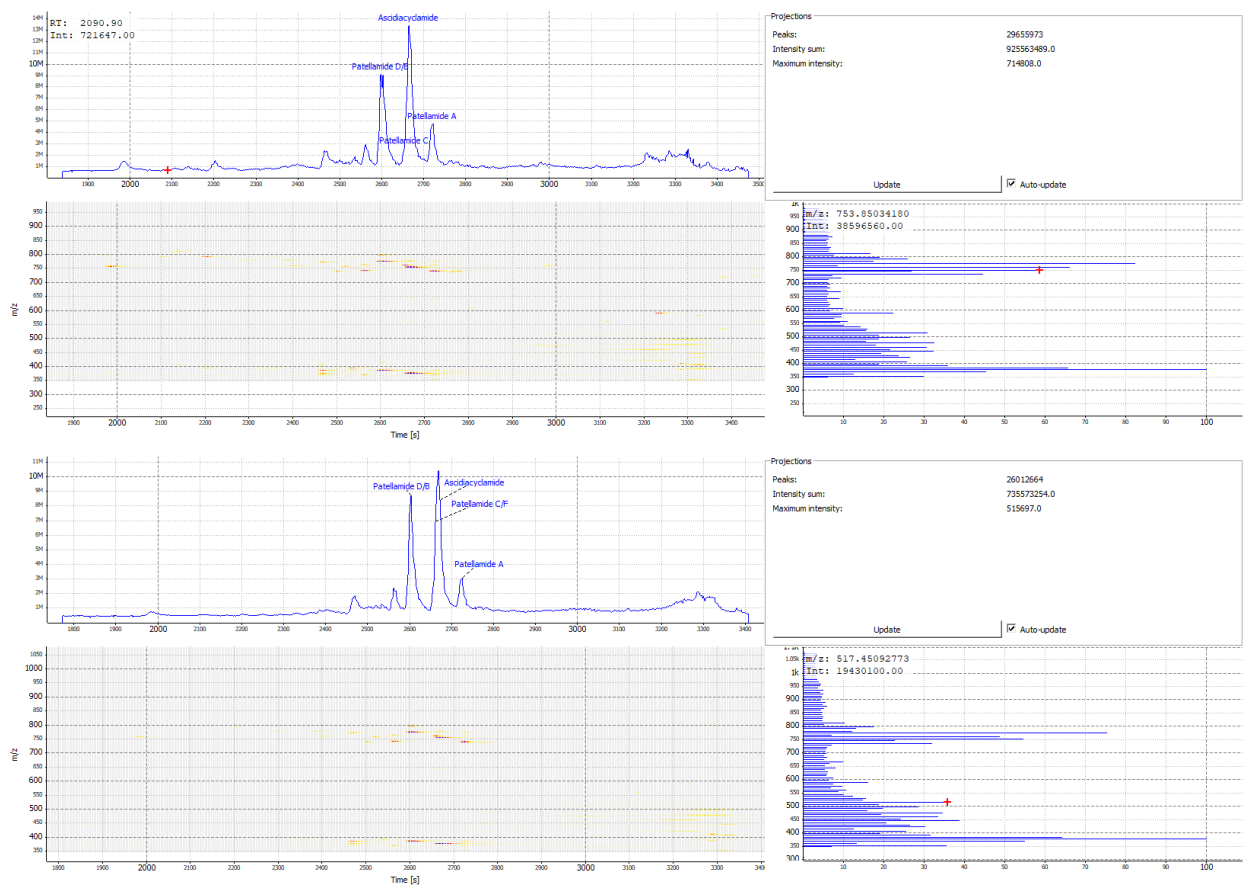


Figure A-CC6: HPLC-MS data of two samples of the filtered cyanobacteria homogenate extracted from the cloacal cavity with addition of copper, measured at the Sciex TripleTOF 6600 system.



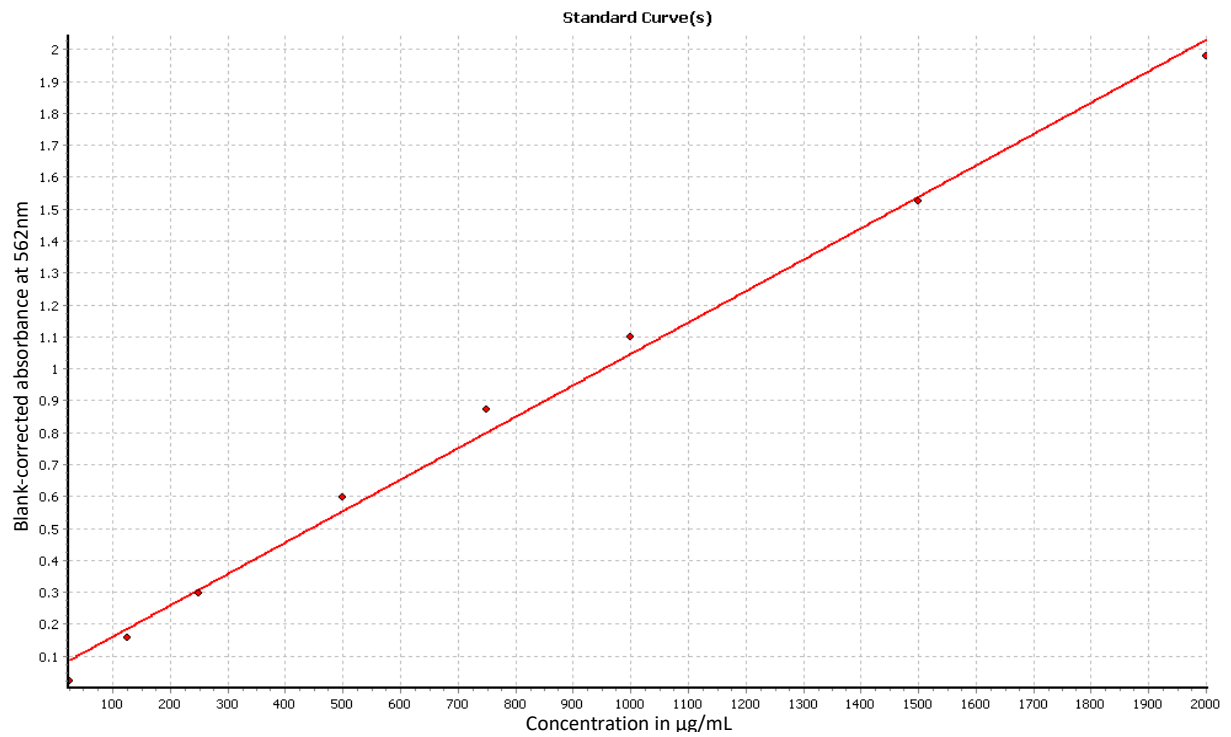


Figure A-CC7: Regression curve for the concentration-dependence of the absorbance at 562nm used for the protein quantification using the Bradford assay ( $Y=0.000984*x+0.062635$ ,  $r^2= 0.9947$ ).

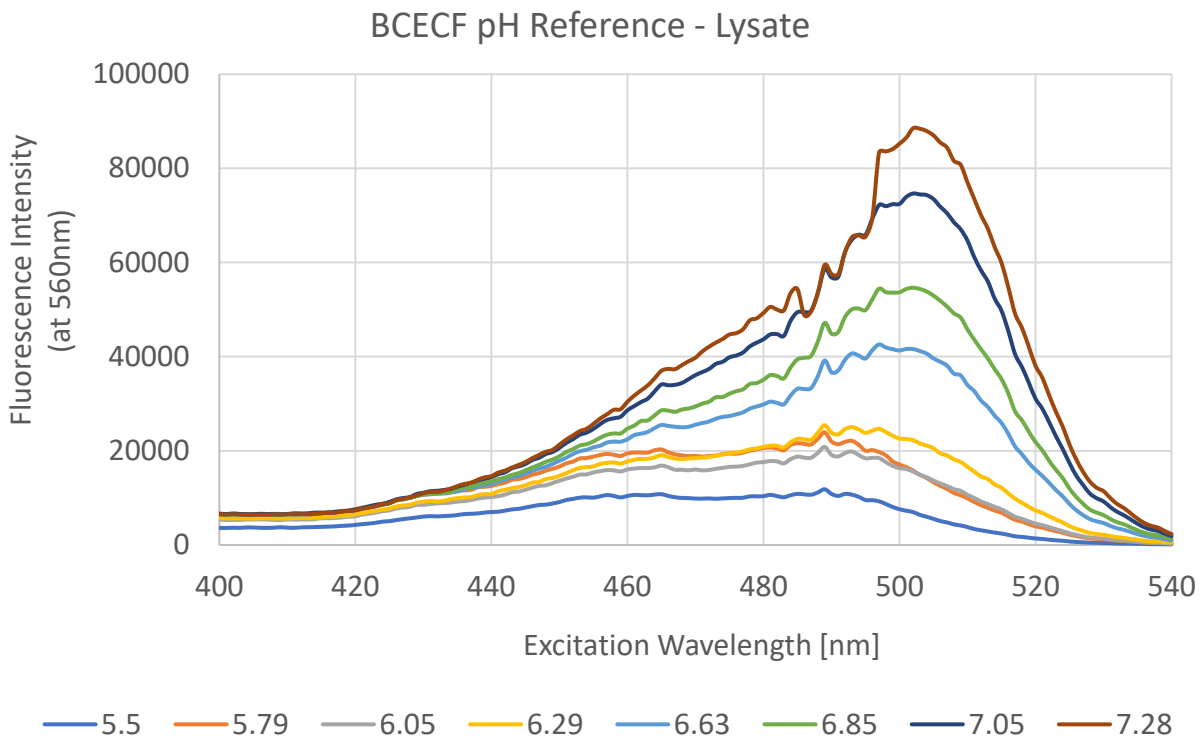
Determination of the intracellular pH value in *Prochloron didemni*

Figure A-pH1: Spectra for the reference measurements of the pH-dependence of the emission intensity at 560nm of 0.05mM BCECF/AM in lysated cells at variable excitation.

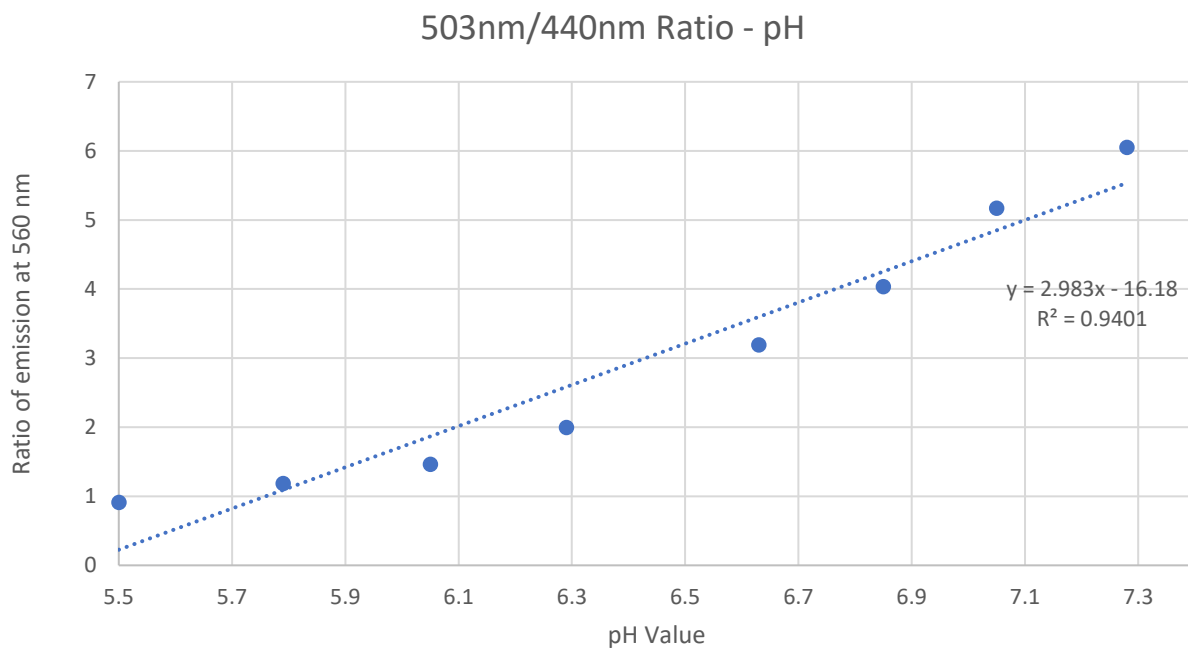


Figure A-pH2: Regression curve for the reference measurements of the pH-dependence of ratio of the emission intensity at 560nm upon excitation at 503 to emission upon excitation at 440 nm of 0.01 mM BCECF/AM in lysated cells ( $Y=2.983 \cdot X - 16.18$ ,  $R^2= 0.9401$ ).

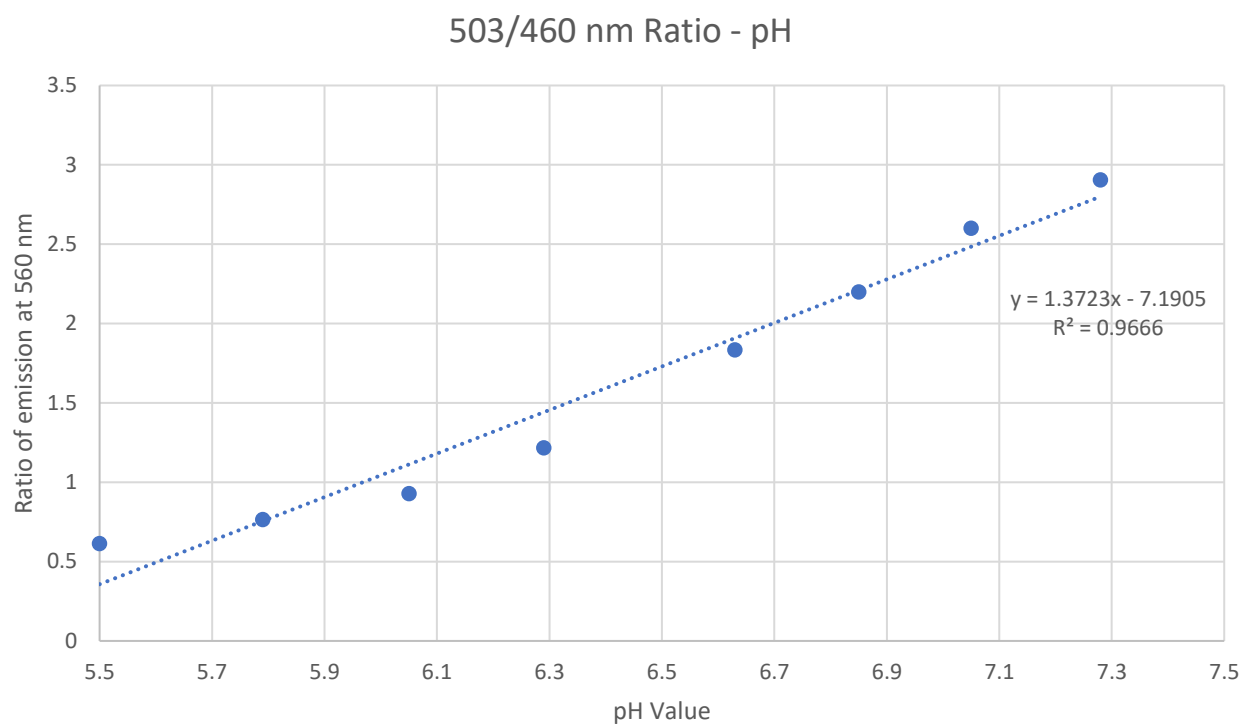


Figure A-pH3: Regression curve for the reference measurements of the pH-dependence of ratio of the emission intensity at 560nm upon excitation at 503 to emission upon excitation at 460 nm of 0.01 mM BCECF/AM in lysated cells ( $Y=1.3723*x-7.1905$ ,  $R^2= 0.9666$ )

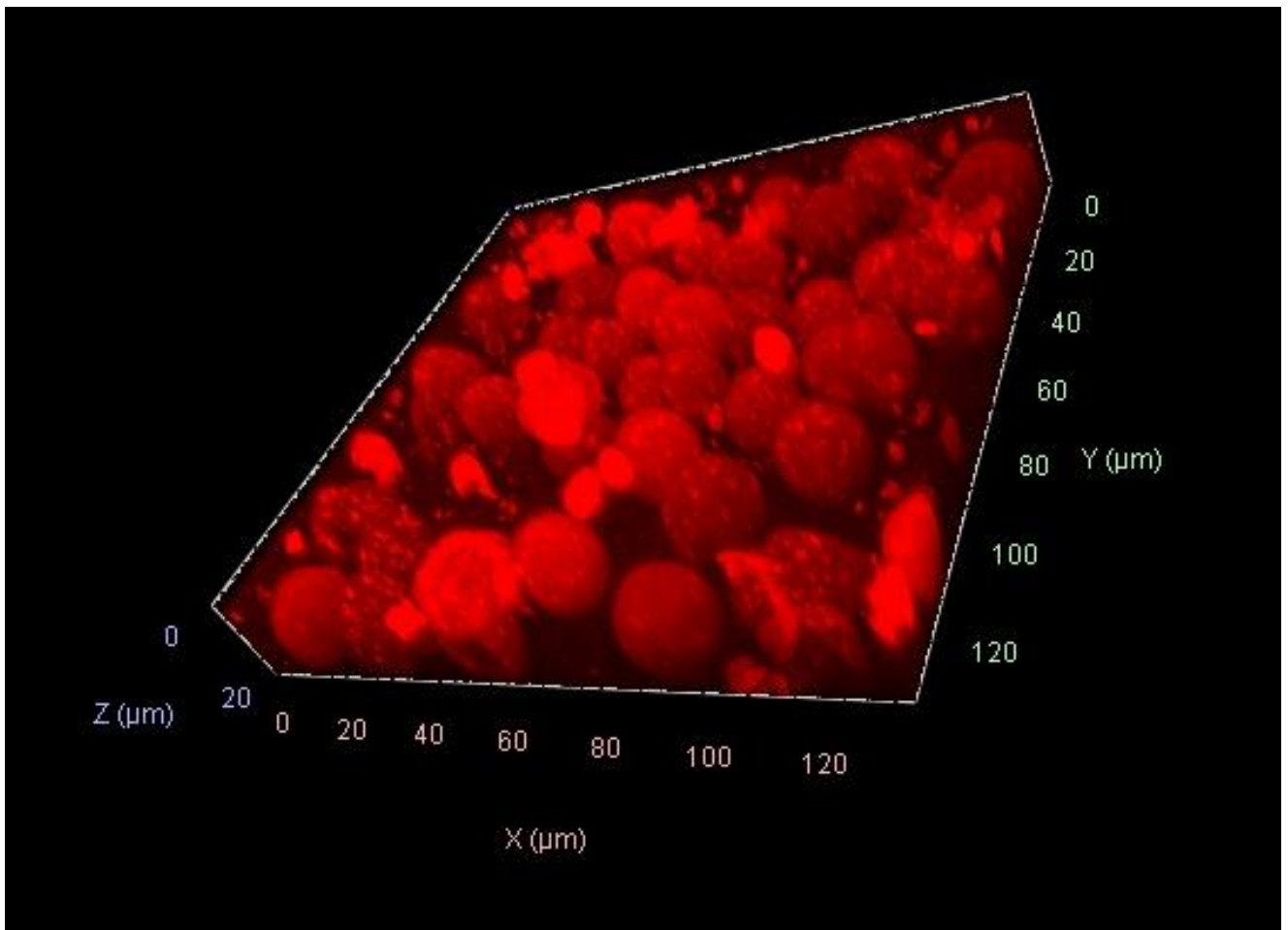


Figure A-pH4: 3D confocal fluorescence microscopy scan of *Prochloron didemni*, loaded with BCECF-dye. The intensity of the red color corresponds to the total emission between 500 and 630nm upon excitation at 488nm.

Patellamide bioactivity towards *Nannochloropsis* spp.

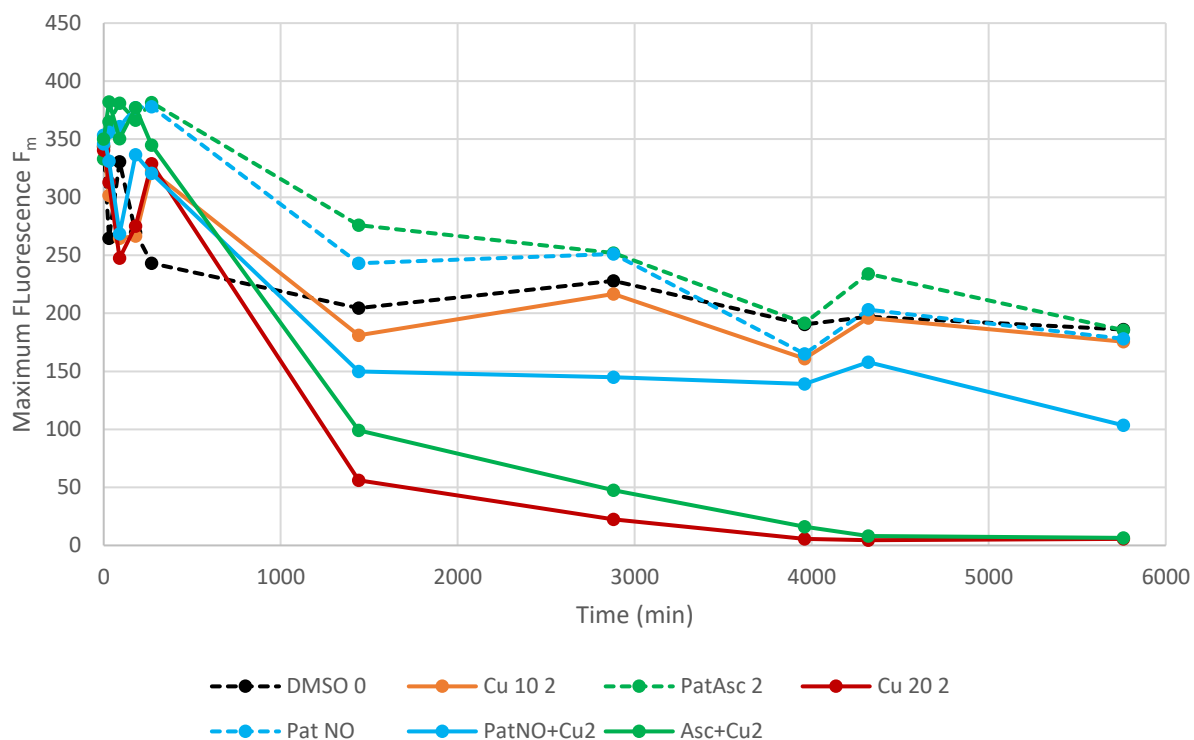


Figure A-BA1: Change of the dark-adapted maximum chlorophyll fluorescence of *Nannochloropsis gaditana* after exposing it to different compounds, first series of measurements.

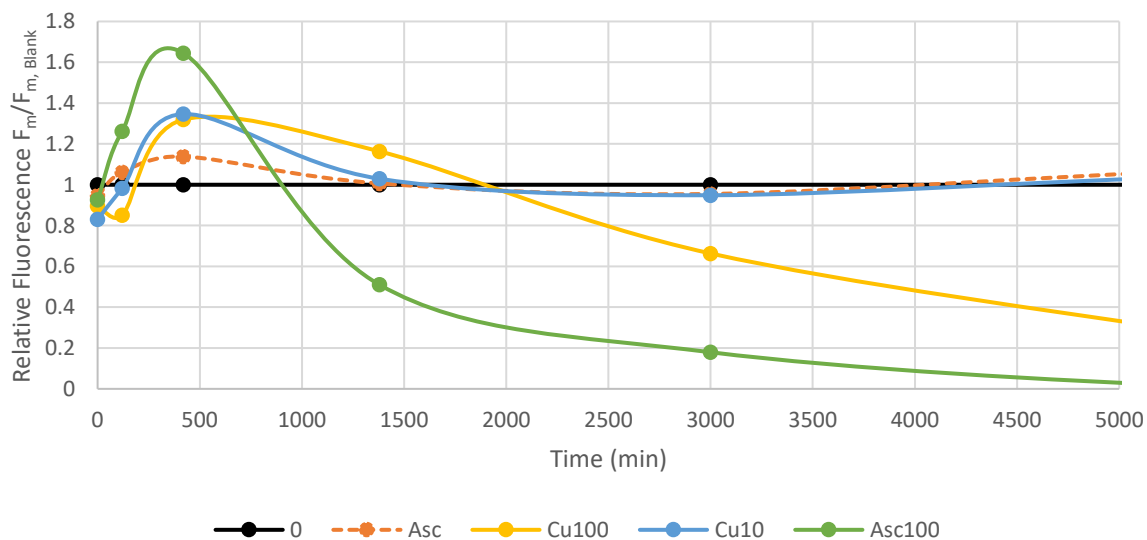


Figure A-BA2: Change of the dark-adapted maximum chlorophyll fluorescence of *Nannochloropsis gaditana* after exposing it to different compounds – values relative to the parameter of the blank, second series of measurements.

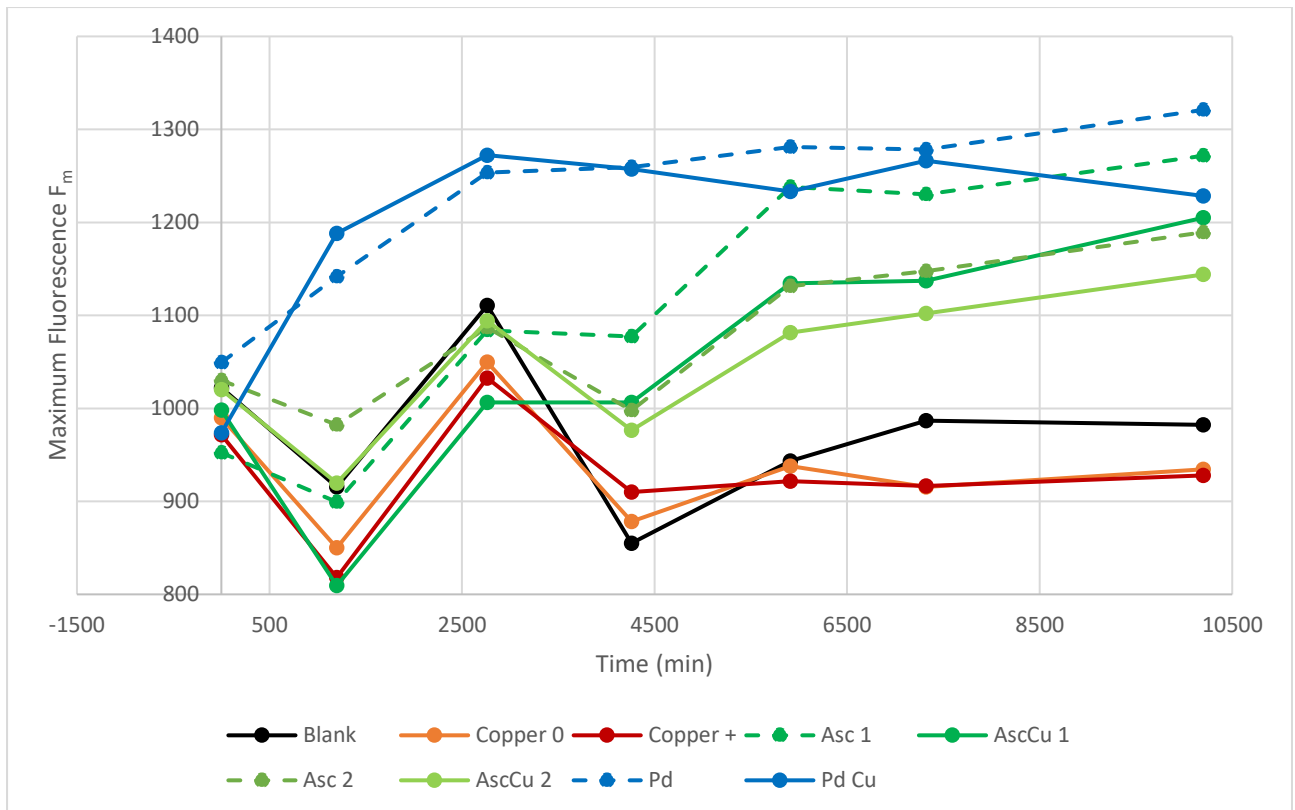
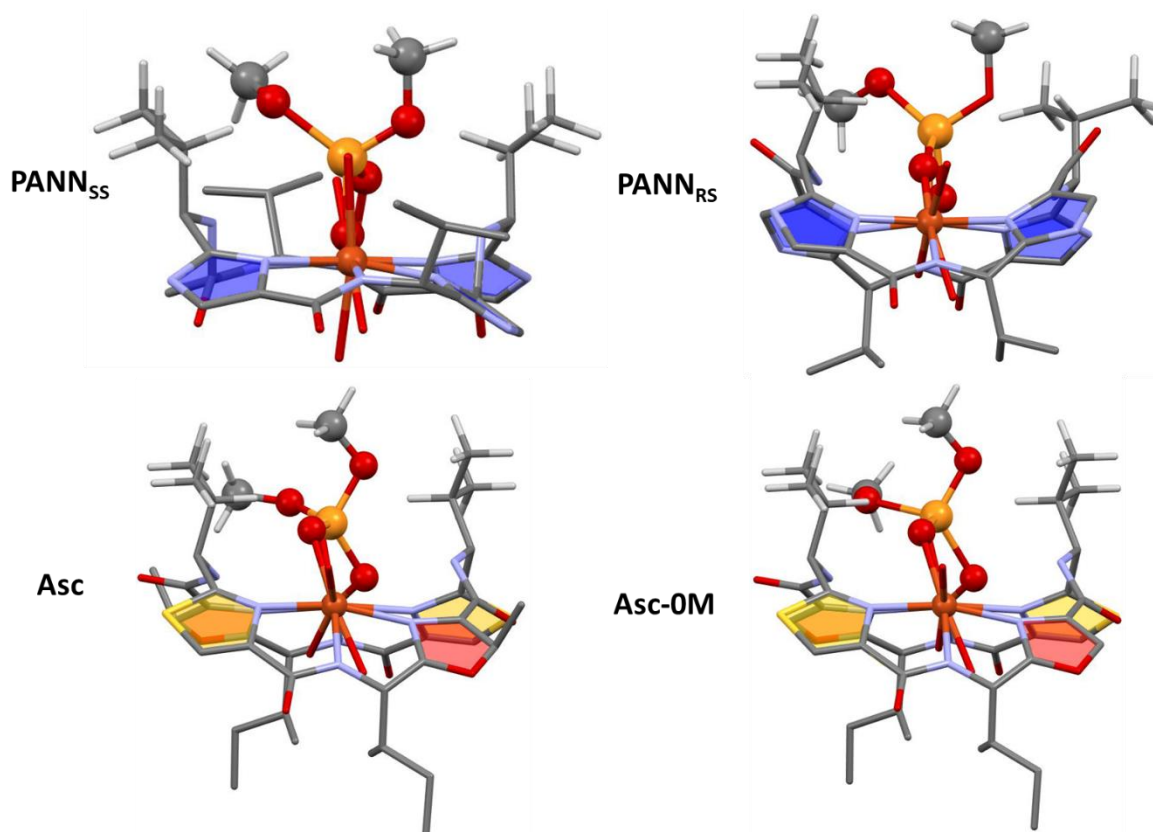


Figure A-BA2: Change of the dark-adapted maximum chlorophyll fluorescence of *Nannochloropsis salina* after exposing it to different compounds – values relative to the parameter of the blank, second series of measurements.

## Phosphodiesterase activity

Table A-P1: Comparison of the hydrolysis data, kinetic profile, pH<sub>max</sub> value and the pK<sub>a</sub> values of different patellamide analogues<sup>[164]</sup>.

catalyst	pH <sub>max</sub>	v <sub>0,max</sub> [Ms <sup>-1</sup> ]	pK <sub>a</sub> (I)	pK <sub>a</sub> (II)	k <sub>cat</sub> [s <sup>-1</sup> ] $\times 10^{-3}$	K <sub>M</sub> [mM]	k <sub>cat</sub> /K <sub>M</sub> [M <sup>-1</sup> s <sup>-1</sup> ]
[Cu <sup>II</sup> <sub>2</sub> (PANN <sub>SS</sub> )(OH)] <sup>+</sup>	6.69	1.4 $\times 10^{-8}$	6.3	7.0	0.4	5.5	0.07
[Cu <sup>II</sup> <sub>2</sub> (PANN <sub>RS</sub> )(OH)] <sup>+</sup>	7.21	1.6 $\times 10^{-7}$	6.9	7.3	4.0	26.4	0.15
[Cu <sup>II</sup> <sub>2</sub> (PAOO <sub>RS</sub> )(OH)] <sup>+</sup>	7.73	3.6 $\times 10^{-8}$	7.0	8.5	6.6	14.7	0.45
[Cu <sup>II</sup> <sub>2</sub> (PASO <sub>RS</sub> )(OH)] <sup>+</sup>	7.57	3.0 $\times 10^{-8}$	7.4	7.7	2.3	4.2	0.53

Figure A-P2: The optimized geometries of TS2 of the phosphodiesterase reaction (only selected hydrogen atoms are shown for clarity; the view is through the two copper(II) centers with the center with the attacking OH<sup>-</sup> at the front). Taken from <sup>[6]</sup>.

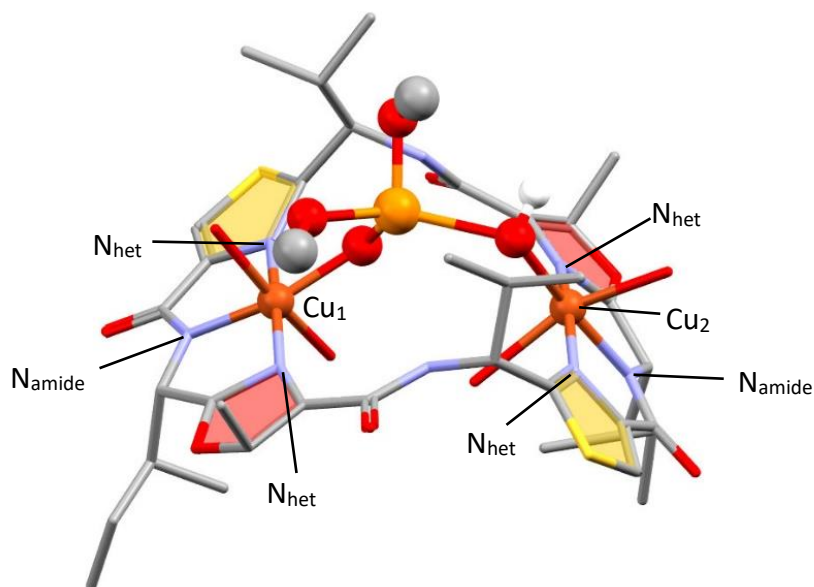


Figure A-P3 / Table A-P3: Comparison of the structural copper(II)-nitrogen bond length during different steps within the catalytic cycle for the dicopper(II) complexes of PANN<sub>SS</sub> and Asc. The structure shown is the ascidiacyclamide complex. Taken from <sup>[6]</sup>.

Step Derivative	1		TS1		2		TS2		3	
	Asc	PANN <sub>SS</sub>	Asc	PANN <sub>SS</sub>	Asc	PANN <sub>SS</sub>	Asc	PANN <sub>SS</sub>	Asc	PANN <sub>SS</sub>
Cu <sub>1</sub> -N <sub>het1</sub>	2.13	1.90	2.27	1.97	2.27	1.97	2.11	1.96	2.11	1.93
Cu <sub>1</sub> -N <sub>amide</sub>	1.93	1.80	1.86	1.80	1.86	1.80	1.89	1.79	1.90	1.80
Cu <sub>1</sub> -N <sub>het2</sub>	2.13	1.86	2.36	1.91	2.36	1.91	2.00	1.98	1.99	1.98
Cu <sub>2</sub> -N <sub>het1</sub>	2.24	1.89	2.01	1.90	2.01	1.90	2.02	1.91	2.02	1.91
Cu <sub>2</sub> -N <sub>amide</sub>	1.92	1.79	1.80	1.81	1.80	1.81	1.95	1.80	1.95	1.80
Cu <sub>2</sub> -N <sub>het2</sub>	2.08	1.91	1.85	1.92	1.85	1.92	2.11	1.96	2.11	1.88



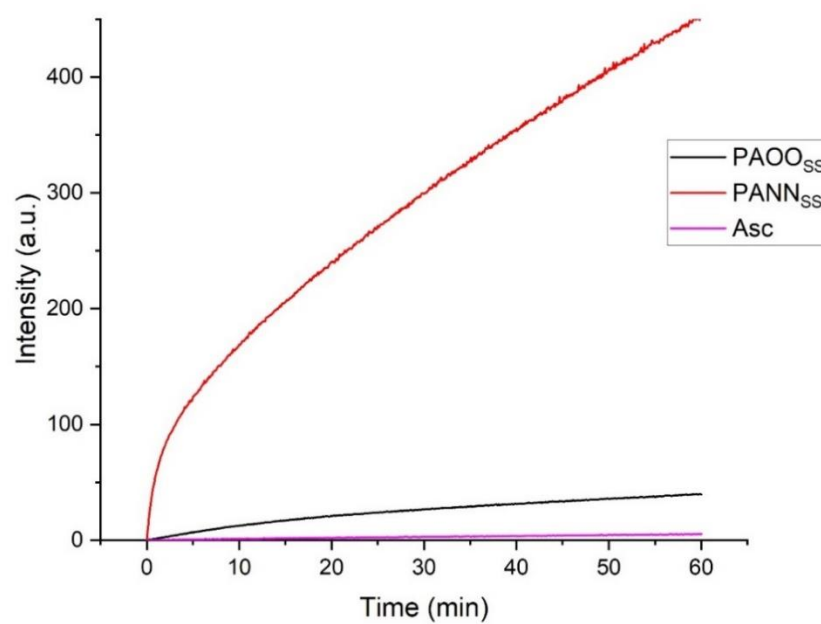


Figure A-P4: Change of the fluorescence intensity at the emission wavelength of  $\lambda=455 \pm 10$  nm caused by the phosphomonoester hydrolysis product 6,8-difluoro-7-hydroxy-4-methylcoumarin (DIFMU) after dephosphorylation. Only PANN<sub>ss</sub> showed significant activity. Taken from [6].

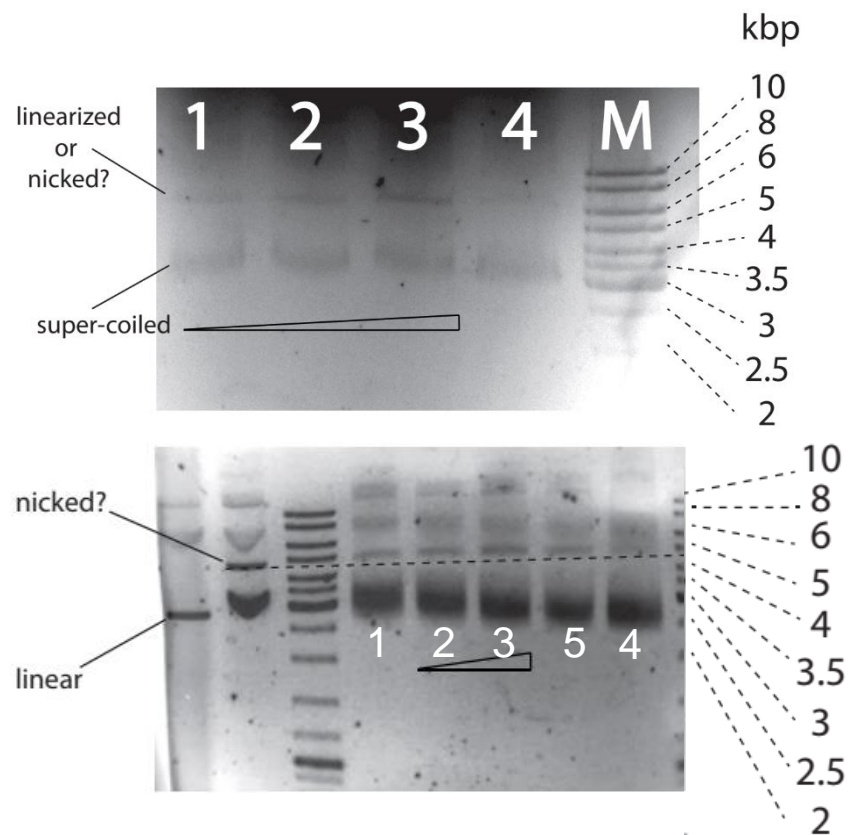


Figure A-P5: Gel electrophoreses of supercoiled ddDNA plasmids, incubated with dicopper(II)-patellamide complexes for 24 hours at 37°C. In all cases, additional lines appeared in the separation. The samples used were 1: PANN<sub>SS</sub>, 2: Cu<sub>2</sub>Asc complex (0.16 mM/L), 3: Cu<sub>2</sub>Asc (0.8 mM/L), 4: control, 5: PANO<sub>SS</sub>.

## Danksagung

Frodo: I wish the Ring had never come to me. I wish none of this had happened.

Gandalf: So do all who live to see such times, but that is not for them to decide. All we have to decide is what to do with the time that is given to us.

from J.R.R. Tolkien, Lord of the Rings

Am Schluss dieser Arbeit, möchte ich Allen danken, die mir mit Rat und Tat – oder Gesellschaft zur Seite standen.

An erster Stelle geht mein Dank an meinen Doktorvater **Prof. Dr. Peter Comba**, der mich in seinen Arbeitskreis aufgenommen und mir dieses interessante und vielfältige Thema für meine Promotion angeboten hatte. Viele Diskussionen und Unterhaltungen gab es auf dem Weg die interessante Frage nach der Funktion der Patellamide zu ergründen. Insbesondere hat es mich gefreut, viele Freiheiten zu bekommen, so dass ich neben Synthese und Rechnungen auch Synchrotron-Messungen, meine Algenversuche und meine biologischen Versuche durchführen konnte und ich im Rahmen der Arbeit sogar zum Tauchen am Great Barrier Reef kam. Danke, dass du mir immer für eine Unterhaltung oder sogar mal für ein Feierabendbier zur Seite standest. Weitere schöne Erfahrungen waren Sommeraktivitäten und Skiseminare (bis auf kniezerreißende Ausnahmen).

Auch danke ich den Mitgliedern meines TAC-Komitees, **Prof. Dr. Franziska Thomas**, **Prof. Dr. Annika Guse** und **Prof. Dr. Kai Johnsson** für ihre Zeit sich alljährlich oder häufiger meinen Fortschritt anzuhören und darüber zu diskutieren. Insbesondere danke ich auch Franziska für die Übernahme der Zweitkorrektur und noch mehr für die interessanten wissenschaftlichen Kollaborationen, von denen unsere beiden AKs viel profitieren konnten, und die interessanten Gespräche. Weiterhin danke ich Annika für ihren Input zu meinen geplanten biologischen Versuchen und die Unterstützung ihres Arbeitskreises bei einigen davon.

Mein herzlicher Dank gilt auch allen internationalen Kollaborationspartnern:

**Prof. Dr. David Fairlie** and his group, for welcoming me in his lab at UQ Brisbane – and offering me all assistance I could (and did) ask for. Without you and your group, many of the interesting measurements would not have been possible. I also thank you and your group for the interesting discussions and advice. Especially I would like to thank **Dr. Tim Hill** for helping me to navigate through the confusing bureaucracy and finding my way around the lab and out of closed rooms (literally). **Dr. James Lim** and **Dr. Cathy Jones** I thank for their assistance with the biological experiments and fluorescence measurements. My thanks go out to **Alun Jones** for his time and work, measuring my samples with his amazing TripleTOF mass spectrometers.

Furthermore, I would like to thank **Prof. Dr. Bernhard Degnan** for his advice and collaboration on the sample collection – and for giving me insight into his interesting and important work. I also thank **Prof. Dr. Lawrence R. Gahan** for his collaboration on the paper publishing the updated copper concentrations.

One more UQ scientist I would like to thank is **Prof. Dr. Jeffrey Harmer** for taking the time to measure EPRs with me. I learned a lot about the technique – and while we didn't see much, this ended up being an important observation anyway.

I would like to thank our collaborators **Prof. Dr. Lars Behrendt** and **Prof. Dr. Michael Kühn** for the invitation to write our nice review paper and especially Lars for all his input and advice on the sample collection in Heron Island.

Hervorzuheben ist außerdem die Zusammenarbeit mit Kollegen (und ehemaligen) am Anorganisch-Chemischen Institut der Uni Heidelberg und es gibt viele bei denen ich mich bedanken möchte. Allen voran bei uns im Arbeitskreis **Dr. Patrick Cieslik**, für all den Rat zu Synthese und anderen Themen am Anfang meiner Arbeit, für die Gespräche und Feierabendkistenbiere, Partys, Game sessions, letztendlich natürlich für das Korrekturlesen meiner Arbeit und für die musikalische Übermalung des Laboralltags. Im Nachbararbeitskreis Linti möchte ich insbesondere **Dr. Philipp Siebenbürger** danken, du hast mich von Anfang an mit offenen Armen an der Uni empfangen, danke für die zahllosen Kochabende, Biere, Gespräche und Diskussionen, DSA-Runden und alles weitere. Auch den anderen verbliebenen und ehemaligen Kollegen in meiner Arbeitsgruppe, **Dr. Thomas Josephy**, **Dr. Katharina Bleher**, **Dr. Saskia Krieg**, **Dr. Martina Lippi** und **Rejith Radhamani** möchte ich danken, für Hilfe und Rat beim Kennenlernen der Instrumente und für den wissenschaftlichen Austausch. Auch dem restlichen Nachbar-AK Linti, **Angela Schwarz**, **Melanie Macher** und **Tobias Saxl**, möchte ich danken für die netten Gespräche und die Gesellschaft, insbesondere beim täglichen gemeinsamen Mittagessen. Ich danke dir, **Maik Jakob**, für die Hilfe mit meinen vielen Bestellungen und deine Hilfsbereitschaft bei Problemen in Labor und mit Geräten.

**Dr. Velmurugan Gunasekaran**, I thank you a lot for all the help with the calculations, the many interesting discussions about these interesting macrocycles, but especially for being a very kind and open person that is always great to talk to.

Außerdem danke auch allen im Matter to Life Programm, die mir auf die eine oder andere Weise geholfen haben, **Dr. Heike Böhm** für ihre Hilfe bei all der Bürokratie am Anfang, **Dr. Jan Heidelberger** und **Dr. Julia Ricken** für Alles in den Jahren darauf. **Prof. Dr. Petra Schwille**, herzlichen Dank für die Empfehlung in diesem einzigartigen neuen Programm zu promovieren. Insbesondere danke ich **Johannes Hahmann** für das Carrien bei den Messungen mit DNA und im Rift und für die lustigen Abende in Aachen. All students in Matter to Life I would like to thank for making this program a great time, and a nice community. Especially the retreats and meet-ups were a lot of fun.

**Dr. Bodo Martin** möchte ich danken für die Hilfe mit Serverzugang und Lizenzen, und für die Einführung in die ungewohnte Welt der Linux-Serververwaltung, die ich nach seinem Wechsel an eine andere Position gebraucht habe.

**Dr. Marion Kerscher** danke ich für die Einführung in die Messung von EPR-Spektren und deren Auswertung.

**Karin Stelzer, Marlies von Schoenebeck-Schilli** und **Dr. Jessica Wiedmeier** möchte ich für all die Hilfe bei Bürokratie, Abrechnungen und Endnotierung danken.

Auch möchte ich allen Forschungsstudenten, Master- und Bachelorstudenten danken, die ich über die Jahre hinweg betreuen durfte: **Jonas Malzacher, Sophia Hamm, Isabel Hanstein, Lissy Phung, Robert Kindler, Martin Degenhardt, Ayşeçan Ünal, Valeria Patini, Moritz Websky, Manuela Brock, Elizaveta Bobkova** und **Philippe de Bary**. Von Einigen hat die Arbeit viel zum Fortschritt des Projektes beigetragen, insbesondere bei der Synthese, einiges war allerdings auch mal ein komplett anderes Thema, dadurch aber eine erfrischende Abwechslung (ja ich spreche über die Rattenschwanz-Radikale).

Auch danke ich meinen Synchrotron-Crews: **Martin Dietl, Wojtek Treyde, Truc Lam Pham, Sunnatullo Fazilev, Tobias Saxl, Marcos Conde-González** und **Philippe de Bary**, die die Trips und langen Arbeitstage zu einer schönen Erfahrung gemacht haben. Insbesondere danke ich auch **Truc Lam** für die interessanten Kollaborationsprojekte und seine Hilfe bei meinen Versuchen die Festphasensynthese zu verwenden. Ich bin gespannt, wie es weiter geht.

A big thanks goes out to the Heron Island Research Station crew, for their hospitality, their help with all the equipment and bureaucracy – and their company on nice BBQ evenings, sunsets, and dive trips (how cool were the whales?).

Den analytischen Abteilungen der Uni Heidelberg danke ich für ihre sorgfältige und schnelle Arbeit, insbesondere Claudia Dienemann für die zahlreichen Massenspektren.

Mein Dank auch an die Feinmechaniker, für die kreative Hilfe bei „Bastelprojekten“ und hartneckigen Säulen (pun intended). Auch danke ich den Reinigungskräften, Schlossern, Glasbläsern und der Verwaltung für ihre Arbeit.

Ich danke neben Patrick auch meinem Vater, **Prof. Peter Baur** für das geduldige Korrekturlesen meiner Dissertation.

Darüber hinaus danke ich Julian, Jacob, Magnus, Philipp, Philip, Philipp, für die schönen Ablenkungen am Wochenende – und den Freunden am Department Patrick, Philipp und Martin für Ablenkungen auch mal unter der Woche.

Am Schluss will ich nun noch meiner Familie danken, ihr wart stets da für mich auch in schwierigen Zeiten. Ihr habt mir geholfen an den Wochenenden zuhause auch mal abzuschalten. Ihr habt immer an mich geglaubt und mich unterstützt.



**GESAMTFAKULTÄT FÜR MATHEMATIK, INGENIEUR-UND NATURWISSENSCHAFTEN**  
**COMBINED FACULTY OF MATHEMATICS, ENGINEERING AND NATURAL SCIENCES**

Eidesstattliche Versicherung gemäß § 8 der Promotionsordnung für die Gesamtfakultät für Mathematik, Ingenieur- und Naturwissenschaften der Universität Heidelberg /

Sworn Affidavit according to § 8 of the doctoral degree regulations of the Combined Faculty of Mathematics, Engineering and Natural Sciences at Heidelberg University.

1. Bei der eingereichten Dissertation zu dem Thema / *The thesis I have submitted entitled*  
**“The biological function of Patellamides and their copper complexes”**

handelt es sich um meine eigenständig erbrachte Leistung / *is my own work.*

2. Ich habe nur die angegebenen Quellen und Hilfsmittel benutzt und mich keiner unzulässigen Hilfe Dritter bedient. Insbesondere habe ich wörtlich oder sinngemäß aus anderen Werken übernommene Inhalte als solche kenntlich gemacht. / *I have only used the sources indicated and have not made unauthorised use of services of a third party. Where the work of others has been quoted or reproduced, the source is always given.*
3. Die Arbeit oder Teile davon habe ich bislang nicht an einer Hochschule des In- oder Auslands als Bestandteil einer Prüfungs- oder Qualifikationsleistung vorgelegt. / *I have not yet presented this thesis or parts thereof to a university as part of an examination or degree.*
4. Die Richtigkeit der vorstehenden Erklärungen bestätige ich. / *I confirm that the declarations made above are correct.*
5. Die Bedeutung der eidesstattlichen Versicherung und die strafrechtlichen Folgen einer unrichtigen oder unvollständigen eidesstattlichen Versicherung sind mir bekannt. / *I am aware of the importance of a sworn affidavit and the criminal prosecution in case of a false or incomplete affidavit.*

Ich versichere an Eides statt, dass ich nach bestem Wissen die reine Wahrheit erkläre und nichts verschwiegen habe. / *I affirm that the above is the absolute truth to the best of my knowledge and that I have not concealed anything.*

.....  
Ort und Datum / *Place and Date*

.....  
Unterschrift / *Signature*